MODELING STORMFLOW IN UNGAUGED BASINS: USING DIGITAL FILTERS, LIDAR, AND THE GEOMORPHOLOGICAL INSTANTANEOUS UNIT HYDROGRAPH

by

WILLIAM FRENCH MASON-DEESE

(Under the Direction of John F. Dowd)

ABSTRACT

This thesis presents a comprehensive model for predicting storm runoff and contributing areas based on precipitation and topography. Independent storms are defined using a procedure by Restrepo-Posada and Eagleson (1982) and stormflow is defined with geochemistry. Recursive digital filters are compared and calibrated to geochemical hydrograph separation on Panola Mountain Research Watershed enabling the digital filters to be used to define stormflow on Coweeta Watershed 18. High resolution topography of the watersheds, derived from LiDAR, is used to extract dense drainage networks. The networks predict surface runoff flow paths and the areas of a watershed that produce runoff. The mean lengths of streams of the networks are used to parameterize the geomorphologic instantaneous unit hydrograph that is used to model storm hydrographs. Finally, modeled storm hydrographs are compared to observed and digitally filtered stormflow. Comparison of observed and modeled storms determines if this model is suitable for ungauged basins.

INDEX WORDS: Baseflow separation, Digital filters, Storm runoff, Stream networks, Geomorphologic instantaneous unit hydrograph

MODELING STORMFLOW IN UNGAUGED BASINS: USING DIGITAL FILTERS, LIDAR, AND THE GEOMORPHOLOGICAL INSTANTANEOUS UNIT HYDROGRAPH

by

WILLIAM FRENCH MASON-DEESE

B.S., Guilford College, 2010

A Thesis Submitted to the Graduate Faculty of The University of Georgia in Partial Fulfillment of the Requirements for the Degree

MASTER OF SCIENCE

ATHENS, GEORGIA

2013

MODELING STORMFLOW IN UNGAUGED BASINS: USING DIGITAL FILTERS, LIDAR, AND THE GEOMORPHOLOGICAL INSTANTANEOUS UNIT HYDROGRAPH

by

WILLIAM FRENCH MASON-DEESE

Major Professor: John F. Dowd

Committee: Todd C. Rasmussen
Thomas R. Jordan

Electron Version Approved:

Maureen Grasso
Dean of the Graduate School
The University of Georgia
December 2013

ACKNOWLEDGEMENTS

I would like to thank professor Dr. John Dowd for being my advisor and for his countless hours writing custom computer programs that made this project possible.

I would like to thank Dr. Thomas Jordan for serving on my committee and helping me to obtain and process the LiDAR data. I would also like to thank Dr. Todd Rasmussen for serving on my committee and helping me to understand and conceptualize this model.

This project was also made possible by the extensive data available at Panola Mountain Research Watershed. I would like to thank Dr. Jake Peters from the USGS for helping to obtain this data and granting access to Panola Mountain Research Watershed. I also wish to thank Richard Cary for the geochemical hydrograph separations he did at Panola which made this project possible.

Extensive data from Coweeta Hydrologic lab was also used for this project. I would like to thank Stephanie Laseter and Chelcy Ford from the USFS at Coweeta for helping to acquire the data.

I would also like to thank my family: my parents Lucinda Mason and William Deese along with my sister Liz Mason-Deese for their continuous support and motivation.

TABLE OF CONTENTS

LIST OF TABLES

LIST OF FIGURES

CHAPTER 1

INTRODUCTION AND LITERATURE REVIEW

Purpose of Study

This thesis consists of a series of manuscripts on modeling stormflow using recursive digital filters and topographic information that enable this model to be applied in ungauged basins. Modeling stormflow is an important topic in the field of hydrology and has many practical applications. Stormflow modeling is essential to infrastructure design including reservoirs, dams, bridges and culverts; it is also necessary for modeling floods, water quality, and solute transport (Kokkonen *et al*. 2003). Most methods of predicting stormflow are data intensive and rely on historical records of rainfall and runoff. However, historical records are not available for most basins across the globe, therefore, predicting stormflow using digital filters and the topography is advantageous and allows for predictions to be made in ungauged basins (Kumar *et al*. 2007).

The methods presented in thesis also estimate which areas of a watershed contribute storm runoff. Identification of contributing areas is essential for proper watershed management and distinguishes areas where fertilizers, pesticides, and solutes will readily runoff into a stream. Identification of contributing areas is also important in determining how construction and development will change the extent of these areas, thus changing the hydrologic response of the basin.

This research is important to the field of hydrology because storm runoff is modeled based on the flow paths that the water follows. Identifying these flow paths and the time at which they contribute is essential to predicting storm runoff and understanding the physical processes that produce runoff in a watershed. Estimating flow paths from digital filters and the topography allows for runoff predictions to be made in ungauged basins.

This thesis presents and tests three hypotheses that lead to a comprehensive stormflow model:

- The first hypothesis is that recursive digital filters can be used to accurately separate a stream hydrograph into components of stormflow and baseflow and that the digital filters can be parameterized for use in ungauged basins. The digital filters are assessed by comparing them to observed geochemical hydrograph separation on Panola Mountain Research Watershed. Optimized and estimated filter parameters are compared to determine if the filters can be applied to ungauged basins.
- The second hypothesis is that self-similar networks can be extracted from high resolution topography. The networks represent surface runoff flow pathways and can be used to estimate contributing areas of a watershed. The self-similar nature of the networks is assessed by calculating Horton ratios.
- The final hypothesis is that self-similar networks extracted from high resolution topography can be used to parameterize the geomorphologic instantaneous unit hydrograph and model storm runoff. The model was fit to storms on Panola Mountain Research Watershed and compared to observed storms. The model was used to predict storms on Coweeta Watershed 18 and compared to digitally filtered stormflow.

Literature Review

The first manuscript details procedures that must be completed prior to modeling storm runoff. The first step is to identify individual storm events. A procedure developed by Restrepo-Posada and Eagleson (1982), based on the assumption that the arrival of independent storms can be described with a Poisson Process, is used to define independent storm events.

Once storms are defined, stormflow is defined by separating observed hydrographs into components of baseflow and stormflow. Recursive digital filtering is a technique that provides realistic baseflow separation (Eckhardt, 2008). Several digital filters, including Lyne and Hollick (1979), Chapman (1991), and Eckhardt (2005) are examined and compared to geochemical separation completed by Cary (2011). Geochemical separation allows for an objective comparison of the digital filters to observed data; it also provides a more concise definition of baseflow and stormflow determined by the flow paths that water follows.

Stormflow is ultimately modeled from the topography. The second manuscript details procedures of deriving a digital elevation model from LiDAR and extracting a dense drainage network. These procedures are implemented using ArcGIS® software by Esri and the program TauDEM (2012) by David Tarboton of Utah State University. The network is used to estimate the areas of the watershed that contribute runoff and the flow paths that the runoff follows. The structure of the network is used to parameterize the geomorphologic instantaneous unit hydrograph, this method assumes that the network is self-similar, or behaves the same way at all scales. The self-similar nature of the networks is assessed using Horton (1945) ratios.

Procedures of Cudennec *et al*. (2004) and Fleurant *et al*. (2006) show how the structure of the drainage network is used to derive the geomorphologic instantaneous unit hydrograph (GIUH). These procedures are described in the third manuscript, as well as procedures for calculating storm hydrographs from the GIUH. Modeled storms are fit and compared to observed storms on Panola Mountain Research Watershed. The model is used to predict storms on Coweeta Watershed 18 and compared to stormflow defined with digital filters, thus simulating an ungauged basin.

These manuscripts offer original research in the field of stormflow modeling. Baseflow separation techniques, such as digital filters, have been compared to other separation techniques but have not been compared to observed data from geochemical hydrograph separation. Comparison to these observed data allow for an objective evaluation of the digital filters and a more concise definition of baseflow and stormflow.

Cudennec *et al*. (2004) uses blue line stream networks from lower resolution maps to derive the GIUH. In this thesis, a dense drainage network is derived from high resolution topography. The topography and drainage network are used to estimate the contributing areas of a watershed, a factor that is overlooked in many hydrologic models. The structure of the drainage network is also used to derive the GIUH. The GIUH is used to calculate storm hydrographs allowing for the results to be compared to observed data. Together, these procedures are useful and unique because they provide a foundation for predicting storm runoff in ungauged basins based solely on the topography and precipitation.

Site Descriptions

The procedures described above are implemented on two separate basins: Panola Mountain Research Watershed and Watershed 18 of Coweeta Hydrologic Laboratory. Both of these watersheds are relatively small, forested, and undisturbed. This model has not yet been tested on larger basins, urban areas, areas with lakes or karstic terrain.

Panola Mountain Research Watershed

Panola Mountain Research Watershed (Panola) is a 41 ha forested watershed located approximately 25 km southeast of Atlanta, Georgia. Panola is located in the southern Piedmont physiological province and has a humid subtropical climate with average temperatures of 15.2°C (Cary 2011). Precipitation is characterized by convective, high intensity, and short duration storms from April through September. The rest of the year is characterized by synoptic weather systems with low intensity and long durations (Peters *et al*. 2003). Panola receives an annual average rainfall of 1,220 mm, of which about 70% is transpired. High baseflows usually occur during the dormant season between November and March; low baseflows occur during the growing season between May and October (Peters *et al*. 2003; Cary 2011).

Panola is 90% forested; the remaining 10% consists of exposed granitic outcrops (Peters *et al*. 2003, Cary 2011). The bedrock is mainly composed of Panola Granite, which is a biotite-oligoclase-quartz, microcline granodiorite and may be interspersed with pods of amphibolitic gneiss (Higgens *et al*. 1988). Soils consist of ultisols that were formed in colluvium and residuum; soils grade into inceptisols on the slopes and at the base of the bedrock outcrop (Peters *et al*. 2003; Cary 2011). Over 75% of the watershed is comprised

of hillslopes with shallow soils (<1 m). Narrow riparian zones with deeper soils (5 m) comprise less than 15% of the watershed. The watershed slopes generally have a northwest aspect.

Data for these analyses were collected at Panola over a 23 year period from October 1985 through September 2008. Precipitation was measured with tipping bucket rain gauges. Stream stage was measured using a sharp-crested compound 90° V-notch weir located at the mouth of the watershed. Measurements were made every five minutes during baseflow conditions and during storm conditions measurements were made in one minute intervals.

Over the 23 year period 642 independent storm events were identified using procedures of Restrepo-Posada and Eagleson (1982). Independent storms were separated by eight consecutive dry hours; the storms had to last longer than one hour and have a minimum volume of 13 mm.

Coweeta Hydrologic Laboratory

Coweeta Hydrologic Laboratory (Coweeta) is located in the Nantahala Mountain Range near Otto, North Carolina. Coweeta was established in the mid 1930s to study the effects of logging on forest hydrology and ecosystems (Swank *et al*. 1988). Long term historical data records and undisturbed watersheds make Coweeta an ideal location for hydrologic research.

Annual average rainfall ranges from 1,870 mm in low elevations to 2,500 mm in higher elevations. Precipitation is relatively evenly distributed throughout the year, with less than 2% falling as snow (Kokkonen *et al*. 2003).

The geology and soils of the Coweeta basin are variable. Soils generally consist of inceptisols and older, more developed ultisols. Soils form on residuum and colluvium of the underlying bedrock (Swank *et al*. 1988). The bedrock geology consists of biotite paragneiss and schist. The topography is rugged with deep valleys forming along zones of weak bedrock that cut through steep ridges. (Adams *et al*. 2005, Higgins *et al*. 1988).

Coweeta Watershed 18 is a 13 hectare watershed located in the southeast portion of the Coweeta Basin. It is a control watershed that has been undisturbed since 1927. Vegetation consists of mixed hardwoods that dominate the canopy and thick rhododendron stands that dominate the understory. The watershed slopes generally have a northwest aspect.

The watershed drains Grady Branch, which flows mainly to the north. Streamflow is measured with a 120° V-notch weir and reported when the gauge stage changes. These data were converted to hourly intervals. Precipitation is measured from a standard rain gauge located adjacent to the watershed and at an elevation of 887 m; precipitation is also reported in hourly intervals. Records of precipitation and streamflow began in 1936 (Swank *et al*. 1988).

For these analyses observations from 2000 through 2010 are used. A period of six consecutive non-rain hours was found to separate independent storms by the procedure of Restrepo-Posada and Eagleson (1982). Over the 10 year period, 448 independent storm events were identified. Storms were also defined to have a minimum duration of an hour and minimum volume of 13 mm.

CHAPTER 2

COMPARISON OF HYDROGRAPH SEPARATION TECHNIQUES; DIGITAL FILTERS VERSUS GEOCHEMICAL END MEMBEFRS[1]

1 Mason-Deese WF, Dowd JF, Cary RH. *Proceedings of the 2013 Georgia Water Resources Conference*, held April 10–11, 2013, at the University of Georgia.
Reprinted here with permission from the publisher.

Abstract

Stormflow is defined as flux resulting from a storm event, while baseflow is thought to be groundwater flux that continuously occurs, most predominantly during non-storm periods. While conceptually these concepts are convenient, it is difficult to ascertain the flow pathways of each component. In this paper we compare common digital filters used to estimate baseflow with a geochemically derived baseflow separation.

A Dynamic End Member Mixing Analysis (DEMMA) on Panola Mountain, Georgia, was used by Cary (2011) to separate four stream flow components using naturally occurring chloride and silica for 22 storm events. DEMMA relies on intensive runoff and chemical sampling, and uses the flow and chemistry hysteresis to separate the hydrograph.

Digital filters estimate baseflow by attenuating the discharge hydrograph. Three digital filters were compared to the DEMMA hydrographs. While parameterized differently, each was a recursive procedure that acts as a low pass filter.

The one parameter filter is simple to use but insensitive to calibration because the parameter is usually not modified. The two parameter filter (Eckhardt 2005) was more robust in its range, but sensitive to calibration.

In general the digital filters over estimate baseflow for Panola (that is, saturated flow), and more closely resemble contributions from subsurface flow (that is, unsaturated and saturated) pathways. This research shows that digital filters are approximating baseflow that occurs over shallow groundwater and deep hillslope flow paths.

Introduction

Separation of baseflow from the hydrograph has been a contentious topic throughout the hydrologic literature and is critical for many types of hydrologic modeling and watershed management. As a result, many techniques for baseflow separation have been developed that vary in objectivity and resemblance to physical processes. Recursive digital filters (RDFs) are one technique that is easy to implement and provides relatively objective and realistic results, although, RDFs have not been compared to geochemically derived hydrograph separation (Nathan and McMahon 1990, Eckhardt 2008).

The objective of this paper is to determine if digital filters can be used to accurately separate stormflow and baseflow from a hydrograph and to determine the flow paths that the digital filters are approximating. The digital filters are assessed by comparison to geochemical hydrograph separation. Optimized filter parameters are also compared to estimated parameters to determine if the filters can be applyed in ungauged basins.

Before baseflow is separated from the hydrograph it must first be defined. Throughout the literature, baseflow has been defined based on residence times and runoff pathways, resulting in several names being given to baseflow including: old water, delayed flow, and through flow (Lanen and Tallaksen 2004). Generally, baseflow is thought to be a component of stream flow which is considered the continuous flow to streams from deep flow paths and is dependent on groundwater reservoirs that have long residence times and react slowly to rainfall events (Aksoy *et al.* 2009, Chapman 1999, Collischonn and Fan 2012, Eckhardt 2005). Hillslope water from the unsaturated zone has been shown to contribute significant amounts of stream flow both early in a storm and as delayed flow (Rasmussen *et al.* 2000, Hewlitt and Hibbert 1965).

Although these definitions are conceptually convenient, runoff processes are complex with many different possible flow paths contributing at different times. For this reason, chemical values are used to define several source waters, and their timing is used to constrain their contribution. This allows for an objective definition of baseflow and stormflow that can be used to assess the digital filters.

Geochemical Hydrograph Separation

Cary (2011) used Dynamic End Member Mixing Analysis (DEMMA) with naturally occurring chemical tracers to separate hydrographs into four flow components for 22 storms on Panola. Naturally occurring chloride and silica are used as conservative tracers to define four end-members: groundwater, deep hillslope water, shallow hillslope water, and event water. Figure 2.1 shows a map of the sampling locations for each end-memeber. Groundwater was collected from wells in saprolite. Deep hillslope water was collected from piezometers in the B-horizon. Shallow hillslope water was collected from zero-tension lysimeters in the top 15 cm of the soil. Event water was collected from rain gauges (Cary 2011).

Synthetic concentrations of chloride and silica are calculated using a four component mixing model:

$$C_S Q_S = C_{GW} Q_{GW} + C_{H1} Q_{H1} + C_{H2} Q_{H2} + C_{EW} Q_{EW} \qquad \textit{Equation 1}$$

where C is concentration, Q is discharge, S is stream water, GW is shallow groundwater, $H1$ is deep hillslope water, $H2$ is shallow hillslope water, and EW is event water. The timing of contributions from each member are adjusted using several operations including beta grading, ratio, stretching, and smoothing.

Results from the end-member mixing model are plotted against discharge to create synthetic hysteresis loops which are compared and fit to the observed hysteresis loops. The discharge, concentration, and timing of the end-members are adjusted until the best fit is achieved for both chloride and silica hysteresis loops. The parameters of the best fit model are used to separate the hydrograph into the four components. Figures 2.2 and 2.3 show an example of hydrograph separation using DEMMA.

Cary (2011) found a threshold of about 50 mm of rain causes hysteresis loops to reverse direction, implying different runoff contributions. Storms below this threshold are characterized by clockwise hysteresis loops while storms above this threshold have counterclockwise hysteresis loops. Cary hypothesizes that at the threshold amount of rain, flow paths within the watershed activate connecting a larger portion of the watershed and delivering chemically distinct waters that reverse the hysteresis loops.

DEMMA was used by Cary (2011) to separate 22 storm hydrographs. In this paper, these geochemically derived hydrograph separations are compared to and used to calibrate recursive digital filters.

Recursive Digital Filters

Recursive digital filters (RDF) were originally designed for signal analysis and processing and more recently have been applied to hydrographs (Lyne and Hollick 1979). RDFs work by mathematically attenuating or enhancing certain frequency bands of a discreet time series (Kaur 2011). Baseflow is associated with long, low frequency waves because it follows deep flow paths, has long residence times, and is sourced from large reservoirs that cause it to have a damped signal. Direct runoff is associated with high

frequency waves because it responds quickly to rainfall. By implementing a low pass filter on the hydrograph, the low frequency baseflow is separated from high frequency direct runoff.

The RDFs do not account for nonlinear storage, bank storage, or water lost from a stream. It is assumed that outflow from the aquifer is linearly proportional to storage and that the recession curve is exponential (Eckhardt 2008). The resulting baseflow hydrograph is a smoothed, damped, and delayed image of the storm hydrograph.

Lyne and Hollick (1979) first introduced the RDF as a method of separating baseflow:

$$b_k = \alpha b_{k-1} + \frac{(1+\alpha)}{2}(y_k + y_{k-1}) \qquad b_k \leq y_k \ . \qquad \textit{Equation 2}$$

Where b is filtered baseflow, k is back shift operator or the time step, y is the observed stream flow, and α is the filter parameter.

Chapman (1991) notes that the Lyne and Hollick algorithm treats baseflow as a constant when there is no storm runoff. Chapman proposes an improved algorithm that uses the recession curve for periods after stormflow has ceased and defines the filter parameter, α, as the recession constant.

$$b_k = \frac{\alpha}{2-\alpha} b_{k-1} + \frac{1-\alpha}{2-\alpha} y_k \qquad b_k \leq y_k \ . \qquad \textit{Equation 3}$$

Eckhardt (2005) argues that the one parameter filters are simplified expressions of a more generalized two parameter filter. Eckhardt proposes a two parameter filter, introducing BFI_{Max} as the second parameter. BFI_{Max} is the largest ratio of baseflow to total streamflow that the algorithm can model:

$$b_k = \frac{(1 - BFI_{Max})\,\alpha\, b_{k-1} + (1 - \alpha)\, BFI_{Max}\, y_k}{1 - \alpha\, BFI_{Max}} \qquad b_k \le y_k . \qquad \textit{Equation 4}$$

The recession constant for a storm is directly calculated by plotting stream discharge versus discharge at the previous time step. The points plot close to a straight line; the slope of this line is defined as the recession constant and generally ranges from 0.90 to 0.97 (Eckhardt 2008, Nathan and McMahon 1990).

The Baseflow Index (BFI) is the long term ratio of baseflow to total stream flow. BFI_{Max} is defined as the largest BFI that the algorithm can model, although, this has no physical meaning and cannot be measured. Eckhardt (2005) suggests predefined values based on the underlying geology and the flow regiment of the stream. A BFI_{Max} value of 0.8 is suggested for perennial streams on porous aquifers; a BFI_{Max} of 0.5 is suggested for ephemeral streams on porous aquifers; and a BFI_{Max} of 0.25 for perennial streams on hard rock aquifers. Independent estimates of BFI can also be used for BFI_{Max}, although, chemical calibration is optimal (Eckhardt 2005).

Methods

The following procedure was used by a custom designed computer program named *PanolaStorms*. Independent storms were derived from analysis of hourly rainfall data using the Poisson Process procedure of Retrepo-Posada and Eagleson (1982). The discharge and geochemical sub-hydrographs, for each selected storm, were converted to hourly values. The filters were fit to the hourly discharge, and the best parameter fits were obtained by finding the smallest root mean square error (RMSE) between the fit and the selected sub-hydrograph. The storms selected and the sub-hydrograph fits were from Cary (2011). The

baseflow index was calculated from the best parameter fit for each filter and for each storm. Note the Lyne and Hollick and Chapman filters fit one parameter, while Eckhardt fit two. For Eckhardt, the RMSE was plotted on a 3-D surface where the optimal parameters occur at the lowest point on the surface or where RMSE is minimized.

Recession constants were measured for each of the 22 storms and then used to parameterize the filters. Eckhardt's (2005) suggested values, and an independent estimate of BFI by Peters *et al.* (2003) were used for BFI_{Max}. Parameters were also optimized for all of the storms by minimizing the RMSE.

Paired student t-tests at 95% confidence were used to determine if the means of the geochemically derived BFI were similar to the means of digitally filtered BFI. T-tests were also used to determine if the estimated parameters were similar to the optimized parameters.

Results and Discussion

The RDFs over-estimate shallow groundwater flow and more closely resemble shallow groundwater plus deep hillslope flow (GW+H1) or shallow groundwater plus deep and shallow hillslope flow (GW+H1+H2). These two source waters were used to optimize the filter parameters. The filters were optimized for 22 storms. Table 2.1 reports characteristics of the 22 storms. Six of the larger storms were characterized by counterclockwise hysteresis loops while the remaining 16 storms had clockwise hysteresis loops.

Plots of the geochemically derived sub-hydrograph and RDFs are produced for each storm. An example of a storm producing counterclockwise hysteresis is depicted in Figure

2.4 and a storm producing clockwise hysteresis is depicted in Figure 2.5. The counterclockwise sub-hydrographs have sharp peaks that respond quickly at the beginning of rainfall events; the smaller clockwise storms are characterized by more subdued and rounded peaks. The digital filters are not able to respond quickly enough and with sharp enough peaks to mimic the observed sub-hydrographs of large counterclockwise storms. However, the digital filters fit the observed sub-hydrographs of the smaller clockwise storms. GW+H1+H2 source waters generally have larger and sharper peaks while GW+H1 have smaller peaks, therefore, the digital filters fit GW+H1 source waters better.

The Lyne and Hollick filter peaks higher and later than the other filters. This is because the Lyne and Hollick filter has no recession constant built into it. The filter will continue to increase or remain equal until it intersects and is set equal to the observed discharge hydrograph.

The results of optimizing the digital filters to GW+H1 are found in Table 2.2 and the results of optimizing the filters to GW+H1+H2 are found in Table 2.3. The filter results are summarized in a series of boxplots. Figure 2.6 depicts the optimized filter parameters for each source; the horizontal line represents the average measured recession constant which is 0.96. Figure 2.7 shows the resulting BFI for each source using optimized parameters, measured recession constants, and estimated BFI_{Max} values. In Figure 2.8, recession constants, BFI_{Max}, BFI, and the RMSE are compared for clockwise and counterclockwise storms. P-values from student t-tests are reported in Table 2.4. P-values greater than 0.05 indicate, at the 95% confidence level, that the means of the geochemical BFIs are not different from the digitally filtered BFI means, and that the optimized parameter means are not different from the measured or estimated parameter means.

Figure 2.6 shows that the optimized recession constants correspond to the recession constants measured from storm hydrographs and that they occur over a relatively narrow range. Except for the Eckhardt filter optimized to GW+H1 that tended to have α values converge at 0.99; Table 2.4 indicates, at the 95% confidence level, that the means of the measured recession constants are not different from the means of the α parameter optimized to each of the source waters. This indicates that measuring recession constants from hydrographs is an accurate and objective method of obtaining the α parameter.

BFI_{Max} values are more difficult to obtain. Figure 2.7 and Table 2.4 show how BFI compares for different estimates of BFI_{Max}. Optimized BFI_{Max} values are statistically similar, at 95% confidence, to Eckhardt's suggested BFI_{Max} of 0.80. However, when the Eckhardt filter is optimized α tends to converge at 0.99, this also causes BFI_{Max} to be inflated. If a BFI_{Max} value of 0.80 is used to parameterize the filter, the resulting BFI is larger than both source waters. A BFI_{Max} value of 0.60 produces results that are statistically similar to GW+H1 source waters.

BFI_{Max} does not appear to be a constant for the watershed, rather, it fluctuates from storm to storm. Figure 2.8 shows counterclockwise storms have a significantly lower BFI_{Max} than clockwise storms, suggesting that BFI_{Max} is not only determined by the geology and type of stream but also by the type of storm. Moreover, examination of RMSE plots show that in most cases BFI_{Max} is the more sensitive parameter. This leads to the conclusion that without an initial or regional estimate of BFI the Eckhardt filter cannot be objectively parameterized.

Figure 2.7 and Table 2.4 compare geochemically derived BFI to BFI resulting from RDFs using estimated and optimized parameters. The mean BFI derived from the

geochemical separation is 55% for GW+H1 and 67% for GW+H1+H2. The mean BFIs of the Lyne and Hollick and Eckhardt filters are statistically similar, at 95% confidence, to GW+H1 source waters. Results from the Lyne and Hollick filter were more variable than the other two filters. The Chapman filters resulted in BFIs that were lower than the geochemical BFI. The Eckhardt filter was only similar when a BFI_{Max} of 0.60 was used which was an independent estimate of BFI from Peters *et al.* (2003). This indicates that the Lyne and Hollick and Eckhardt filters can be used to separate baseflow from a hydrograph and that the filters are defining baseflow as water sourced from groundwater and deep hillslope flow paths.

The type of filter used is the main determinate of the resulting BFI. Despite slight variations in the recession constant the Lyne and Hollick filter produces a BFI of around 60% and the Chapman a BFI of around 50%. The Eckhardt filter is more robust, where as, the resulting BFI is controlled by the BFI_{Max} parameter. If an independent estimate of BFI is known, the filter can be run changing BFI_{Max} until the average resulting BFI is close to the initial estimate.

Figure 2.8 shows that the filters minimize the RMSE the most for clockwise storms because the storms have smaller, less pronounced peaks that the filters are better able to fit. The filters cannot respond quickly enough to fit the larger, more pronounced peaks of counterclockwise storms. As a result, the filtered peaks are delayed and the RMSE is greater. Shallow hillslope water generally increases the sub-hydrograph peak or adds a second, delayed peak that are both difficult for the filters to fit and as a result, increase RMSE.

The assumptions that baseflow is comprised solely of groundwater that has a delayed response to rainfall is challenged by the geochemically derived sub-hydrograph, which is comprised of a large proportion of hillslope water that responds rapidly to rainfall. The RDFs are approximating these shallow groundwater and deep hillslope pathways, although, the timing is always late and the shape is too smooth.

Conclusion

Geochemical hydrograph separation is used to define baseflow as water resulting from shallow groundwater and hillslope pathways. Several digital filters were compared and fit to the geochemical sub-hydrograph in order to determine what flow paths the digital filters are defining as baseflow and to determine how to parameterize the digital filters.

Baseflow filtered by the Lyne and Hollick filter is comparable to the geochemically estimated groundwater and deep hillslope water, although, the Lyne and Hollick filter produces delayed peaks, and does not account for recession. The Chapman filter underestimates baseflow with peaks and recession tails that are too low. The Eckhardt filter provides similar results to geochemically separated groundwater and deep hillslope water, although, the best fits produce delayed peaks and a smoother shape than the observed sub-hydrograph.

The α parameter is easily estimated from the recession constant and generally does not change, however, the Eckhardt filter also requires an estimate of the BFI_{Max} parameter. The BFI_{Max} parameter is sensitive and subject to change based on the type of storm but can be estimated from a regional estimate of BFI.

The Lyne and Hollick and Eckhardt filters, using an estimate of the recession constant and an estimate of BFI for BFI_{Max}, can be applied to produce statistically similar results to geochemically derived hydrograph separations. The digital filters are defining baseflow as flow from groundwater and deep hillslope pathways, although, the timing is delayed and the shape is too smooth. This insight could lead to the formulation of a new digital filter that better matches the shape and timing of the observed sub-hydrographs.

Table 2.1: Characteristics of storms at Panola that were examined by Cary (2011).

Date	Storm Number	Return Period	Peak Discharge (mm/min)	Antecedent Precipitation Index	Precipitation (mm)	Hysteresis Direction
04/23/88	22	3	0.050	40.7	54.1	counterclockwise
02/10/95	44	4	0.063	10.1	85.09	counterclockwise
04/27/97	58	8	0.081	31.8	87.63	counterclockwise
03/02/01	87	0.75	0.014	39.8	52.53	counterclockwise
02/05/02	97	0.75	0.010	27.2	58.93	counterclockwise
06/16/04	113	1.5	0.030	60.8	38.35	counterclockwise
07/24/86	4	1	0.022	43.8	32.51	clockwise
04/25/88	23	0.5	0.009	82	17.27	clockwise
11/05/93	28	0.75	0.014	53.6	33.53	clockwise
12/10/93	30	0.5	0.006	33.1	20.07	clockwise
01/11/94	32	0.75	0.014	31.4	30.48	clockwise
01/27/94	33	0.75	0.014	19.6	29.46	clockwise
11/28/94	42	0.75	0.014	47.1	22.61	clockwise
09/21/96	53	1.1	0.027	48.5	33.53	clockwise
11/01/99	72	1	0.024	11.7	52.83	clockwise
03/16/00	76	0.05	0.008	18	24.38	clockwise
06/19/00	79	1.5	0.034	20.2	72.39	clockwise
01/29/01	84	0.5	0.005	17	22.35	clockwise
02/22/03	105	0.75	0.013	34.8	24.64	clockwise
11/18/03	111	0.75	0.017	13.5	42.38	clockwise
11/02/04	116	0.75	0.019	13.7	52.07	clockwise
04/30/05	122	0.75	0.010	28.2	32.26	clockwise

Table 2.2: Digital filters were optimized to groundwater plus deep hillslope water. The Baseflow Index (BFI) is reported for each of the digital filters and for the geochemically derived BFI. The table is continued...

	Storm	GW + H1	Optimized BFI (%)		
Date	Number	BFI (%)	Lyne-Hollick	Chapman	Eckhardt
04/23/88	22	36	58	49	53
02/10/95	44	33	38	34	31
04/27/97	58	31	49	46	41
03/02/01	87	66	56	49	57
02/05/02	97	65	57	49	55
06/16/04	113	66	65	51	62
07/24/86	4	57	53	43	51
04/25/88	23	57	72	65	72
11/05/93	28	60	53	45	53
12/10/93	30	69	67	52	68
01/11/94	32	53	42	41	42
01/27/94	33	46	57	46	54
11/28/94	42	66	68	55	68
09/21/96	53	30	60	51	60
11/01/99	72	41	28	27	27
03/16/00	76	72	74	51	74
06/19/00	79	24	16	25	21
01/29/01	84	69	60	49	60
02/22/03	105	64	71	50	70
11/18/03	111	74	66	50	65
11/02/04	116	48	55	47	55
04/30/05	122	74	73	58	73

Table 2.2: Continued... The measured α parameter is reported for each storm as well as the optimized α value by filter. Optimized BFI_{MAX} is also reported for the Eckhardt filter. The minimized Root Mean Square Error (RMSE) is reported for each storm by filter. The digital filters were optimized by minimizing the RMSE of the filter's fit to the groundwater plus deep hillslope sub-hydrograph.

	Storm	Measured	Optimized α			Optimized	Minimized RMSE		
Date	Number	α	Lyne-Hollick	Chapman	Eckhardt	BFI_{MAX}	Lyne-Hollick	Chapman	Eckhardt
04/23/88	22	0.94	0.94	0.92	0.94	0.55	0.077	0.062	0.060
02/10/95	44	0.97	0.98	0.98	0.94	0.36	0.183	0.158	0.139
04/27/97	58	0.96	0.95	0.95	0.92	0.43	0.138	0.121	0.116
03/02/01	87	0.96	0.98	0.96	0.99	0.96	0.067	0.068	0.065
02/05/02	97	0.96	0.97	0.95	0.97	0.57	0.042	0.040	0.038
06/16/04	113	0.93	0.87	0.83	0.91	0.64	0.054	0.043	0.038
07/24/86	4	0.95	0.85	0.91	0.99	0.87	0.006	0.006	0.003
04/25/88	23	0.97	0.99	0.99	0.99	0.74	0.007	0.015	0.006
11/05/93	28	0.97	0.96	0.94	0.99	0.98	0.018	0.022	0.017
12/10/93	30	0.96	0.97	0.96	0.99	0.97	0.012	0.021	0.011
01/11/94	32	0.96	0.99	0.98	0.99	0.74	0.024	0.023	0.023
01/27/94	33	0.96	0.97	0.95	0.99	0.96	0.017	0.026	0.015
11/28/94	42	0.96	0.97	0.95	0.98	0.70	0.035	0.050	0.030
09/21/96	53	0.93	0.96	0.96	0.99	0.89	0.006	0.010	0.003
11/01/99	72	0.96	1.00	0.99	0.99	0.82	0.004	0.005	0.004
03/16/00	76	0.95	0.91	0.85	0.99	0.99	0.018	0.026	0.016
06/19/00	79	0.95	1.00	0.99	0.99	0.80	0.008	0.007	0.004
01/29/01	84	0.97	0.98	0.96	0.99	0.75	0.007	0.012	0.008
02/22/03	105	0.98	0.95	0.92	0.99	0.87	0.017	0.041	0.016
11/18/03	111	0.98	0.93	0.91	0.99	0.88	0.014	0.024	0.013
11/02/04	116	0.90	0.93	0.92	0.99	0.98	0.022	0.024	0.018
04/30/05	122	0.97	0.98	1.00	0.99	0.96	0.012	0.038	0.011

Table 2.3: Digital filters were optimized to groundwater plus deep hillslope and shallow hillslope water. The Baseflow Index (BFI) is reported for each of the digital filters and for the geochemically derived BFI. The table is continued...

Date	Storm Number	GW+H1+H2 BFI (%)	Optimized BFI (%)		
			Lyne-Hollick	Chapman	Eckhardt
04/23/88	22	47	71	50	54
02/10/95	44	52	52	46	44
04/27/97	58	41	49	46	45
03/02/01	87	78	59	7	60
02/05/02	97	76	57	49	55
06/16/04	113	77	65	51	62
07/24/86	4	73	53	43	51
04/25/88	23	72	76	65	75
11/05/93	28	76	55	46	56
12/10/93	30	81	72	52	73
01/11/94	32	66	45	44	45
01/27/94	33	62	58	47	54
11/28/94	42	73	71	54	69
09/21/96	53	42	61	52	61
11/01/99	72	55	28	27	27
03/16/00	76	80	75	51	78
06/19/00	79	28	16	25	21
01/29/01	84	87	92	50	75
02/22/03	105	70	71	50	70
11/18/03	111	85	66	50	65
11/02/04	116	62	55	47	55
04/30/05	122	81	73	58	73

Table 2.3: Continued... The measured α parameter is reported for each storm as well as the optimized α value by filter. Optimized BFI_{MAX} is also reported for the Eckhardt filter. The minimized Root Mean Square Error (RMSE) is reported for each storm by filter. The digital filters were optimized by minimizing the RMSE of the filter's fit to the groundwater plus deep hillslope plus shallow hillslope sub-hydrograph.

	Storm	Measured	Optimized α			Optimized	Minimized RMSE		
Date	Number	α	Lyne-Hollick	Chapman	Eckhardt	BFI_{MAX}	Lyne-Hollick	Chapman	Eckhardt
04/23/88	22	0.94	0.84	0.76	0.81	0.54	0.105	0.080	0.079
02/10/95	44	0.97	0.95	0.94	0.93	0.47	0.163	0.172	0.170
04/27/97	58	0.96	0.95	0.95	0.94	0.48	0.128	0.114	0.114
03/02/01	87	0.96	0.97	0.95	0.99	0.97	0.067	0.069	0.065
02/05/02	97	0.96	0.97	0.95	0.97	0.57	0.042	0.040	0.038
06/16/04	113	0.93	0.87	0.83	0.91	0.64	0.054	0.044	0.037
07/24/86	4	0.95	0.85	0.91	0.99	0.87	0.006	0.006	0.003
04/25/88	23	0.97	0.98	0.98	0.98	0.70	0.019	0.026	0.017
11/05/93	28	0.97	0.94	0.93	0.99	0.98	0.019	0.023	0.017
12/10/93	30	0.96	0.95	0.94	0.99	0.98	0.014	0.025	0.013
01/11/94	32	0.96	0.99	0.96	0.97	0.51	0.030	0.026	0.026
01/27/94	33	0.96	0.97	0.94	0.99	0.96	0.022	0.029	0.020
11/28/94	42	0.96	0.96	0.93	0.97	0.69	0.050	0.064	0.044
09/21/96	53	0.93	0.95	0.95	0.99	0.87	0.013	0.014	0.010
11/01/99	72	0.96	1.00	0.99	0.99	0.83	0.005	0.005	0.005
03/16/00	76	0.95	0.90	0.79	0.99	0.98	0.021	0.028	0.018
06/19/00	79	0.95	1.00	0.99	0.99	0.80	0.008	0.007	0.004
01/29/01	84	0.97	0.25	0.00	0.37	0.75	0.016	0.025	0.011
02/22/03	105	0.98	0.95	0.92	0.99	0.87	0.017	0.041	0.016
11/18/03	111	0.98	0.93	0.91	0.99	0.88	0.014	0.024	0.013
11/02/04	116	0.90	0.93	0.92	0.99	0.98	0.023	0.025	0.019
04/30/05	122	0.97	0.98	1.00	0.99	0.96	0.012	0.038	0.011

Table 2.4: P-values from student t-tests comparing digital filters at Panola. Baseflow Indexes (BFI) from measured α values are compared to geochemically derived BFI of two source waters: groundwater and deep hillslope (GW+H1) and groundwater, deep and shallow hillslope (GW+H2+H1). BFIs resulting from optimized parameters are also compared to geochemically defined BFI. Recession constants measured from storm hydrographs are compared to the optimized α parameter. The estimated BFI_{Max} values are compared to the optimized BFI_{Max}. The grey boxes indicate p-values that exceed 0.05 indicating that the two means are not different within 95% confidence.

P-values from t-tests comparing Digital Filters at Panola

Geochemical	BFI from Measured α		
Source Water	Lyne Hollick	Chapman	Eckhardt
GW + H1	0.19	0.01	0.83
GW + H1 + H2	0.01	< 0.01	< 0.01

Geochemical	BFI from Optimized Parameters		
Source Water	Lyne Hollick	Chapman	Eckhardt
GW + H1	0.52	0.01	0.85
GW + H1 + H2	0.03	< 0.01	< 0.01

Geochemical	Measured α compared to Optimized α		
Source Water	Lyne Hollick	Chapman	Eckhardt
GW + H1	0.81	0.15	< 0.01
GW + H1 + H2	0.19	0.11	0.70

Estimated BFI_{Max}	Optimized BFI_{Max} GWH1	Optimized BFI_{Max} GWH1H2
0.25	< 0.01	< 0.01
0.60	< 0.01	< 0.01
0.80	0.83	0.72

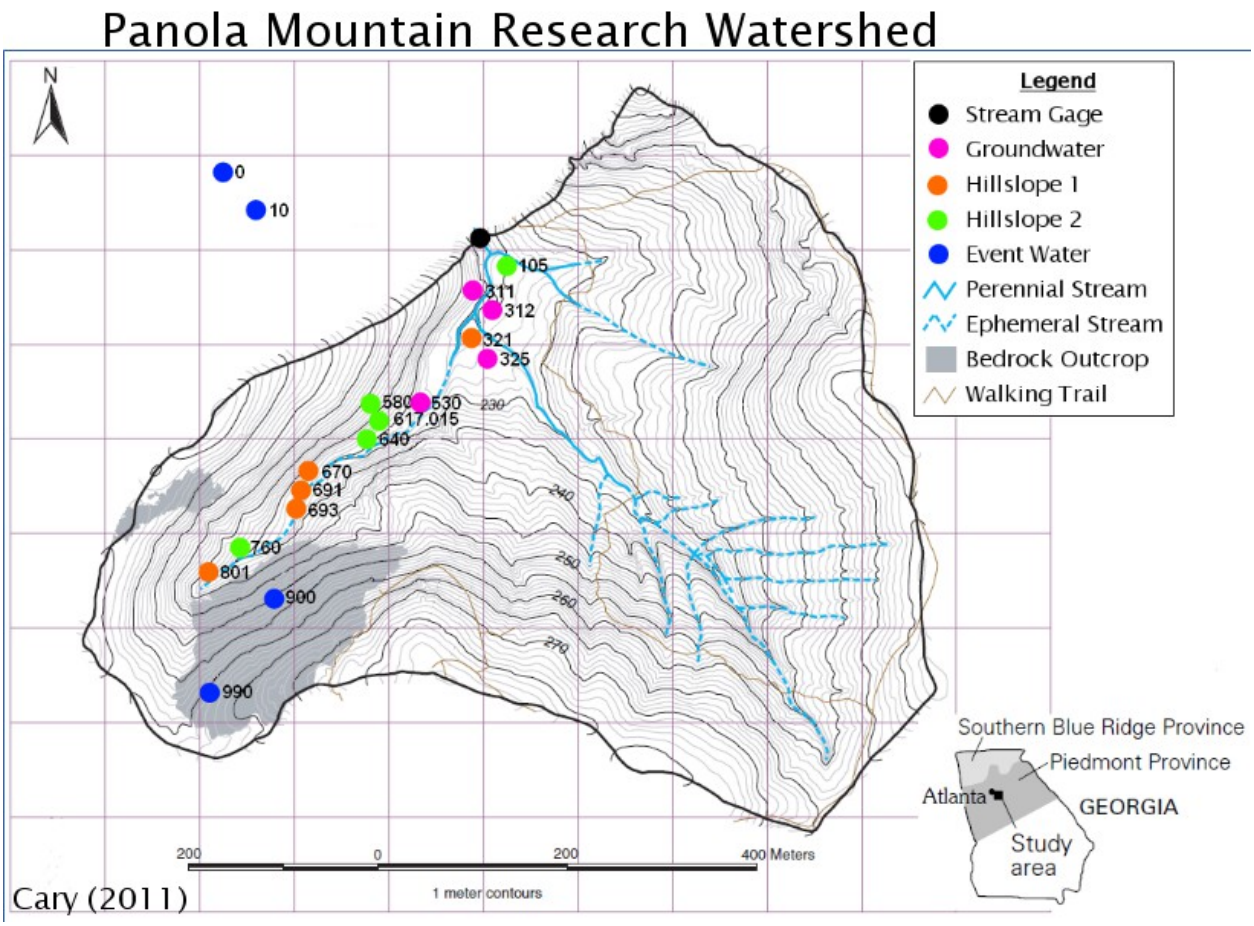

Figure 2.1: Map of Panola showing the sampling locations used to define end-memebers. Groundwater was measured from wells in the saprolite; Hillslope 1 is deep hillslope water measured with piezometers in the B-Horizon; Hillslope 2 is shallow hillslope water and was measured with zero-tension lysimeters in the top 15 cm of soil; Event water is measured from rain gauges.

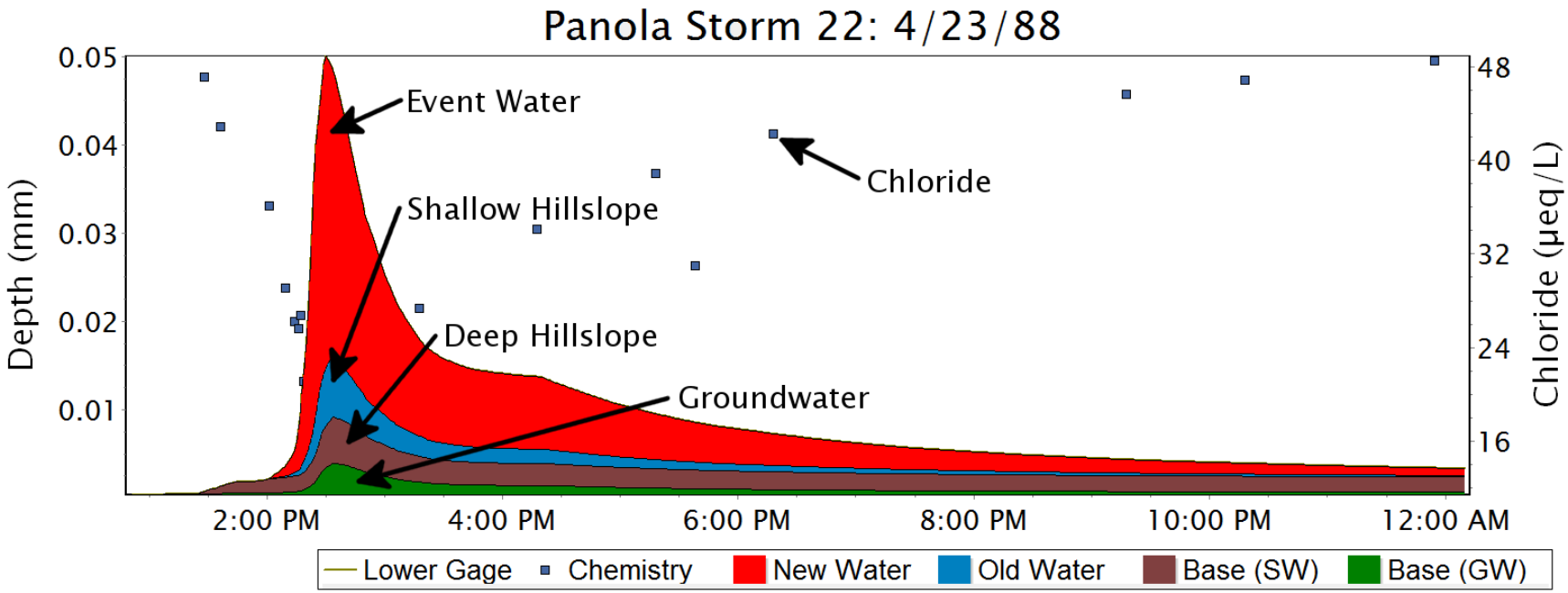

Figure 2.2:Hydrograph separation using Dynamic End-Member Mixing Analysis for Panola storm 22 on 4/23/1988.

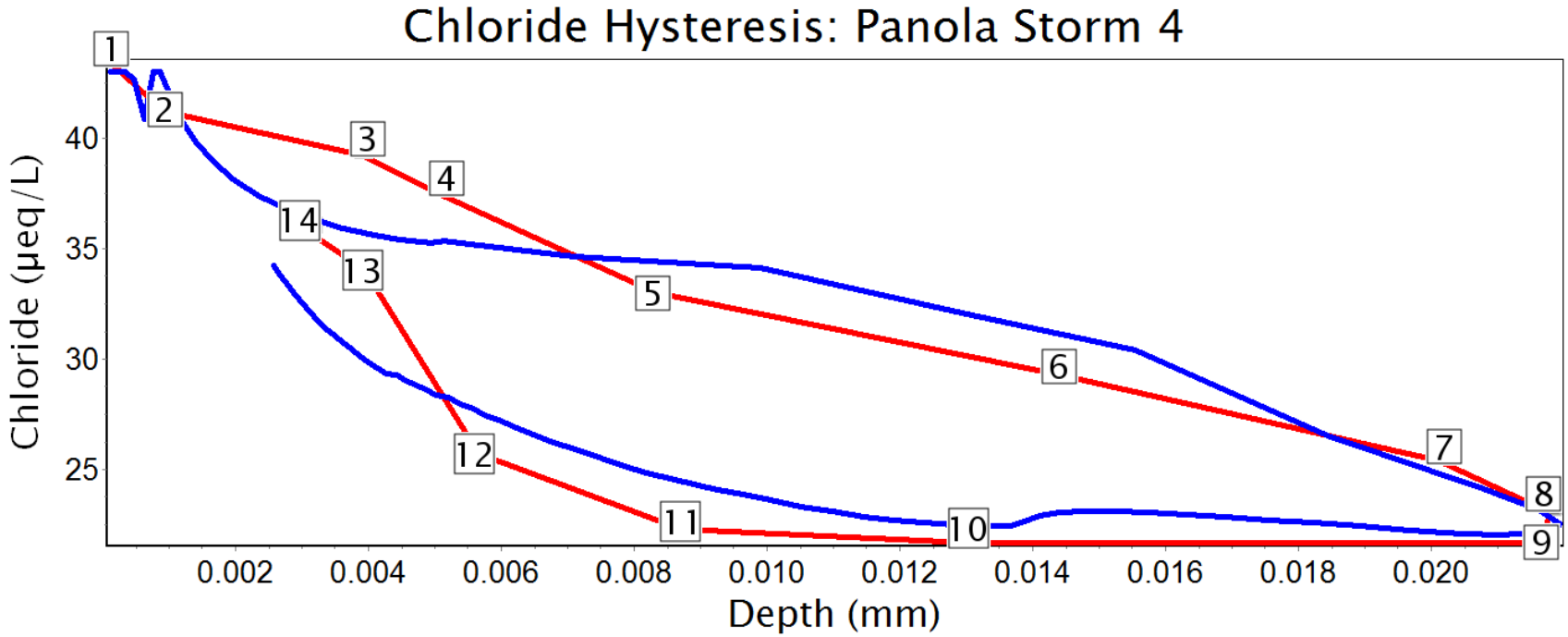

Figure 2.3:Observed and estimated hysteresis loops of chloride during Panola storm 4 on 7/24/86. The boxes on the estimated hysteresis loop (red) denote the direction (clockwise). The blue loop is the observed hysteresis.

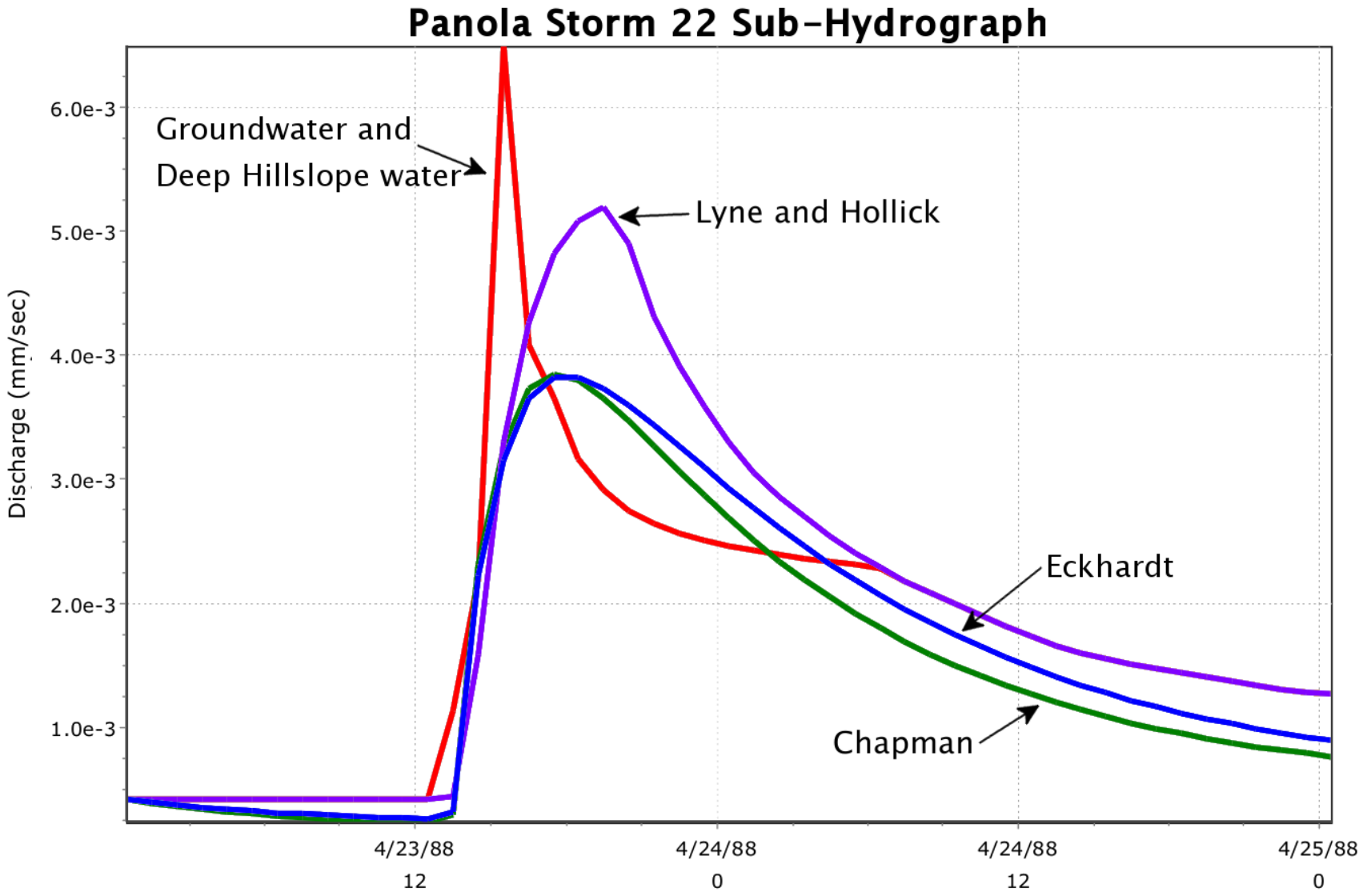

Figure 2.4: Digital filters fit to the groundwater and deep hillslope sub-hydrograph for Panola storm 22 which occurred on 4/23/88 and had counterclockwise hysteresis. The Lyne and Hollick α is 0.94, Chapman α is 0.92, the Eckhardt α is 0.94 and BFI_{Max} is 0.55.

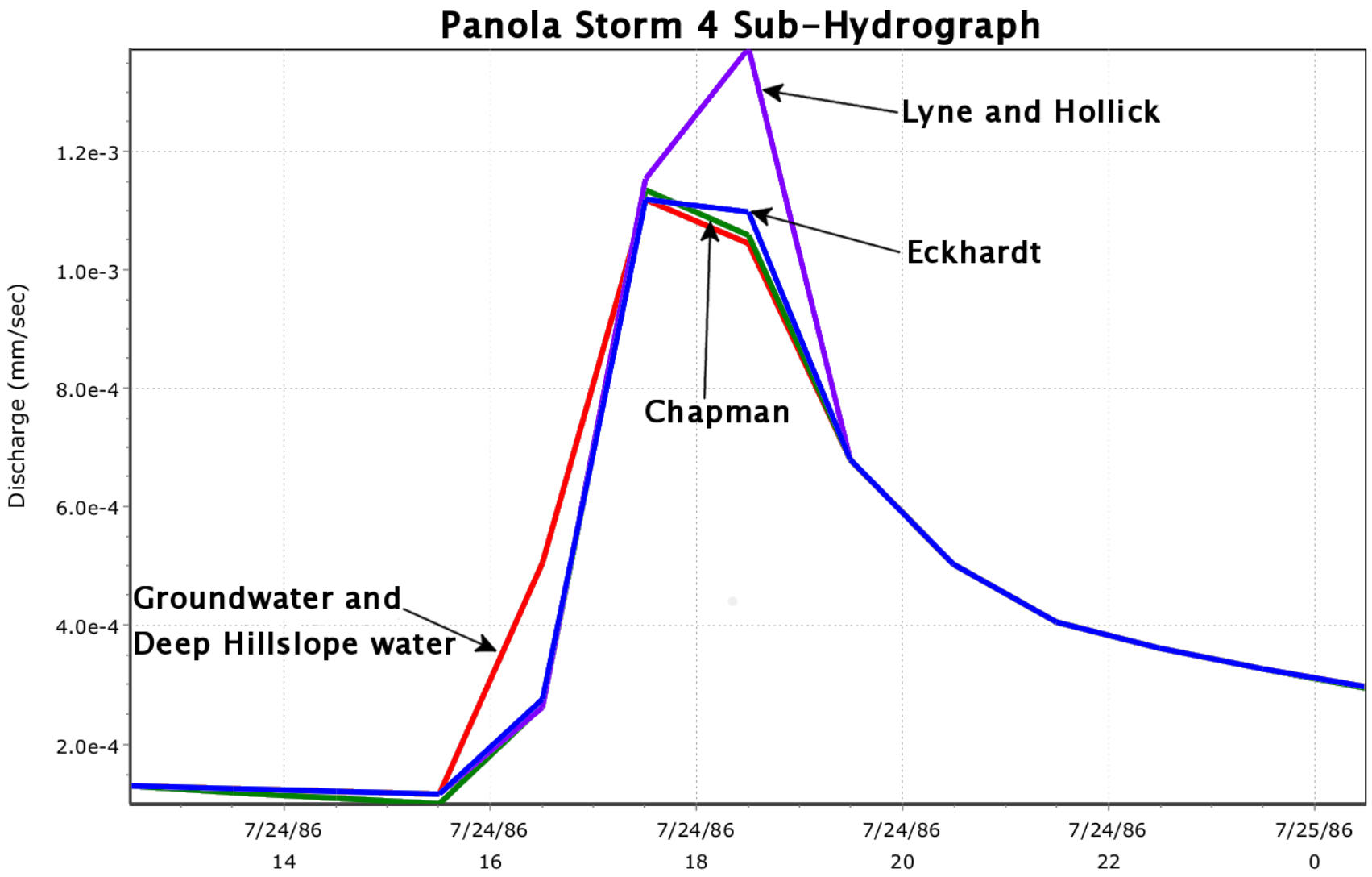

Figure 2. 5: Digital filters fit to the groundwater and deep hillslope sub-hydrograph of storm 4 which occurred on 7/24/86 and had clockwise hysteresis. The Lyne and Hollick α is 0.85, Chapman α is 0.91, the Eckhardt α is 0.96 and BFI_{Max} is 0.68.

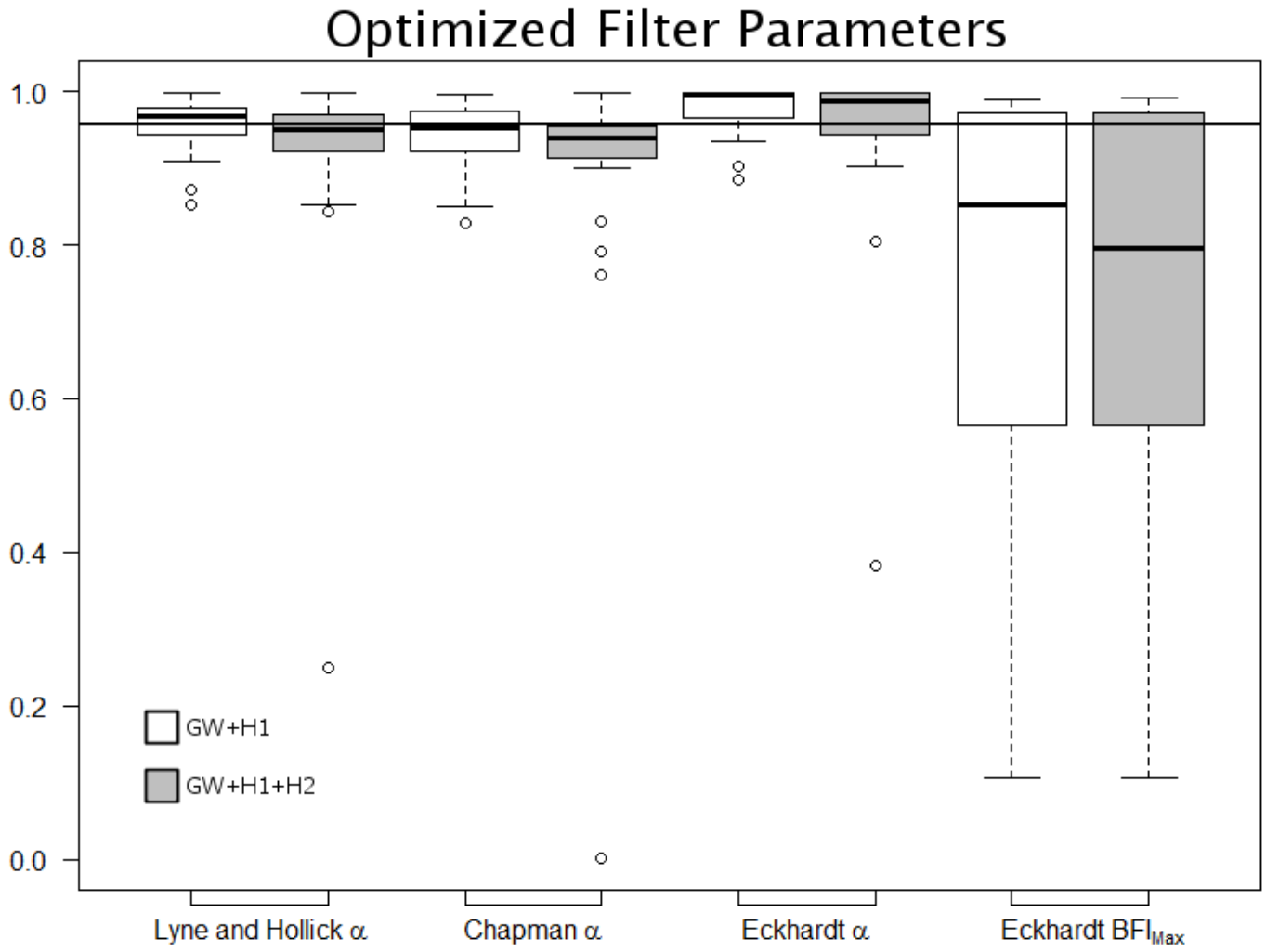

Figure 2.6: Optimized filter parameters. The line at 0.96 is the average measured recession constant.

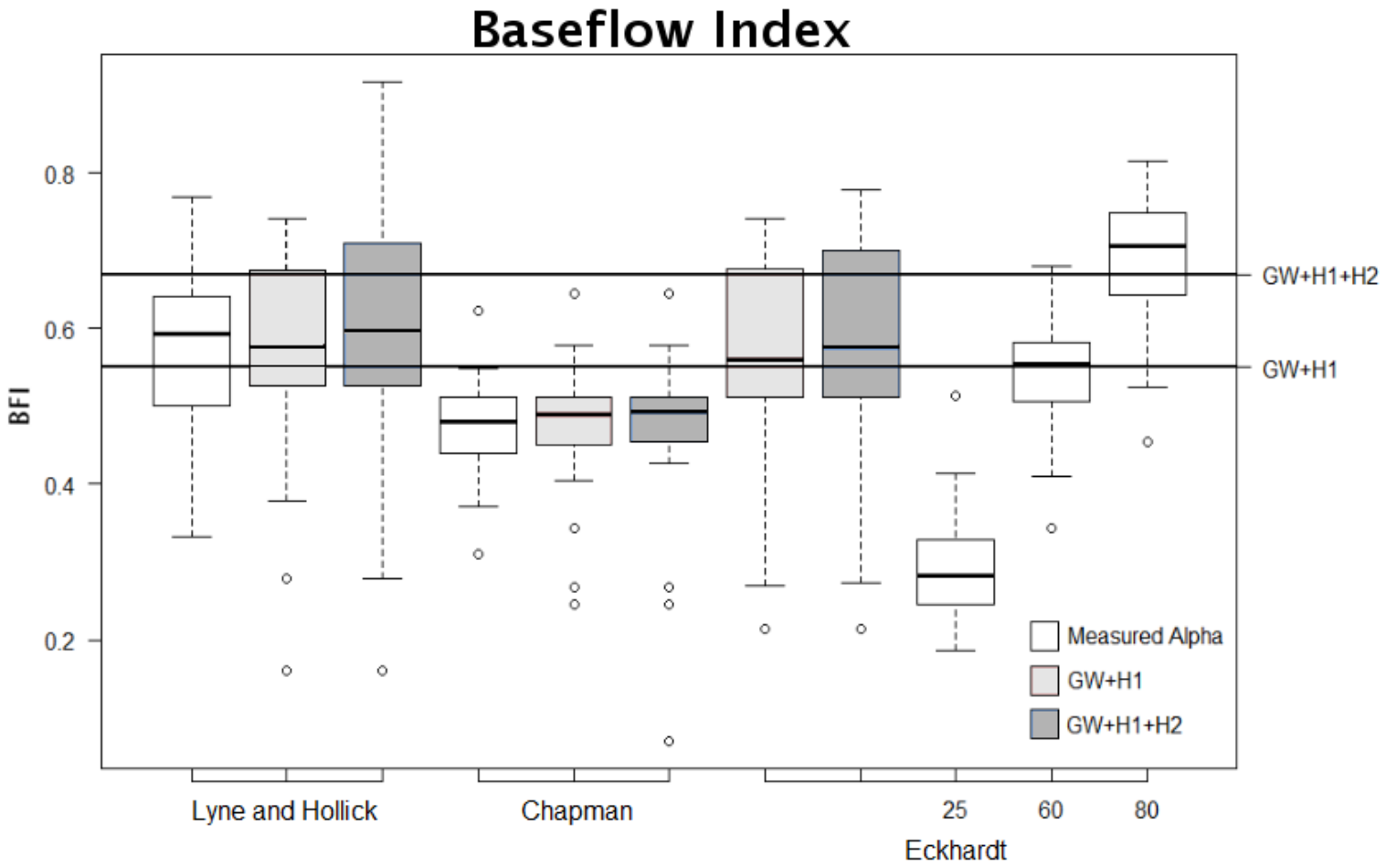

Figure 2.7: Boxplot of baseflow indexes for each digital filter for measured alphas and optimized parameters for each source water. BFI_{Max} values of 25, 60, and 80 are also shown. The line at 0.55 is the mean BFI of groundwater and deep hillslope water and the line at 0.67 is the mean BFI of groundwater, deep hillslope, and shallow hillslope water.

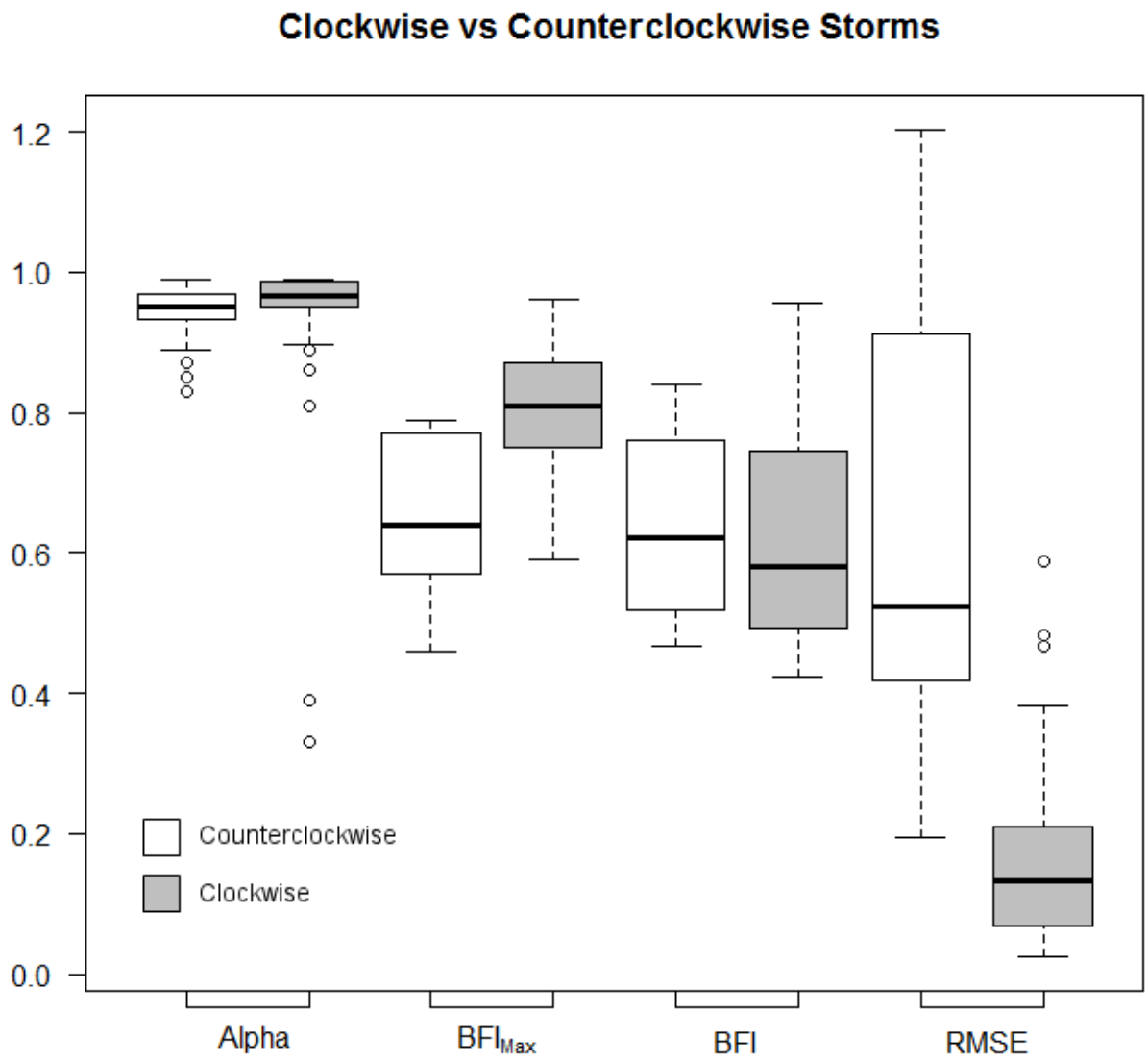

Figure 2.8: Boxplots of optimized parameters, BFI, and RMSE for clockwise and counterclockwise storms.

Literature Cited

Aksoy H, Kurt I, Eris E. 2009. Filtered smoothed minima baseflow separation method. *Journal of Hydrology* **372**(1-4): 94–101.

Cary R. 2011. Dynamic EMMA: Investigating watershed flow pathways using geochemistry and timing at Panola Mountain Research Watershed, Georgia. Thesis University of Georgia, Athens, Georgia.

Chapman T. 1991. Evaluation of automated techniques for base-flow and recession analyses – COMMENT. *Water Resour. Res.* **27**(7): 1783–1784.

Chapman T. 1999. A comparison of algorithms for stream flow recession and baseflow separation. *Hydrological Processes* **13**(5): 701–714.

Collischonn W, Fan FM. 2012. Defining parameters for Eckhardt's digital baseflow filter. *Hydrological Processes.*

Eckhardt K. 2005. How to construct recursive digital filters for baseflow separation. *Hydrological Processes* **19**(2): 507–515.

Eckhardt K. 2008. A comparison of baseflow indices, which were calculated with seven different baseflow separation methods. *Journal of Hydrology* **352**(1-2): 168–173.

Hewlett J, Hibbert A. 1963. Moisture and energy conditions within a sloping soil mass during drainage. *Journal of Geophysical Research* **68**(4).

Kaur G, Kaur R. 2011. Design of recursive digital filters using multiobjective genetic algorithm. *International Journal of Engineering Science & Technology* **3**(7): 5614.

Lanen HA, Tallaksen LM. 2004. Hydrological drought : Processes and estimation methods for streamflow and groundwater. *Developments in water science* **48**. Elsevier: Amsterdam; Boston.

Lyne V, Hollick M. 1979. Stochastic Time variable rainfall runoff modelling. Hydrology and Water Resources Symposium, Institute of Engineers Australia, Perth; 89-92.

Nathan RJ, McMahon TA. 1990. Evaluation of automated techniques for base flow and recession analyses. *Water Resources Research* **26**(7): 1465–1473.

Peters N, Freer J, Aulenbach B. 2003. Hydrologic dynamics of the Panola Mountain Research Watershed, Georgia, USA. *Ground Water* **41**(7): 973–988.

Rasmussen TC, Baldwin RH, Dowd JF, Williams AG. 2000. Tracer vs. pressure wave velocities through unsaturated saprolite. *Soil Science Society of America Journal* **64**(1): 75–85.

Restrepo-Posada PJ, Eagleson PS. 1982. Identification of independent rainstorms. *Journal of Hydrology* **55**(1-4): 303–319.

CHAPTER 3

EXTRACTION OF SELF-SIMILAR STREAM NETWORKS FROM LIDAR[2]

2 Mason-Deese WF, Dowd JF. To be submitted to *Open Journal of Modern Hydrology.*

Abstract

High resolution topography derived from LiDAR is used to extract dense surface runoff networks. Four extraction techniques, with different assumptions, produced networks with different structures. D_8 networks assume single flow directions, D_8PD networks assume single flow directions and that concave topography preferentially produces runoff, D_∞ networks assume multiple flow directions, and D_∞PD networks assume multiple flow directions and that concave topography preferentially produces runoff. The extracted networks describe the flow paths that surface runoff follows and the areas of the watershed that produce runoff.

Horton laws are calculated and used to assess the self-similar nature and fractal geometry of the networks. The networks were found to be self-similar in terms of bifurcation, stream lengths, and contributing area. D_8 networks were slightly more self-similar than D_∞ networks. Self-similarity also increased as the density of the network increased.

Introduction

When modeling storm runoff in a forested watershed it is often assumed that rainfall intensities never exceed the infiltration capacity of the soil. As precipitation infiltrates into the soil, areas become saturated bringing the flow of water to the surface in the form of saturation excess flow. The areas that become saturated, or variable source areas (VSA), are generally located adjacent to streams where the watertable is near the surface. These areas also extend into concave hollows and up the hillslope in the form of ephemeral and intermittent channels that form a drainage network (Hewlett and Hibbert 1967; Hewlett and Nutter 1970).

This network is valuable for several reasons: it estimates the flow paths that surface runoff is following; it can be used to estimate the areas that are producing runoff; and it can be used to predict storm runoff from a watershed. This paper describes methods of extracting a dense surface drainage network from high resolution topography derived from LiDAR. The network is used to estimate contributing areas of a watershed and the timing of the contributions.

Stream networks follow a branching structure and are considered to be fractal objects (Tarboton *et al.* 1988). Therefore, networks exhibit statistical self-similarity, or each part of the network is similar to the network as a whole (Cudennec *et al.* 2004, Fleurant *et al.* 2006). This means that the same properties can be used to to describe a network at all scales. Horton laws or Horton ratios (Horton 1945) have been found to remain constant at all scales for a given basin and are often used to quantify the self-similarity and scaling properties of a network.

Tarboton *et al.* (1988) found that Horton ratios can be used to calculate the fractal dimension of a watershed and that fractal dimensions approach two, which is consistent with the assumption that stream networks drain the entire surface of a watershed and are space filling. In this paper, Horton ratios are used to assess the fractal dimensions and the self-similar nature of the extracted stream networks.

LiDAR

The process of stream network extraction begins with the topography which is derived from LiDAR. Light Detection And Ranging (LiDAR) uses laser pulses to measure distances to points. To measure topography, a LiDAR system consisting of a system controller, transmitter, and receiver is mounted inside of an aircraft which follows designated flight lines above the area of interest. As the plane flies over, the transmitter emits laser pulses in the near-infrared range, around 1064 nm. A scanning mirror directs the laser pulses in a tract perpendicular to the flight line. The receiver receives the backscattered laser pulses which travel near the speed of light. The travel time of each pulse is used to calculate the distance of each point. A GPS in the aircraft and on the ground are used to locate the airplane and each point (ASPRS 2007).

LiDAR systems are capable of receiving multiple returns from a single laser pulse. As a laser pulse hits the ground it covers a near circular area called the instantaneous laser footprint. It is possible for multiple objects to be located within a laser footprint causing multiple returns for each laser pulse. If the footprint hits only one object it will have only one return, the “first and only” return. These data are processed post flight and used to help classify LiDAR points (ASPRS 2007).

Bare earth LiDAR points are necessary to produce a DEM. Bare earth points are separated using semi-automatic filters which must be checked manually. The filters typically look at first and only returns, and last returns. The elevation of each return is compared to the elevation of its nearest neighbors to classify points as bare earth. The results are analyzed manually to correct misclassified points (ASPRS 2007).

Two LiDAR data sets are used to extract stream networks on two watersheds: Panola Mountain Research Watershed (Panola) and Coweeta Watershed 18 (Coweeta).

Georgia Department of Natural Resources:

LiDAR for Panola was flown as a collaborative project by the National Oceanic and Atmospheric Administration (NOAA) and the Environmental Protection Division (EPD) of Georgia Department of Natural Resources (GADNR) as part of a project that covered Pickens, Rockdale, and Troup Counties. The project was flown in March 2012 during leaf-off conditions. The point density was required to be at least one point per square meter to accommodate one meter horizontal accuracy. The vertical accuracy is given as 3.8 cm. Bare earth points are classified as Class 2 and water bodies as Class 9. The raw LiDAR point files, in *laz* format, were downloaded from NOAA's digital coast website[3]. The bare earth points were used to interpolate a one meter DEM for Panola which is seen in Figure 3.1.

National Center for Airborne Laser Mapping:

The National Center for Airborne Laser Mapping (NCALM), as part of the Seed Money Survey Campaign, funded LiDAR to be flown for Coweeta Hydrologic Lab for the project *LiDAR estimation of Forest Leaf Structure, Terrain and Hydrophysiology*, by Katherine

3 http://www.csc.noaa.gov/dataviewer/#

Windfeldt of the University of Minnesota-Twin cities. The LiDAR data are available at Open Topography[4]. Vertical accuracy for the data set is between five and 30 cm and the horizontal accuracy is around one meter (Windfeldt 2009). A one meter DEM was interpolated from the bare earth LiDAR points and is seen in Figure 3.2.

The project was flown on August 26th, 2009, out of Macon County airport in Franklin, North Carolina. The survey area consists of a 6.25 km by 6.7 km rectangle around Coweeta Hydrologic Laboratory which was covered by 36 flight lines in the North-South direction. The project was flown at an altitude of 600 m with a total flying distance of 222 km and covering an area of 43 km^2. All points in overlapping areas were utilized and 69% of the area flown was covered by overlapping flight lines (Windfeldt 2009).

The LiDAR was collected with an Optech GEMINI Airborne Laser Terrain Mapper operating at a pulse rate frequency of 100 kHz and at a wavelength of 1047 nm. The scanning mirror operated at a frequency of 45 Hz with a scan angle of 21° of which the outside 3° were removed (Windfeldt 2009).

Network Extraction

Stream network extraction is completed using ArcGIS® software by Esri and the program Terrain Analysis Using Digital Elevation Models (TauDEM) by David Tarboton of Utah State University. The complete workflow for extracting stream networks in TauDEM and ArcMAP is found in Appendix A.

Network extraction begins with the digital elevation model (DEM) obtained from LiDAR. Small artificial pits are often introduced into the terrain when the DEM is

4 www.opentopography.org

interpolated which causes water not to drain off the surface of the DEM. The pits are filled so that the lowest edge will drain into the adjacent cell. This procedure smooths over small errors in the DEM and produces a hydrologically conditioned DEM in which all cells will drain by overland flow to the basin outlet (Tarboton and Ames 2001). This method removes any existing closed depressions in the topography and does not account for surface storage. If a lake or a river were present, breaklines would need to be inserted into the DEM to separate water bodies from the land surface.

The conditioned DEM is used to calculate flow directions for each cell using two methods, the D_8 and D_∞ methods. The D_8 method assigns flow from each cell to one of the eight neighboring cells based on the direction of steepest downward slope. This method is subject to bias from the gridded structure of the DEM. To avoid bias the D_∞ method can be used which assigns multiple flow directions. This method uses a triangular facet around each cell to find the angle of steepest downward slope. If the angle falls between neighboring cells the flow is proportioned between the two cells based on the angle. This method alleviates some of the bias introduced by a gridded DEM. It also allows for divergent flow and is better suited for braided stream structures (Tarboton and Ames 2001).

The calculated flow directions are used to generate a flow accumulation map. The algorithm assumes that each cell yields one unit of runoff that is routed through the watershed based on the flow directions. The number of cells flowing through each cell are counted generating a map of the number of upstream cells draining through each cell. On a one meter DEM, this map is analogous to the upstream area draining to each cell (Tarboton and Ames 2001).

Concave hollows and sections of concave hillslope have been shown to concentrate flow paths and are likely locations for runoff to occur (Zaslavsky and Rogowski 1969, Sidle *et al.* 2000). Using the DEM sections of concave slope are flagged and weighted for runoff production. An algorithm introduced by Peucker and Douglas (1975) examines each quadrant of four adjacent cells and flags the highest cell of each quadrant. The remaining unflagged cells are considered upwardly curved or concave. The distribution of concave cells generally resemble a stream network, although, it lacks connectivity and requires thinning (Band 1986). A flow accumulation map is generated by weighting the concave cells for runoff production.

Flow accumulation maps are used to extract stream networks by setting a threshold upstream area at which overland flow occurs. All cells with an upstream area above the designated threshold are considered part of the stream network. Lowering the threshold extends the network up into the hillslope and increases the density of the network.

Stream networks produced from D_∞ flow directions lack connectivity because multiple flow directions allow for divergent flow. Some cells on the flow accumulation map will exceed the threshold for overland flow and be considered part of the stream network. If an area of low slope is encountered downstream, the flow paths will diverge and the cells will not meet the threshold for overland flow resulting in an unconnected stream link. The unconnected links are deleted by converting the stream network to a geometric network and testing for connectivity.

The cells above the designated threshold for overland flow are converted to a polyline shapefile representing the stream network. TauDEM (2012) automatically

calculates several attributes for each link in the network including: Strahler order, length, slope, and upstream area.

Contributing Area

Estimating contributing area is an important aspect of hydrologic research. Contributing areas become saturated and produce runoff, therefore, solutes from these areas will enter a stream. These areas also spatially identify the source of runoff and can be used to estimate the timing of runoff from different parts of the watershed. Contributing areas and the timing of their contributions are also used to model storm hydrographs. Contributing area is identified by using stream networks and the slope of the surrounding topography.

The extracted stream network is a polyline shapefile that represents the shape and structure of the stream network; however, it does not represent the VSA or area around the stream that is likely to become saturated and produce runoff. To estimate the VSA the viewshed function in Esri's ArcGIS® is used to look upslope from the network to identify low lying areas around the stream that will likely become saturated. The function looks out a certain radius from the stream network and identifies the cells that are within a certain elevation of the network. These low lying areas adjacent to the network are assumed to become saturated and produce runoff.

The extent of these areas depends on the density of the stream network used to estimate the area; as the network grows so will the contributing areas. The extent of the areas also vary by changing extent of the area around the network that is examined. The extent can be changed by changing the radius around the network and the height above the network. As the radius and height increase the contributing areas will increase up the

hillslope and grow farther away from stream networks. This method estimates the area of stream channels and low lying areas adjacent to channels.

To estimate the timing of runoff contributions Manning's equation is applied to the network. Mannings equation is given as (Manning 1891):

$$V = \frac{1}{n} R_h^{2/3} S^{1/2} \qquad \textit{Equation 1}$$

where n is Manning's roughness coefficient and was estimated for each Strahler order of the network. R_h is the wetted radius of the channel and was estimated for each stream link by Strahler order and upstream contributing area. S is the slope of the channel and was calculated from the DEM for each stream length. V is the average velocity and is solved for each link of the network. The travel time for each link is calculated and summed to the basin outlet. Travel times to the basin outlet are then known for each stream link. Travel times are interpolated across the watershed to produce an isochrone map of travel times to the basin outlet. The complete process of applying Manning's equation and interpolating an isochrone map is given in Appendix B.

Isochrone maps are used to calculate transfer functions for basins. The frequency of travel times, obtained from the isochrone map, is equivalent to the transfer function. The transfer function describes how much area contributes runoff over time given a pulse of runoff applied to the entire watershed. This distribution is important because it can be used to predict storm hydrographs (Clark 1945).

Self-Similarity

Horton's Laws (Horton 1945) can be used to assess the self-similar nature and fractal geometry of a stream network (Tarboton *et al.* 1988). Several of Horton's laws

including bifurcation ratios, length ratios, and area ratios are calculated for each network. Horton's laws are calculated by first classifying the stream network by Strahler order (Strahler 1957). The most upstream links of a network are first order streams. If two streams of equal order intersect the resulting stream is of the next highest order. If a high and low order stream intersect the resulting stream retains the highest order.

Horton ratios are calculated by:

$$R_B = \frac{N_{i-1}}{N_i}, \qquad R_L = \frac{L_i}{L_{i-1}}, \qquad R_A = \frac{A_i}{A_{i-1}} \qquad \textit{Equation 2}$$

where R_B is the bifurcation ratio; N is the number of streams in the i^{th} order; R_L is the length ratio; L is the mean length of streams in the i^{th} order; R_A is the area ratio; A is the mean contributing area for the i^{th} order. Ratios for the entire basin are obtained from the slopes of the straight lines formed by plotting log R_B, log R_L, and log R_A against Strahler order. How well the plots of Horton ratios conform to a straight line determines how self-similar a network is. R^2 values and p-values from f-tests of the linear regressions are analyzed to assess the self-similarity of the networks.

Tarboton *et al.* (1988) shows that Horton ratios can be used to estimate fractal dimensions of the basin. The fractal dimension for the main stream length which relates channel length to basin area and describes the sinuosity of the network is calculated by:

$$D_S = \frac{2\log(R_L)}{\log(R_A)} \qquad \textit{Equation 3}$$

The branching of the network is described by the fractal dimension D_B, which is calculated from the bifurcation and length ratios:

$$D_B = \frac{\log(R_B)}{\log(R_L)} \qquad \textit{Equation 4}$$

Bifurcation and area ratios are used to calculate the area dimension which describes how sub-basins fill the watershed:

$$D_A = \frac{2\log(R_B)}{\log(R_A)} \qquad \textit{Equation 5}$$

D_A is also equal to the product of D_S and D_B: $D_A = D_S \times D_B$.

The area dimension describes how the sinuosity and the branching of the network fill the area of the watershed. For a network that is space filling the dimension approaches two (Tarboton 1988).

Results and Discussion

The process starts with a one meter DEM that has been interpolated from bare earth points obtained with LiDAR. The DEM of Panola is seen in Figure 3.1 and the DEM of Coweeta is seen in Figure 3.2.

Stream networks were extracted using four variations of the procedures described above. D_8 networks were made with D_8 flow directions; D_8 PD networks were made with D_8 flow directions and Peucker Douglas (1975) weights of concave cells; D_∞ networks were made using D_∞ flow directions; and D_∞PD networks were made with D_∞ flow directions and Peucker Douglas (1975) weights of concave cells. Dense drainage networks from each extraction method are shown for Panola in Figure 3.3 and for Coweeta in Figure 3.4. The networks and the surrounding topography were used to estimate the contributing areas of the watersheds. Figures 3.5 and 3.6 show the contributing areas that were estimated from networks of different densities. As the density of the network increases the contributing area also increases.

Figures 3.3 and 3.4 show that the different extraction techniques generate noticeably different networks. The D_8 networks are characterized by long first order streams that cover the watershed in a relatively uniform manner. The D_8 PD networks are also characterized by long first order streams, although, the networks do not cover the watershed as uniformly as the D_8 networks because only concave cells are weighted for runoff production.

The D_∞ networks are characterized by shorter but more numerous stream segments and a higher degree of branching. The disconnected stream links of the D_∞ networks have been removed which serves to thin the network. The networks are more concentrated with stream segments clustered together in what resembles braided streams. Concentration of stream segments leave larger areas of the watershed unconnected by streams. As a result, the unconnected areas do not contribute runoff.

Several networks were extracted at different thresholds. Table 3.1 reports a summary of the extracted networks at Panola and Table 3.2 at Coweeta. The type of network, extraction threshold, contributing area, Strahler order, and drainage density are reported for each network. Horton ratios, R^2 values, p-values, and fractal dimensions are also reported for each network. Boxplots of Horton ratios and the area dimension are shown in Figures 3.7 and 3.8.

Horton ratios are calculated from a linear regression through values from each Strahler order. The strength and significance of the regressions are assessed with R^2 values and with p-values from f-tests. P-values less than 0.05 imply that the regression explains 95% of the variation in the data. P-values are reported for each network in Tables 3.1 and 3.2.

T-tests are used to calculate p-values and compare the mean Horton ratios of the different network extraction techniques. P-values less than 0.05 indicate that, at 95% confidence, the means are different. Tables 3.3 and 3.4 report p-values comparing different networks at Panola and Coweeta

In terms of bifurcation, all of the Panola networks are considered self-similar because all the networks have p-values less than 0.05 indicating that the regression explains at least 95% of the variation. All of the Coweeta networks are also self-similar in terms of bifurcation except for the $D_\infty PD$ network at an extraction threshold of 10 which has a p-value of 0.1 and a R^2 value 0.41. D_∞ and $D_\infty PD$ networks produced slightly higher bifurcation ratios at Panola, however at both Panola and Coweeta, there is no statistically significant difference between the means of the different techniques. Higher bifurcation ratios mean that higher order streams have more stream links.

The Panola networks are not as self-similar in regards to stream lengths, although D_8 networks are more self-similar than D_∞ networks. The Panola D_8 network with a threshold of 1000 is not self-similar. The D_∞ network extracted at a threshold of 25 and the $D_\infty PD$ network extracted at a threshold of one are the only two networks, using multiple flow directions at Panola, that are self-similar. Therefore, using single flow directions is more likely than using multiple flow directions to produce networks that are self-similar in terms of stream lengths. The single flow direction networks also have significantly higher length ratios than the multiple flow direction networks. This implies that the stream lengths of D_8 and D_8PD networks change more across Strahler orders while D_∞ and $D_\infty PD$ stream lengths change relatively little across Strahler orders.

The networks at Coweeta are more self-similar in terms of stream lengths. The only networks that are not self-similar are the D_8PD and D_∞PD networks extracted at a threshold of 10. D_8 networks at Coweeta have significantly higher length ratios than D_∞PD networks. This implies that the stream lengths of D_8 networks change more across Strahler orders than D_∞PD stream lengths.

All of the networks at Panola are self-similar in terms of upstream areas and all of the networks at Coweeta are self-similar in terms of upstream areas except for the D_∞PD network extracted at a threshold of 10. This implies that all of the extraction techniques produce streams that are self-similar in terms of upstream area. For both Panola and Coweeta, single flow direction networks have significantly higher area ratios than multiple flow direction networks. This implies that the area drained by each Strahler order changes more across Strahler orders for single flow direction networks while the area drained by each Strahler order changes significantly less for multiple flow direction networks. This is possibly because the multiple flow direction networks have been thinned and leave larger areas of the watershed unconnected. Therefore first order streams of multiple flow directions networks would drain a larger area than first order streams of single flow direction networks that extend further into the hillslope and cover the watershed more uniformly.

Self-similarity increases with the density of the network. The networks found to be non-similar were usually the least dense networks. For stream lengths at Panola, the only multiple flow direction networks that were self-similar were the most dense networks. This implies that dense networks promote self-similarity. Cudennec *et al.* (2004) noticed

that the highest order stream segment is not self-similar because there are usually only a few stream segments in the highest order and it only drains to one outlet. In a denser network the highest stream order has less weight in a regression because there are more points and therefore might provide a better fit.

Figures 3.7 and 3.8 also show results of the area dimension for Panola and Coweeta. The area dimension describes how the branching and sinuosity of a network fill the area of a watershed. The area dimension is also the product of the channel length dimension and the branching dimension. A space filling network that drains the entire area of a watershed has an area dimension that approaches two. Fractal dimensions for Panola are reported in Table 3.1 and Coweeta in Table 3.2.

Area dimensions of single flow direction networks at Panola average around one, this indicates that the networks are not space filling. The D_∞ networks average around 1.5 which is closer to space filling. The dimensions of the main channel lengths for Panola networks are relatively low for all networks. The branching dimensions are significantly higher, averaging just below three for D_8 networks and 13.5 for D_∞ networks. This implies that branching accounts for most of the space filling of the networks, especially for D_∞ networks.

Coweeta networks follow the same general patterns. D_∞ networks have a significantly larger area dimension than D_8 networks. This implies that D_∞ networks are closer to space filling. The dimension of the main channel length is low for all networks while the branching dimension is higher. Higher branching dimensions imply that the space filling of the network is mainly governed by the branching patterns of the network.

None of the networks have an area dimension of two, therefore, none of the networks are space filling. Tarboton (1996) shows that when using Horton ratios to calculate fractal dimensions the area dimension can never equal two. The assumption of space filling implies that the entire watershed produces runoff and is drained by the network, although, if some areas of the watershed never produce runoff the assumption of space filling does not apply and the area dimension would be expected to be less than two. Networks created using the Peucker Douglas (1975) algorithm assume that concave areas are the only areas that produce runoff and therefore, do not comply with the assumption of space filling. However, the flow directions, not the Peucker Douglas weighting, are determining the differences in area dimensions.

D_8 networks appear to be the most space filling because they have uniform branching which covers most of the watershed. The D_∞ and Peucker Douglas networks result in larger areas of the watershed that are not connected which implies that the area dimension would be lower. However, this does not agree with the calculated area dimensions.

Manning's (1891) equation was applied to each type of network and used to calculate travel times to the basin outlet. Network travel times were interpolated across the watershed to produce an isochrone map of travel times to the basin outlet. Isochrone maps of Panola are seen in Figure 3.9 and maps of Coweeta are seen in Figure 3.11. The distribution of the frequency of travel times obtained from the isochrone maps provide the basin's transfer function which describes, over time, how much area contributes runoff given a pulse of runoff applied to the entire watershed. Transfer functions for each of the

four network extraction techniques are seen for Panola in Figure 3.10 and for Coweeta in Figure 3.12.

Conclusion

Stream networks were extracted from LiDAR derived DEMs of Panola Mountain Research Watershed and Coweeta Watershed 18. The DEMs were first hydrologically conditioned enabling them to be used to calculate flow direction maps. The flow direction maps were used to route water across the watershed; the number of upstream cells flowing through each cell was used to produce a flow accumulation maps. Streams were extracted from flow accumulation maps by setting a threshold at which overland flow occurs.

Four different methods: D_8, D_8PD, D_∞, and D_∞PD were used to extract networks. Different thresholds were used to extract networks of different densities. The networks were examined and compared by calculating Horton ratios which were used to assess the self-similar nature and fractal geometry of the networks.

The extracted networks were also used to calculate travel times and to produce isochrone maps of travel times to the basin outlet. The distribution of the frequency of travel times depicts how much area will contribute overtime from a pulse of runoff and is equivalent to the basin transfer function. Transfer functions determine how a basin responds to runoff and can ultimately be used to model storm runoff based on flow paths identified from the topography, however, these methods assume that the networks are self-similar (Cudennec *et al.* 2004).

Networks on both Panola and Coweeta exhibit self-similarity in terms of bifurcation. Panola networks made from multiple flow directions (D_∞ and D_∞PD) were not similar in

terms of stream lengths. This appears to be because these networks have a high degree of branching and the stream lengths remain about the same length across all Strahler orders. Networks at Coweeta were self-similar in terms of stream lengths, although, the least dense networks tended not to be self-similar. All of the dense networks at both Panola and Coweeta were self-similar in terms of upstream area. The results show that these methods can be used to extract self-similar drainage networks.

In general denser networks exhibit a higher degree of self-similarity. This is because denser networks have more stream orders and a hierarchical effect where the highest stream orders are not as self-similar. The highest stream order results in one outlet draining the entire basin, and therefore, is not similar to the rest of the network (Cudennec *et al.* 2004). As the number of orders grow the lack of self-similarity of the highest orders becomes less important.

Calculation of fractal dimensions provide a way of comparing the structure and fractal natures of the networks. The area dimension describes how a network fills the watershed and approaches two if the network fills the space of the watershed. D_∞ networks were closer to space filling with D_8 networks producing an area dimension of one. This is the opposite as expected because the D_8 networks appear to fill more of the watershed while D_∞ networks leave large areas unconnected. Tarboton (1996) suggests that Horton ratios will never produce a space filling network and suggests Tokunaga cyclicity as a method for calculating fractal dimensions which might provide more meaningful results.

Overall the D_8 networks produce the most self-similar networks, although, the D_8 networks are not the most conceptually appealing because they do not allow for weights of concave cells and do not allow for multiple flow directions. It is difficult to ascertain which

extracted networks are closest to the actual active networks. Detailed field observations during a storm are needed to try to ascertain the active flow paths during a storm. Nevertheless, comparison of extracted networks to the self-similar nature in which stream networks are expected to behave is useful in comparing the different techniques of stream extraction.

Further research could include examination of different methods of defining streams. Instead of using a constant threshold at which overland flow occurs a dynamic threshold could be used based on slope, soils, wetness index, or other factors. The DEMs used for this study were produced with the natural neighbors technique to interpolate a one meter DEM. Different methods of interpolating DEMs, such as tinning, as well as, different resolution DEMs should be examined to determine the effects on network extraction.

Table 3.1: Summary of Panola networks. Network refers to the different extraction assumptions. Threshold is the upstream area at which overland flow occurs. Area is the % of the watershed area that contributes runoff. Order is the basin Strahler order. Density is the length of streams divided by the watershed area. Bifurcation, length ratio, and area ratio are how the number of streams, the length of streams, and the upstream area change by Strahler order and are obtained by regression. R^2 values give the strength of the regression and p-values less than 0.05 imply significance at 95% confidence. D_S is sinuosity, D_B is branching, and D_A is the fractal dimension.

Network	Threshold	Area %	Order	Density m^{-1}	Bifurcation	R^2(B)	P-value (B)	Length Ratio	R^2 (L)	P-value (L)	Area Ratio	R^2(A)	P-value (A)	D_s	D_B	D_A
D_8	50	76	6	0.170	1.83	0.98	0.001	1.34	0.89	< 0.001	4.53	1.00	< 0.001	0.39	2.08	0.80
D_8	100	78	6	0.115	1.99	0.91	< 0.001	1.38	0.98	0.005	4.41	1.00	< 0.001	0.44	2.12	0.93
D_8	250	36	5	0.065	1.83	0.97	0.003	1.30	0.86	< 0.001	4.51	1.00	< 0.001	0.34	2.33	0.80
D_8	500	22	5	0.040	2.36	0.91	0.002	1.18	0.76	0.023	4.39	0.99	< 0.001	0.23	5.06	1.16
D_8	1000	12	5	0.025	2.86	0.79	0.013	1.31	0.88	0.053	3.77	0.99	< 0.001	0.41	3.86	1.59
D_8PD	1	84	7	0.239	1.75	0.99	< 0.001	1.27	0.82	0.005	4.45	1.00	< 0.001	0.32	2.33	0.75
D_8PD	5	61	6	0.116	1.81	0.99	< 0.001	1.26	0.93	0.002	4.23	1.00	< 0.001	0.32	2.55	0.83
D_8PD	10	46	6	0.082	2.77	0.84	0.010	1.28	0.97	< 0.001	4.35	0.99	< 0.001	0.34	4.13	1.39
D_8PD	20	32	5	0.056	1.89	0.99	0.001	1.23	0.95	0.005	4.25	1.00	< 0.001	0.29	3.02	0.88
D_8PD	45	19	5	0.036	2.16	0.95	0.005	1.29	0.97	0.003	3.96	0.99	< 0.001	0.37	3.02	1.12
D_∞	25	75	8	0.323	2.14	0.94	< 0.001	1.11	0.71	0.009	3.17	0.96	< 0.001	0.18	7.25	1.32
D_∞	50	51	7	0.172	2.26	0.91	0.001	1.05	0.34	0.170	3.40	0.94	< 0.001	0.08	16.15	1.33
D_∞	100	31	7	0.088	2.79	0.83	0.004	1.04	0.22	0.288	3.31	0.96	< 0.001	0.06	28.73	1.71
D_∞	250	16	6	0.041	2.45	0.87	0.007	1.17	0.65	0.052	3.18	0.96	0.001	0.26	5.87	1.55
D_∞	500	10	5	0.026	2.02	0.98	0.001	1.16	0.59	0.127	2.91	0.96	0.003	0.27	4.83	1.32
$D_\infty PD$	1	69	8	0.285	2.43	0.83	0.002	1.13	0.85	0.001	3.32	0.96	< 0.001	0.20	7.28	1.48
$D_\infty PD$	5	34	7	0.095	2.17	0.93	< 0.001	1.02	0.17	0.358	3.00	0.95	< 0.001	0.04	39.81	1.40
$D_\infty PD$	10	22	6	0.058	2.42	0.90	0.004	1.09	0.63	0.059	3.38	0.94	< 0.001	0.14	10.09	1.45
$D_\infty PD$	20	15	6	0.038	3.10	0.80	0.016	1.11	0.56	0.087	3.19	0.96	< 0.001	0.19	10.44	1.95
$D_\infty PD$	45	9	5	0.024	2.08	0.89	0.015	1.16	0.76	0.053	2.81	0.96	< 0.001	0.28	5.00	1.41

Table 3.2: Summary of Coweeta networks. Network refers to the different extraction assumptions. Threshold is the upstream area at which overland flow occurs. Area is the % of the watershed area that contributes runoff. Order is the basin Strahler order. Density is the length of streams divided by the watershed area. Bifurcation, length ratio, and area ratio are how the number of streams, the length of streams, and the upstream area change by Strahler order and are obtained by regression. R^2 values give the strength of the regression and p-values less than 0.05 imply significance at 95% confidence. D_S is sinuosity, D_B is branching, and D_A is the fractal dimension.

Network	Threshold	Area %	Order	Density m^{-1}	Bifurcation	R^2(B)	P-value (B)	Length Ratio	R^2 (L)	P-value (L)	Area Ratio	R^2(A)	P-value (A)	D_s	D_B	D_A
D_8	10	86	7	0.177	1.67	0.88	0.002	1.42	0.98	< 0.001	3.87	0.97	< 0.001	0.52	1.46	0.76
D_8	20	70	7	0.113	2.10	0.77	0.010	1.38	0.97	< 0.001	3.89	1.00	< 0.001	0.47	2.32	1.09
D_8	40	50	6	0.066	1.57	0.84	0.010	1.41	0.99	< 0.001	3.99	0.99	< 0.001	0.49	1.32	0.65
D_8	80	35	6	0.037	2.25	0.71	0.036	1.28	0.93	0.002	3.85	1.00	< 0.001	0.37	3.23	1.20
D_8	155	16	5	0.021	1.60	0.93	0.007	1.22	0.90	0.013	3.95	0.99	< 0.001	0.29	2.36	0.69
D_8PD	1	64	6	0.064	1.51	0.78	0.019	1.45	0.97	< 0.001	4.18	1.00	< 0.001	0.52	1.10	0.57
D_8PD	2	54	6	0.046	2.36	0.71	0.035	1.26	0.83	0.011	4.21	0.99	< 0.001	0.32	3.75	1.20
D_8PD	3	45	6	0.035	2.25	0.73	0.030	1.25	0.90	0.004	3.85	1.00	< 0.001	0.33	3.69	1.20
D_8PD	5	34	6	0.023	2.13	0.81	0.014	1.20	0.71	0.035	3.50	1.00	< 0.001	0.29	4.19	1.20
D_8PD	10	22	5	0.012	2.41	0.78	0.048	1.17	0.44	0.224	4.04	0.99	< 0.001	0.22	5.75	1.26
D_∞	10	93	8	0.237	2.10	0.85	0.001	1.31	0.97	< 0.001	2.46	0.92	< 0.001	0.60	2.76	1.65
D_∞	20	68	7	0.138	2.25	0.80	0.006	1.31	0.97	< 0.001	2.58	0.83	0.004	0.56	3.03	1.71
D_∞	40	41	7	0.066	2.12	0.77	0.009	1.20	0.93	< 0.001	2.29	0.84	0.004	0.45	4.03	1.81
D_∞	80	24	6	0.033	1.53	0.84	0.011	1.17	0.87	0.007	2.02	0.81	0.014	0.44	2.76	1.21
D_∞	155	16	6	0.019	2.08	0.69	0.042	1.13	0.77	0.022	2.17	0.78	0.020	0.31	6.07	1.90
$D_\infty PD$	1	35	7	0.051	1.91	0.75	0.012	1.26	0.96	< 0.001	2.23	0.83	0.004	0.58	2.78	1.62
$D_\infty PD$	2	24	6	0.031	1.59	0.87	0.007	1.13	0.81	0.015	2.08	0.85	0.009	0.34	3.78	1.27
$D_\infty PD$	3	20	6	0.024	2.16	0.71	0.035	1.14	0.90	0.004	2.32	0.82	0.013	0.31	5.84	1.83
$D_\infty PD$	5	15	6	0.017	2.02	0.70	0.038	1.14	0.78	0.020	2.13	0.78	0.020	0.36	5.23	1.87
$D_\infty PD$	10	11	5	0.011	1.41	0.63	0.109	1.06	0.42	0.239	1.90	0.73	0.066	0.17	6.11	1.06

Table 3.3: Panola p-values from pairwise t-tests comparing the mean bifurcation, length, and area ratios for each type of network. Mean fractal dimensions are also compared.

Panola P-Values

Bifurcation	D_8	D_8PD	D_∞
D_8PD	1.000	-	-
D_∞	1.000	1.000	-
$D_\infty PD$	1.000	0.980	1.000

Length	D_8	D_8PD	D_∞
D_8PD	1.000	-	-
D_∞	< 0.001	0.002	-
$D_\infty PD$	< 0.001	0.002	1.000

Area	D_8	D_8PD	D_∞
D_8PD	1.000	-	-
D_∞	< 0.001	< 0.001	-
$D_\infty PD$	< 0.001	< 0.001	1.000

Fractal Dimension	D_8	D_8PD	D_∞
D_8PD	1.000	-	-
D_∞	0.174	0.080	-
$D_\infty PD$	0.055	0.025	1.000

Table 3.4: Coweeta p-values from pairwise t-tests comparing the mean bifurcation, length, and area ratios for each type of network. Mean fractal dimensions are also compared.

Coweeta P-Values

Bifurcation	D_8	D_8PD	D_∞
D_8PD	1.000	-	-
D_∞	1.000	1.000	-
$D_\infty PD$	1.000	1.000	1.000

Length	D_8	D_8PD	D_∞
D_8PD	1.000	-	-
D_∞	0.425	1.000	-
$D_\infty PD$	0.024	0.261	1.000

Area	D_8	D_8PD	D_∞
D_8PD	1.000	-	-
D_∞	< 0.001	< 0.001	-
$D_\infty PD$	< 0.001	< 0.001	1.000

Fractal Dimension	D_8	D_8PD	D_∞
D_8PD	1.000	-	-
D_∞	0.019	0.055	-
$D_\infty PD$	0.075	0.210	1.000

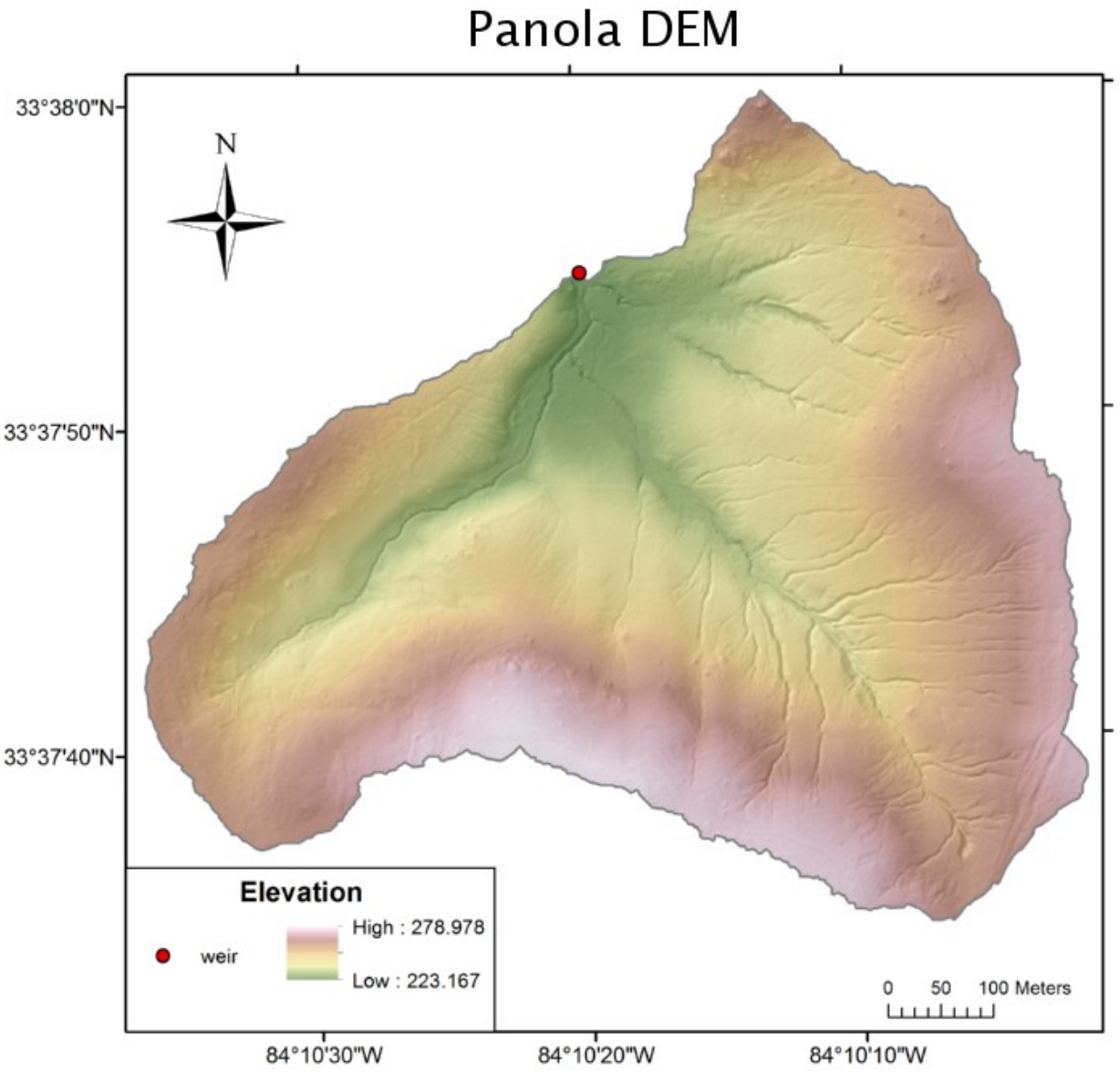

Figure 3.1: One meter resolution digital elevation model interpolated from bare earth LiDAR points on Panola Mountain Research Watershed.

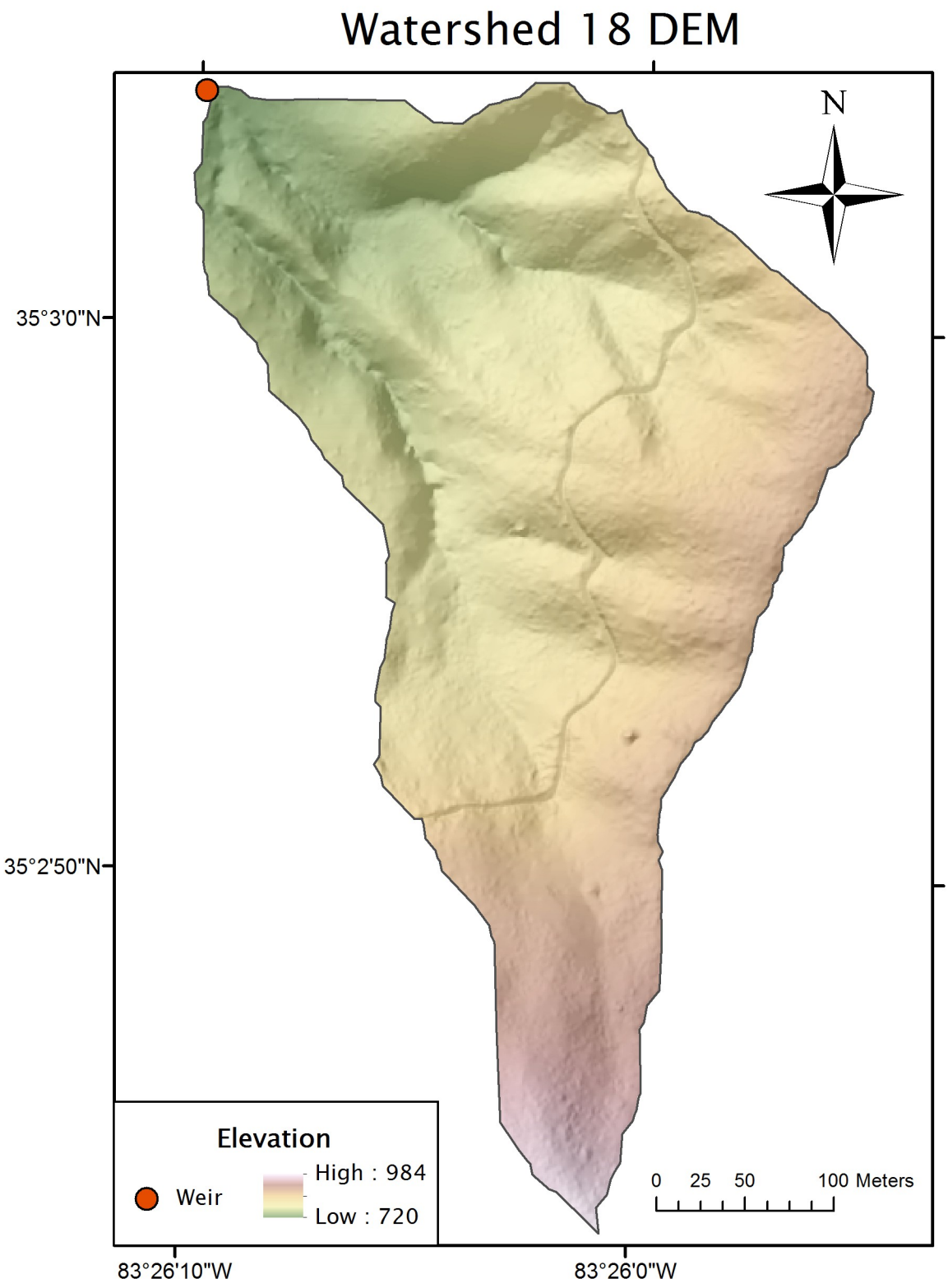

Figure 3.2: One meter resolution digital elevation model interpolated from bare earth LiDAR points on Watershed 18 of Coweeta Hydrologic Laboratory.

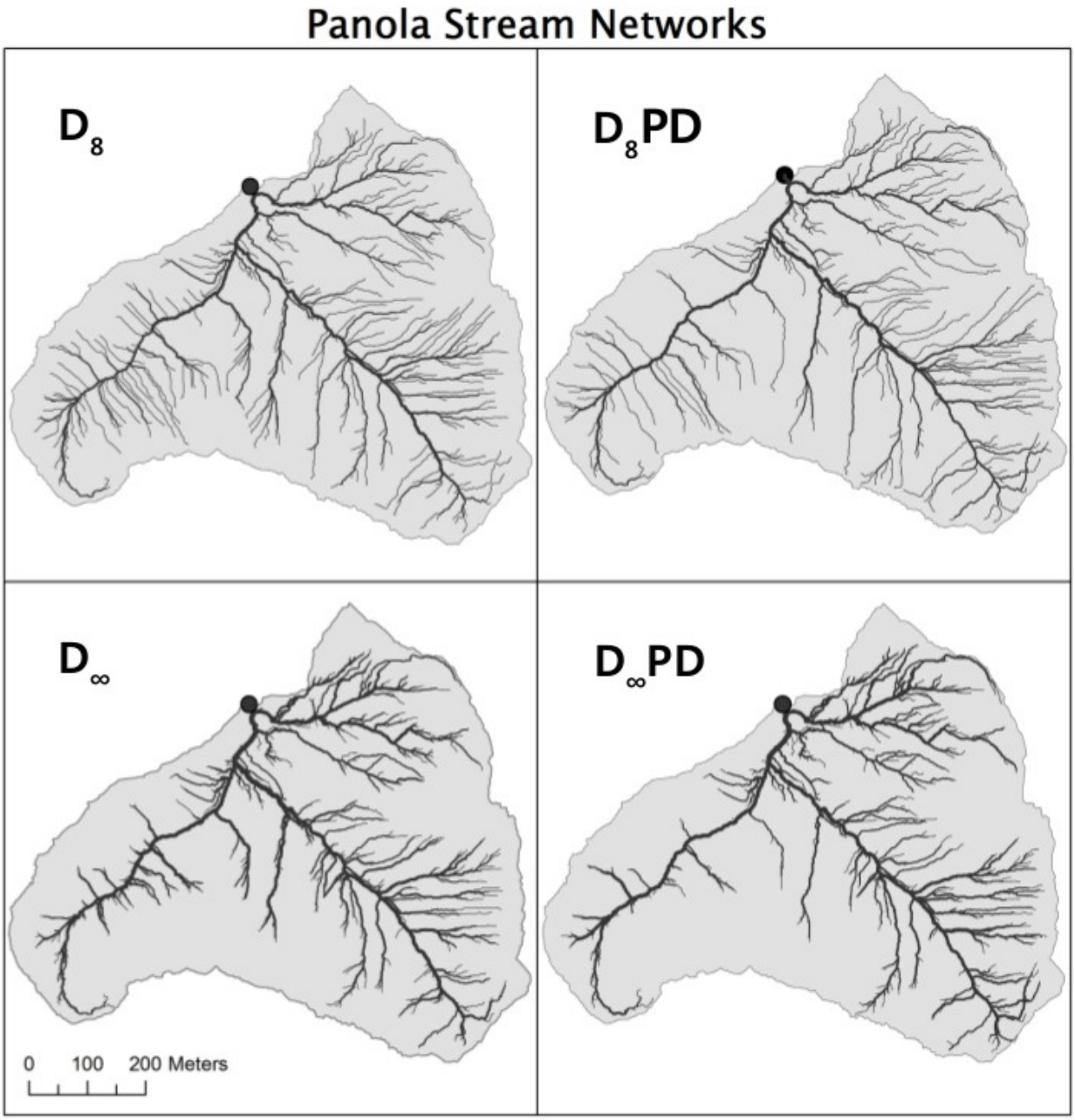

Figure 3.3: Panola stream networks. Drainage density for all networks is approximately 0.045 m^{-1}. D_8 (single flow direction) threshold is 400; D_8PD (single flow direction and weighted concave cells) threshold is 30; D_∞ (multiple flow directions) threshold is 200; and $D_\infty PD$ (multiple flow directions and weighted concave cells) threshold is 15.

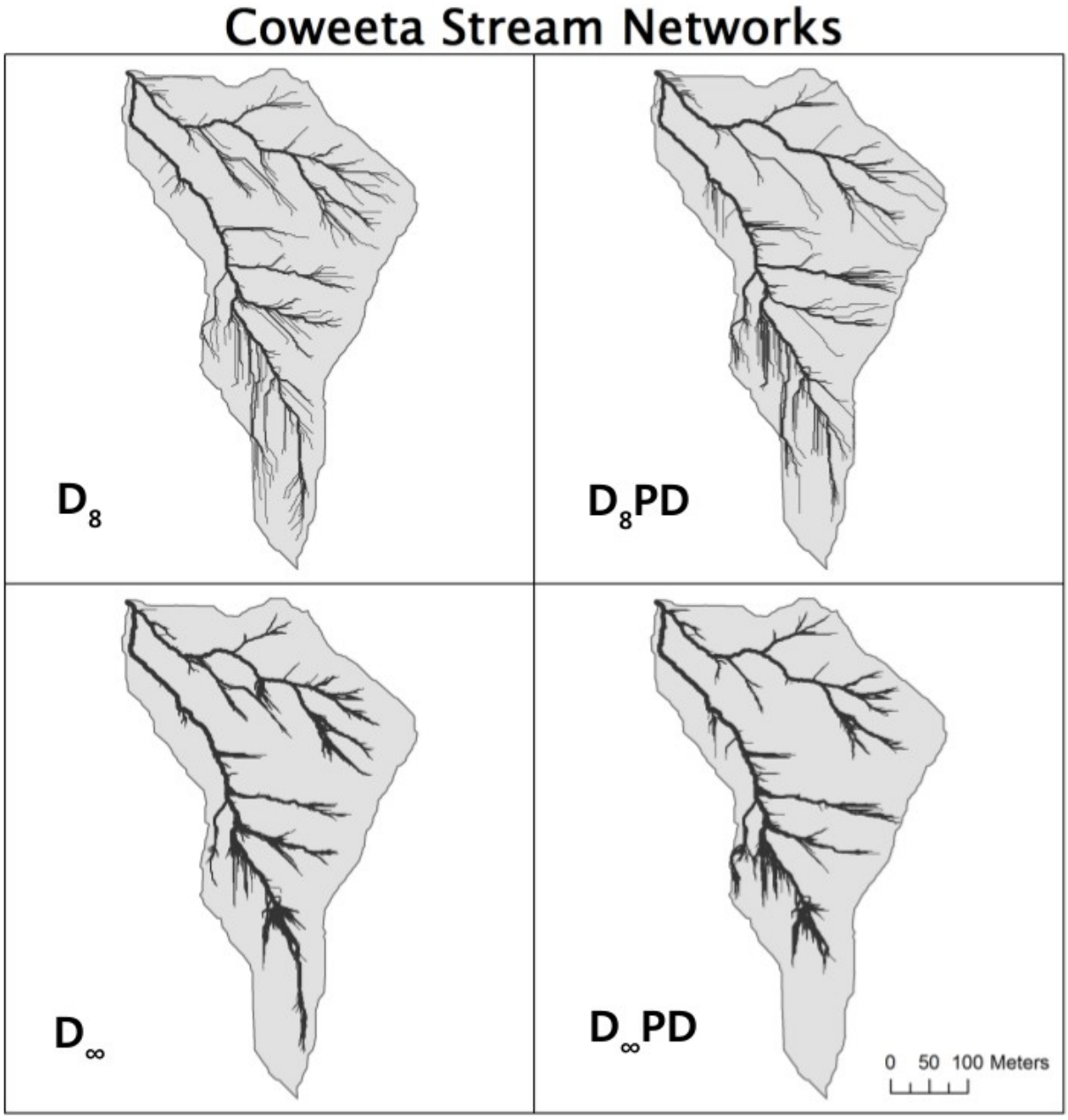

Figure 3.4: Coweeta stream networks. D_8 (Single flow direction) threshold is 155; D_8PD (single flow direction and weighted concave cells) threshold is 5; D_∞ (multiple flow directions) threshold is 80; D_∞PD (multiple flow directions and weighted concave cells) threshold is 2. The drainage density for D_8 networks is 0.075 m^{-1}; drainage density for D_∞ networks is 0.1 m^{-1}.

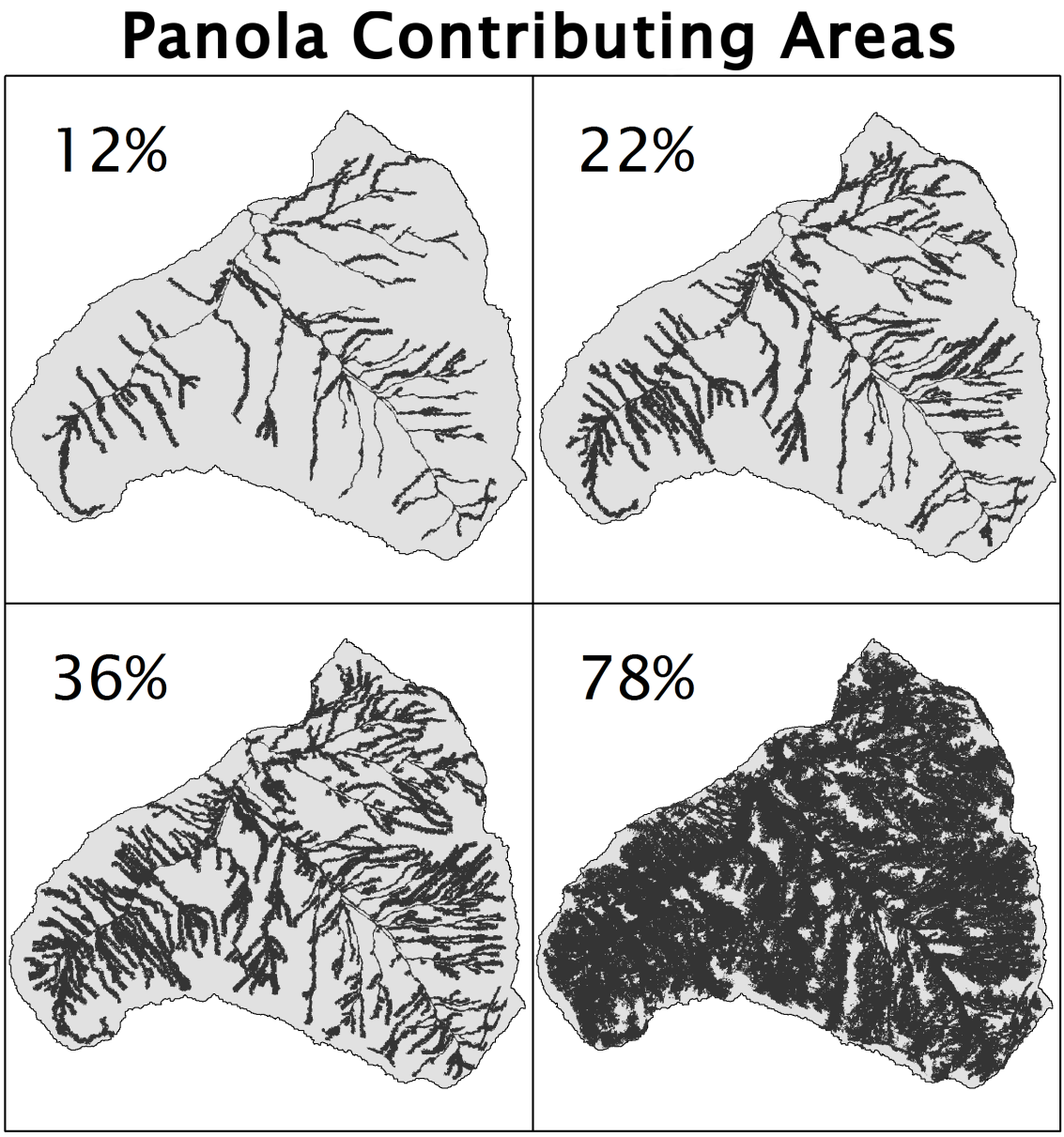

Figure 3.5: Contributing areas on Panola estimated from D_8 networks. Percentages refer to the percent of the watershed area identified as contributing area.

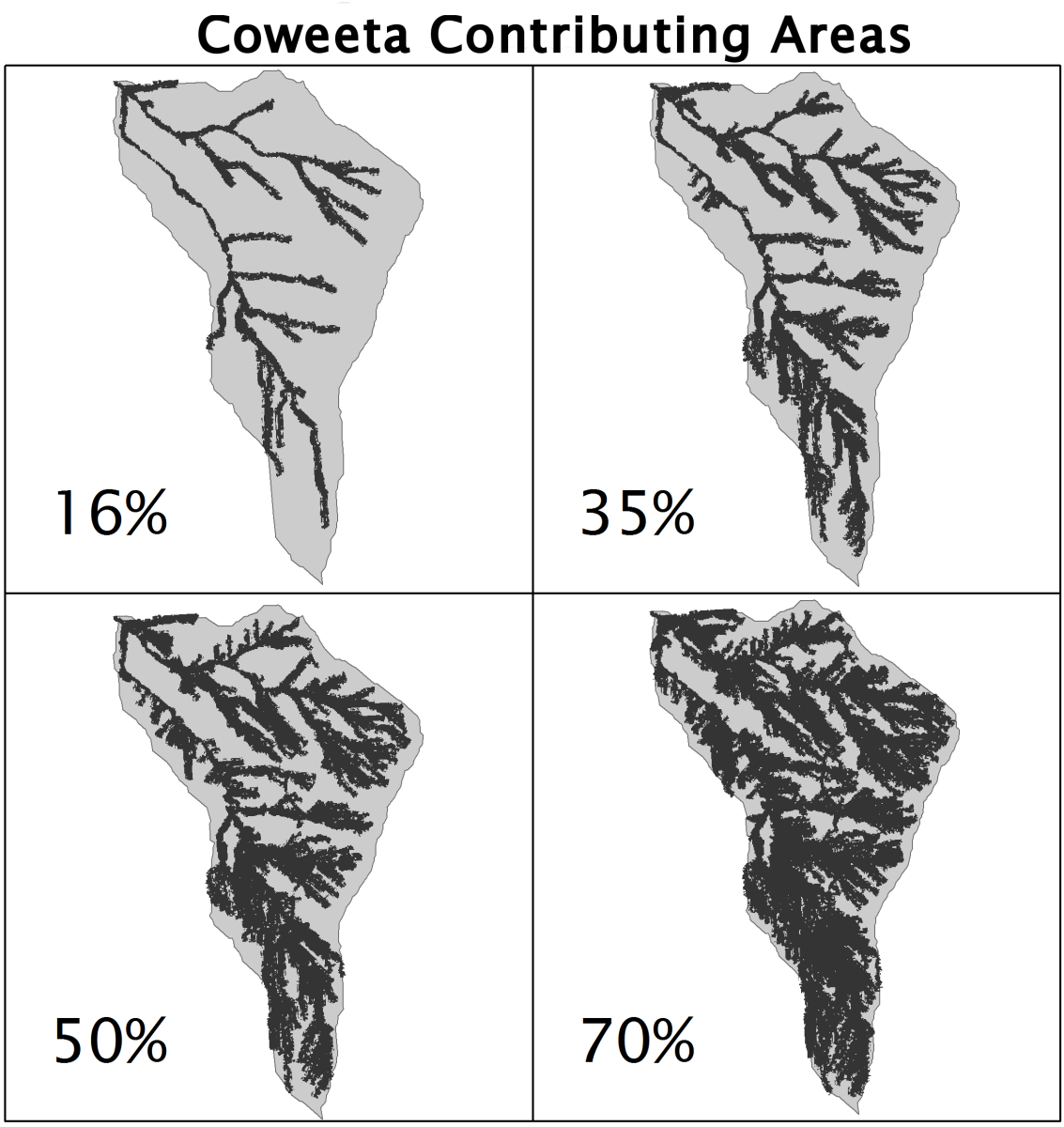

Figure 3.6: Contributing areas on Coweeta estimated from D_8 networks. The percentage refers to the percent of the watershed area that is contributing.

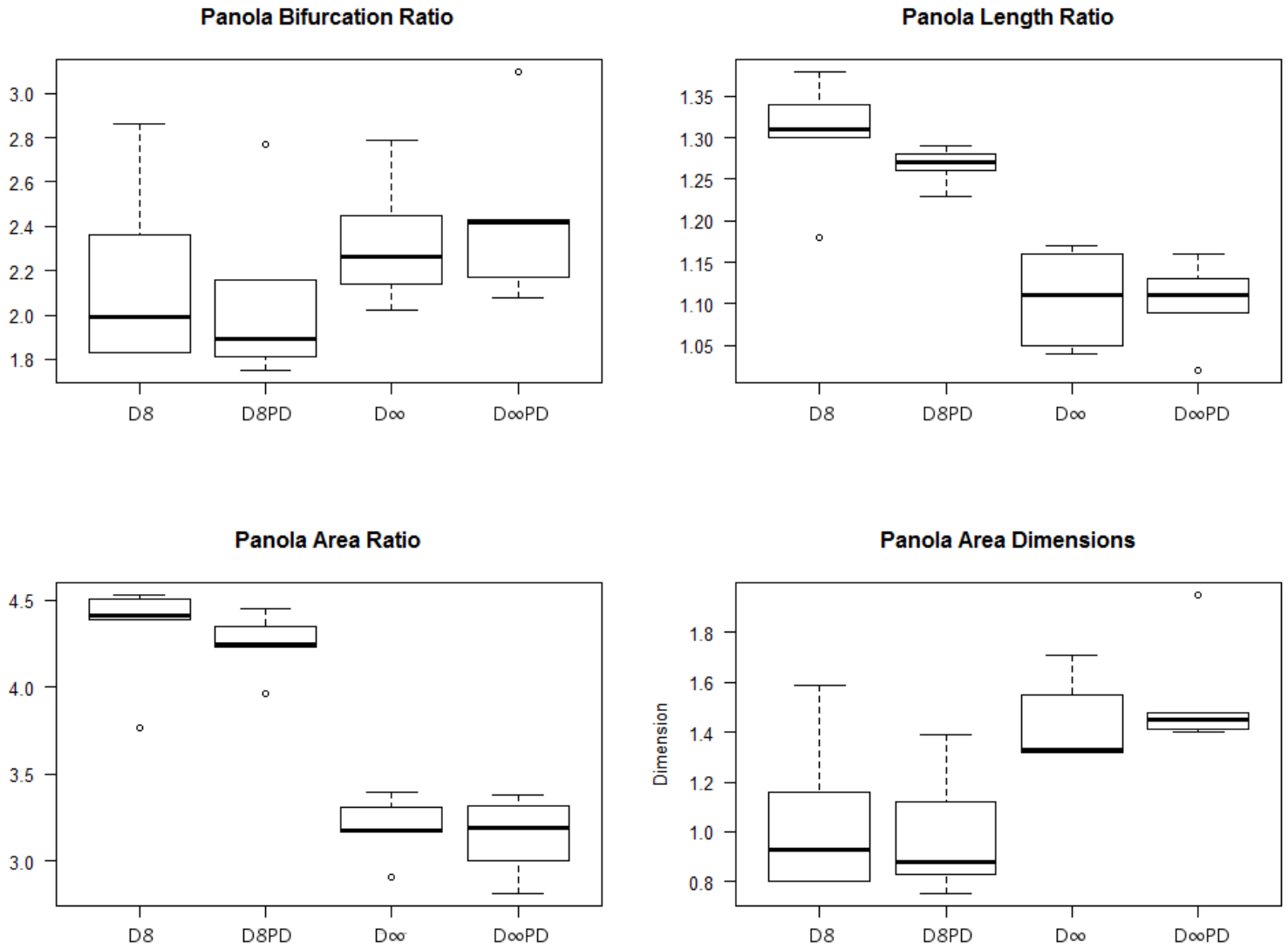

Figure 3.7: Boxplots for Panola bifurcation ratio, length ratio, area ratio, and the area fractal dimension.

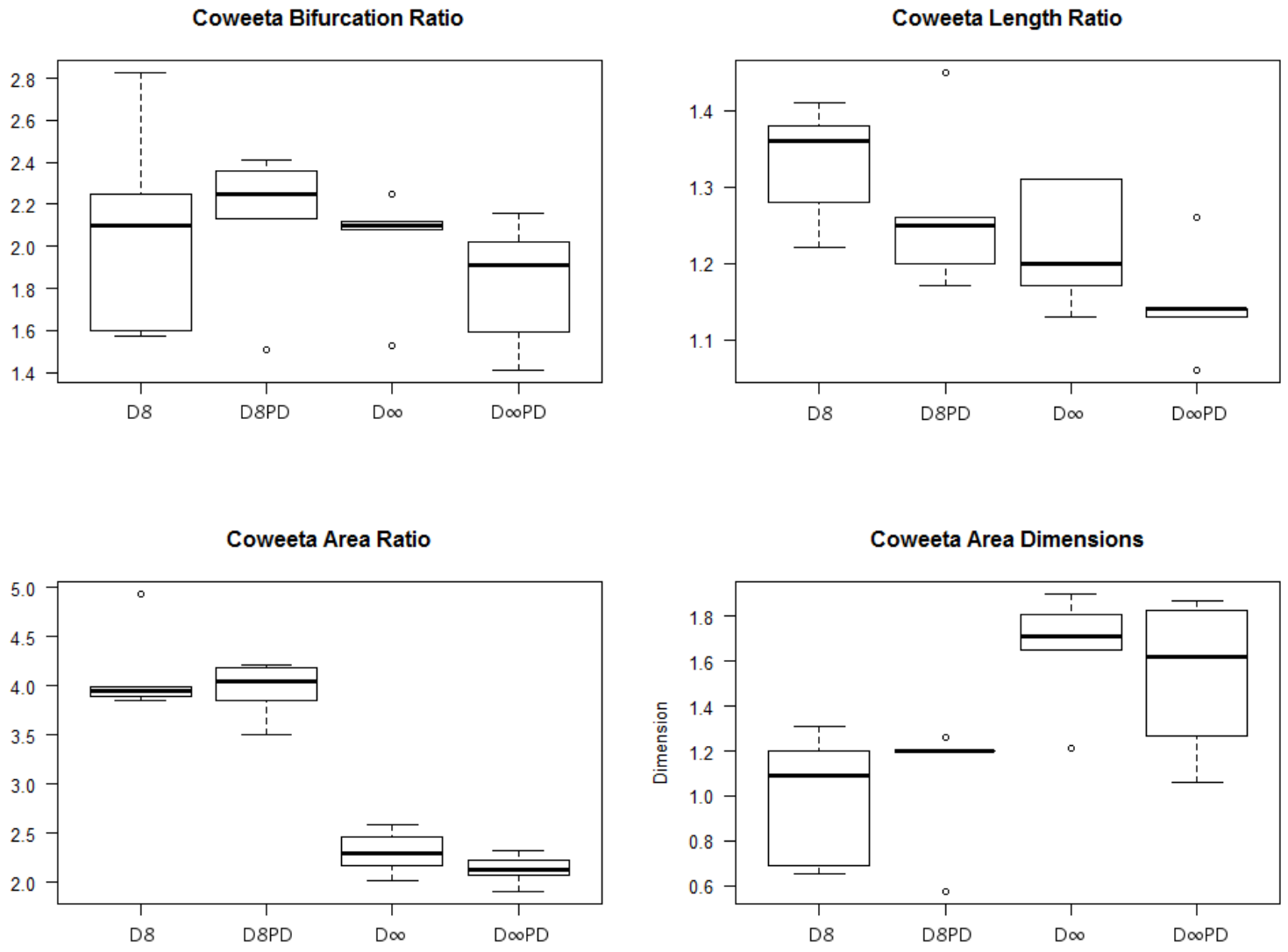

Figure 3.8: Boxplots of Coweeta bifurcation ratio, length ratio, area ratio and the area fractal dimension.

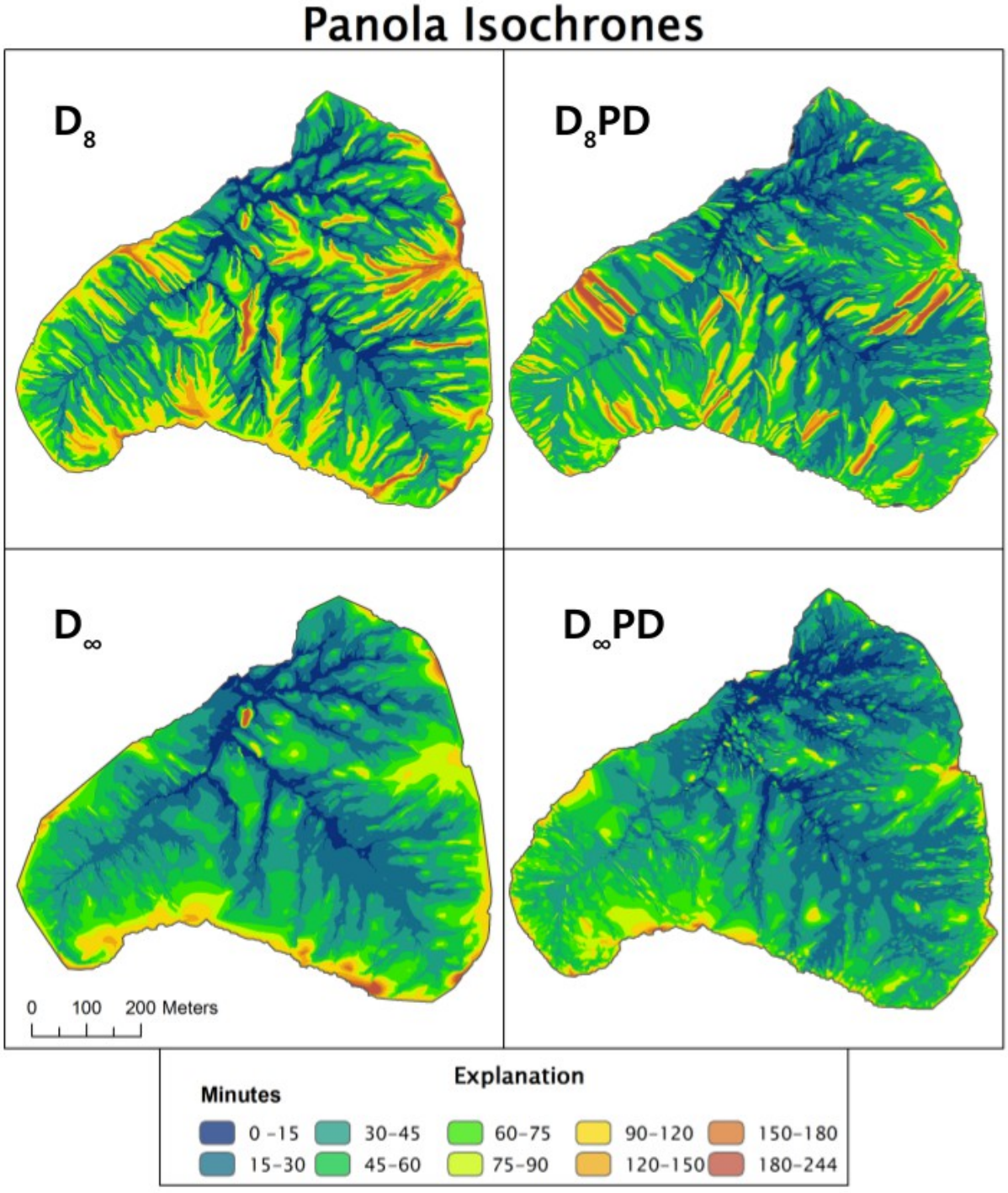

Figure 3.9: Panola isochrone maps.

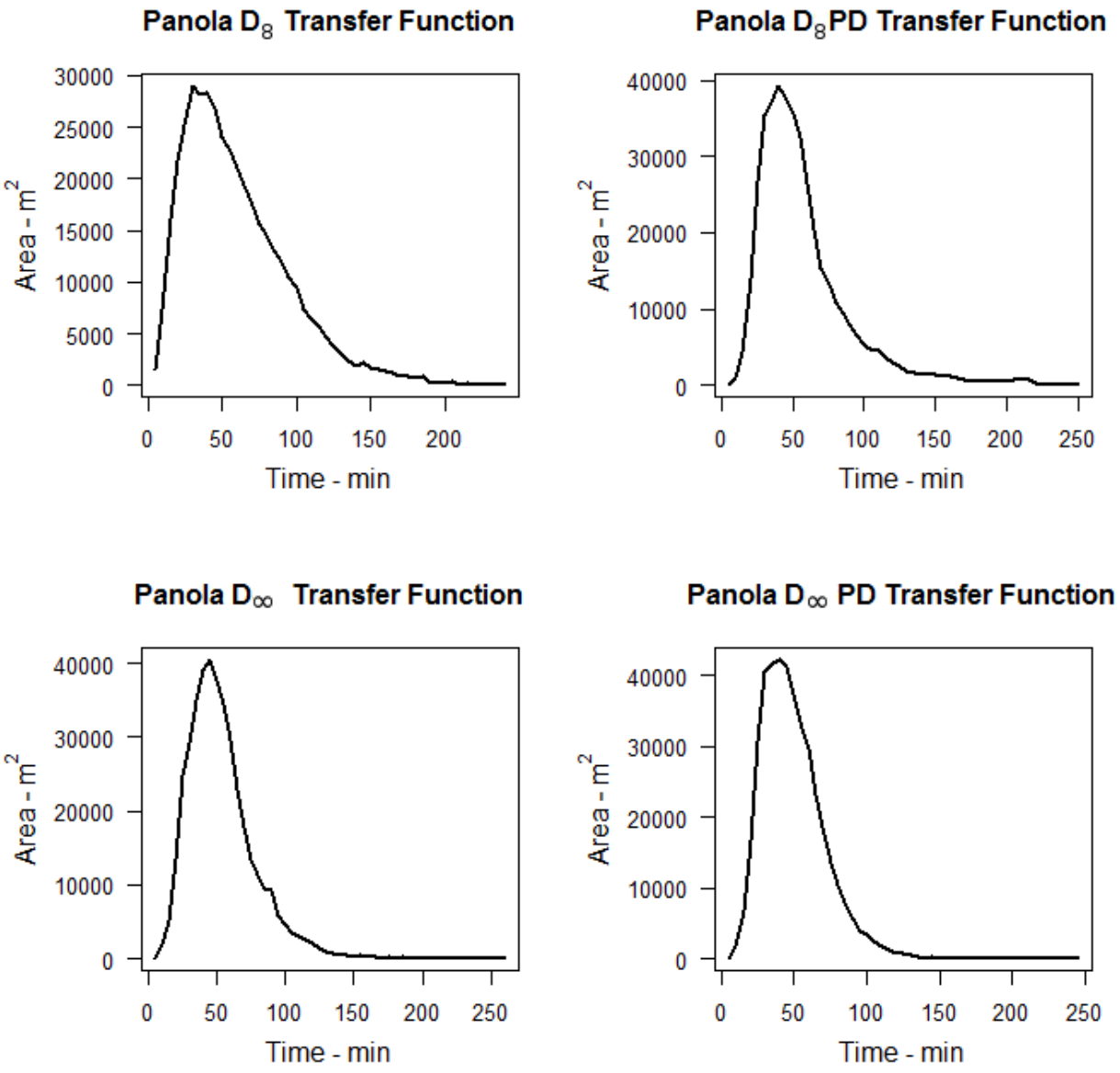

Figure 3.10: Transfer functions for Panola. Transfer functions are the distribution of the frequency of travel times to the basin outlet obtained from the isochrone maps.

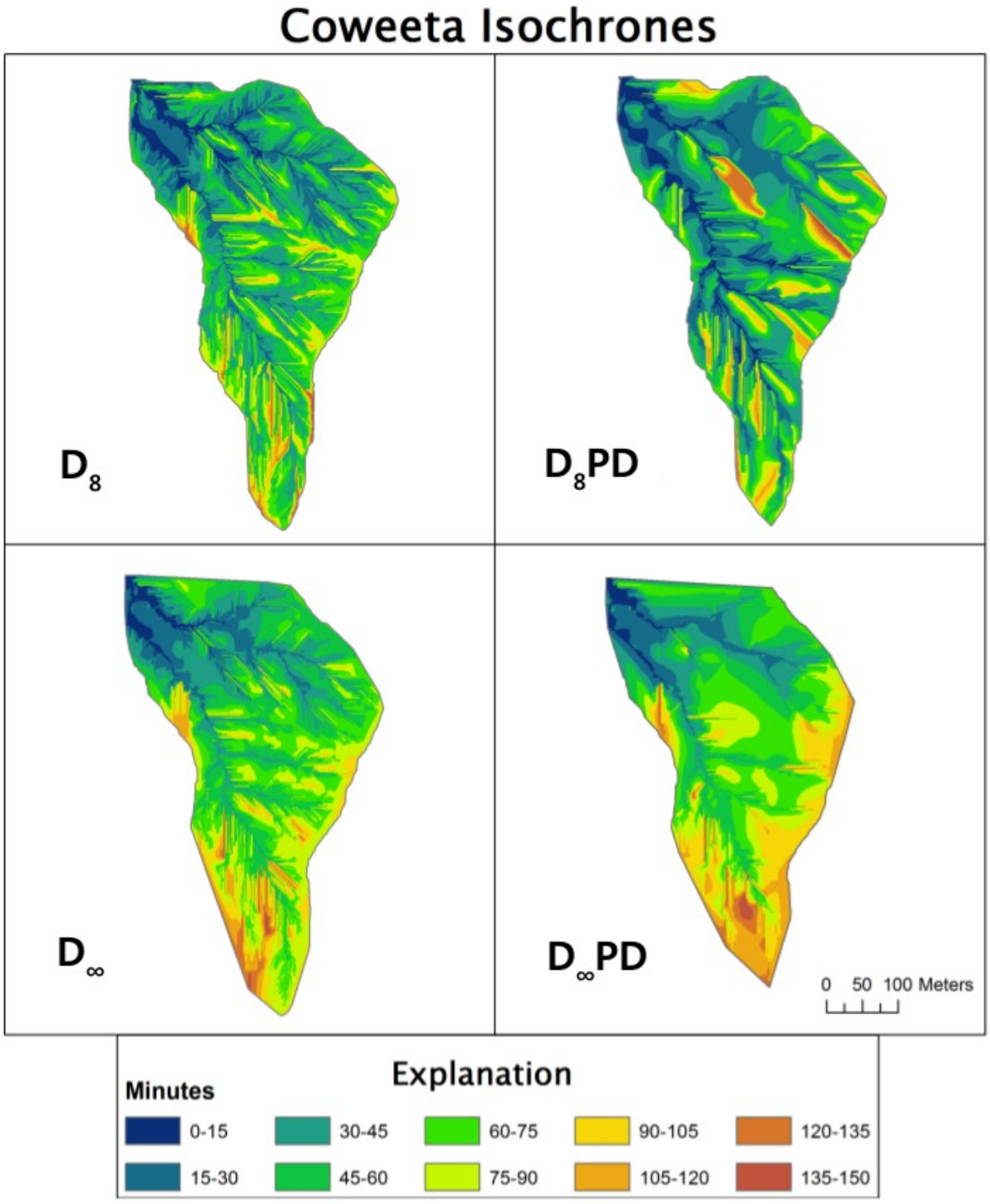

Figure 3. 11: Coweeta isochrone maps.

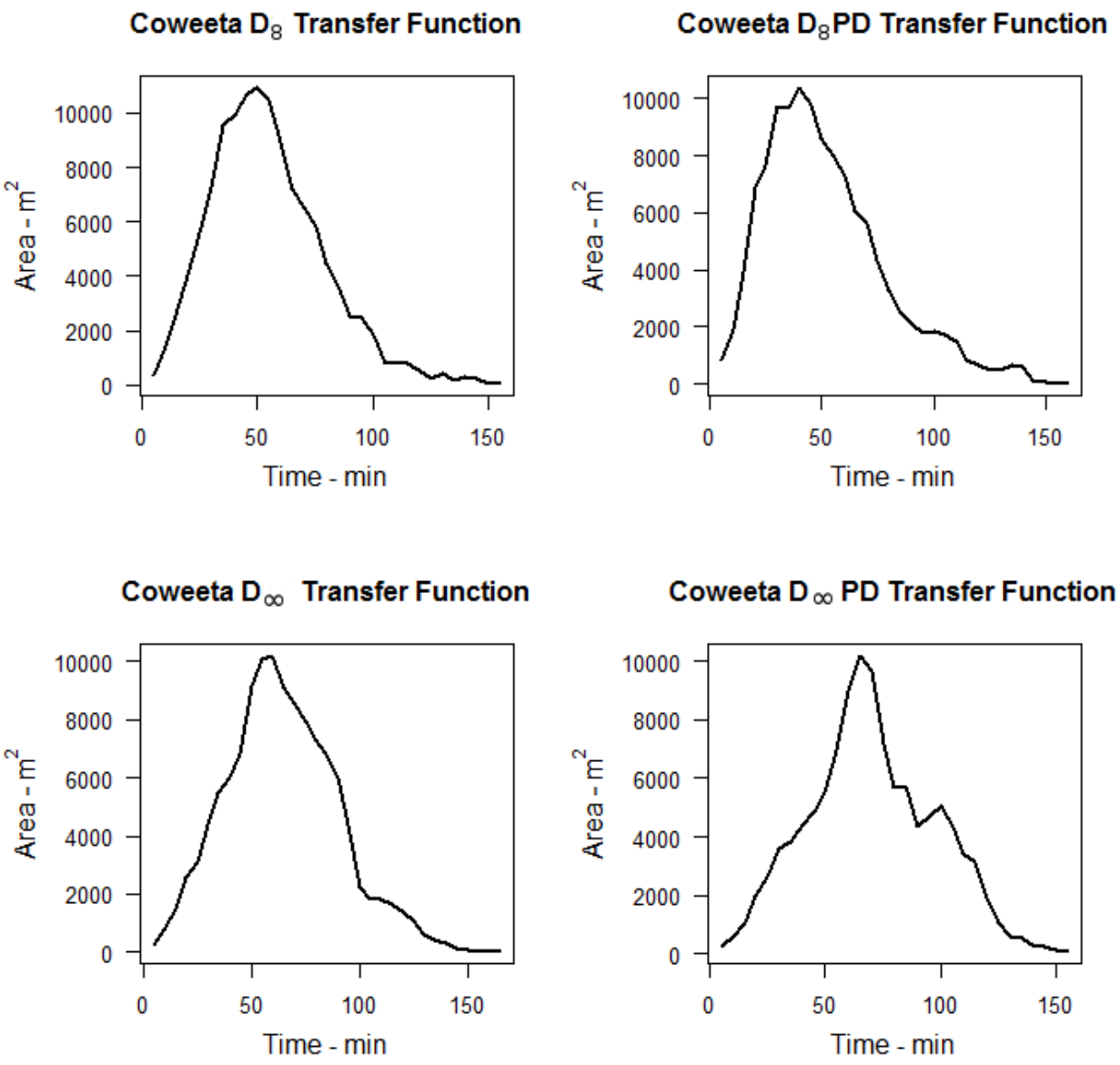

Figure 3.12: Transfer functions for Coweeta. Transfer functions are the distribution of the frequency of travel times to the basin outlet obtained from the isochrone maps.

Literature Cited

American Society for Photogrammetry and Remote Sensing. 2007. Digital Elevation Model technologies and applications: the DEM users manual, 2nd ed. American Society of Photogrammetry and Remote Sensing: Bethesda, Md.

Band LE. 1986. Topographic partition of watersheds with digital elevation models. *Water Resources Research* **22**(1): 15-24.

Clark CO. 1945. Storage and the unit hydrograph. *Transactions, American Society of Civil Engineers* **10**: 1419-1446.

Cudennec C, Fouad Y, Sumarjo Gatot I, Duchesne J. 2004. A geomorphological explanation of the unit hydrograph concept. *Hydrol. Process.* **18**(4): 603–621.

Hewlett JD, Hibbert AR. 1967. Factors affecting the response of small watersheds to precipitation in humid regions. *Forest Hydrology*: 275-290.

Hewlett JD, Nutter WL. 1970. The varying source area of streamflow from upland basins. *Proceedings of the Symposium on Interdisciplinary Aspects of Watershed Management* Bozeman, MT; 65-83.

Horton RE. 1945. Erosional development of streams and their drainage basins; Hydrophysical approach to quantitative morphology. *Geologic Society of America Bulletin* **56**: 275:370.

Manning R. 1891. On the flow of water in open channels and pipes. *Transactions of the Institution of Civil Engineers of Ireland* **20**: 161-207.

Peucker TK, Douglas DH. 1975. Detection of surface-specific points by local parallel processing of discrete terrain elevation data. *Comput. Graphics Image Process*. **4**: 375-387.

Sidle RC, TsuboyamaY, Noguchi S, Hosoda I, Fujieda M, Shimizu T. 2000. Stormflow generation in steep forested headwaters: a linked hydrogeomorphic paradigm. *Hydrological Processes* **14**(3): 369–385.

Strahler AN. 1957. Quantitative analysis of watershed geomorphology. *American Geophysical Union Transactions* **38**(6): 913-920.

Tarboton DG. 2012. Terrain Analysis Using Digital Elevation Models (TauDEM). *Available at*: http://hydrology.usu.edu/taudem/taudem5.0/. *Accessed in* January 2013.

Tarboton DG. 2003. Terrain Analysis Using Digital Elevation Models in Hydrology. 23rd ESRI International Users Conference, San Diego, California, July 7-11.

Tarboton DG, Ames DP. 2001. Advances in the mapping of flow networks from digital elevation data. *World Water and Environmental Resources Congress*: Orlando, Florida, May 20-24, ASCE.

Tarboton DG. 1996. Fractal river networks, Horton Laws, and Tokunaga cyclicity. *Journal of Hydrology* **187**: 105-117.

Tarboton DG, Bras RL, Rodriguez-Iturbe I. 1988. The Fractal Nature of River Networks. *Water Resources Research* **24**(8): l3l7-l322.

Windfeldt K. 2009. LiDAR estimation of Forest Leaf Structure, Terrain and Hydrophysiology Airborne Project Mapping Report. National Center for Airborne Laser Mapping. University of Minnesota-Twin cities.

Zaslavsky D, Rogowski AS. 1969. Hydrologic and Morphologic Implications of Anisotropy and Infiltration in Soil Profile Development. *Soil Science Society of America Proceedings* **33**: 594-599.

CHAPTER 4

MODELING STORMFLOW WITH THE GEOMORPHOLOGIC INSTANTANEOUS UNIT HYDROGRAPH[5]

5 Mason-Deese WF, Dowd JF, Rasmussen TC. To be submitted to *Hydrological Processes*.

Abstract

The geomorphologic instantaneous unit hydrograph (GIUH) is used to model and predict storm runoff for several storms at Panola Mountain Research Watershed and Coweeta Watershed 18. The GIUH is a two parameter gamma distribution that is parameterized by the average length of streams in each Strahler order. This allows flow paths from dense surface runoff networks to be used to model stormflow. The resulting GIUH is used to calculated the unit hydrograph which is scaled by precipitation and contributing area to synthesize storm hydrographs. Nash-Sutcliffe efficiency coefficients are used to compare the modeled storms to observed storm runoff.

Introduction

The geomorphologic instantaneous unit hydrograph (GIUH) is an important tool for predicting stormflow in ungauged basins (Cudennec *et al.* 2004, Fleurant *et al.* 2006, Kumar *et al.* 2007). Geomorphologic parameters can easily be obtained from high resolution topography which is becoming increasingly available. The topography is used to extract a dense stream network for a basin. The average length of streams in each Strahler order is used to describe surface runoff from the basin and to parameterize a gamma distribution that forms the GIUH based on procedures of Cudennec *et al.* (2004) and Fleurant *et al.* (2006). The GIUH is used to calculate the unit hydrograph. Unit hydrographs are produced for each time step of a storm and scaled by precipitation and contributing area. The convolution of hydrographs from each time step of a storm produces the storm hydrograph.

This model is fit to storms on Panola Mountain Research Watershed (PMRW) by using the observed data to back-calculate contributing areas. Coweeta Watershed 18 is treated as an ungauged basin, and the model is used to predict storms on Coweeta by estimating the contributing areas. Model results are assessed by comparing modeled and observed peak discharges as well as Nash-Sutcliffe (1970) efficiency coefficients.

Unit Hydrograph

The unit hydrograph is a common and relatively simple method of modeling storm runoff. The unit hydrograph describes the basin's response to one unit of effective rainfall, or runoff, that is applied uniformly across the basin over a given duration of time (Clark 1945, Fleurant *et al.* 2006). Depending on where in the watershed the runoff is generated and how far it is from the basin outlet, the runoff will take different amounts of time to

reach the outlet. The unit hydrograph describes the distribution of runoff over time at the basin outlet. The shape or distribution of the unit hydrograph is affected by the structure of runoff flow paths, the shape of the watershed, the slope, soils, and geology. This method assumes that precipitation has a constant intensity over the given duration of time and that precipitation falls uniformly across the basin (Clark 1945, Fleurant *et al.* 2006).

The unit hydrograph describes how the basin responds to runoff. The volume of runoff produced is also needed in order to model storms. The volume of runoff produced during a storm is determined by the watershed area and the rainfall excess which is the amount of rainfall that turns into runoff. The runoff volume and unit hydrograph are used by convolution to model storm runoff with following equation:

$$Q(t) = A \int_0^t i(\tau) u(t-\tau) d\tau \qquad \textit{Equation 1}$$

Where $Q(t)$ is storm runoff, A is the area of the watershed, $i(\tau)$ is rainfall excess, and $u(t-\tau)$ is the response function or unit hydrograph. This method also assumes that the unit hydrograph scales linearly with different size unit rainfalls (Clark 1945, Fleurant *et al.* 2006).

Unit hydrographs of various durations can be calculated from the instantaneous unit hydrograph (IUH). The IUH was first introduced as a method of predicting stormflow by Clark (1945). The IUH describes runoff at the outlet of the basin resulting from one unit of effective rainfall applied instantaneously and uniformly across the basin. Nash (1957) described IUH with a series of cascading linear reservoirs that take the shape of a gamma distribution. Both, the Nash and the Clark models use a gamma distribution parameterized

by measurements made from observed hydrographs. Therefore, these models require historical discharge data for calibration and are unsuited for ungauged basins.

Geomorphologic Instantaneous Unit Hydrograph

Rodriguez-Iturbe and Valdes (1979) developed the geomorphologic instantaneous unit hydrograph which gives a physical meaning to the IUH by basing it on the probability density function (pdf) of travel times to the basin outlet. The GIUH can be used in ungauged basins because the parameters are derived from geomorphologic properties that are measured from the topography.

In this paper, the methods of Cudennec *et al.* (2004) and Fleurant *et al.* (2006) are used to calculate the GIUH. The GIUH is the basin response function, and is assumed to be equal to the convolution of response functions from each Strahler order of the basin's stream network. Each Strahler order's response function is equivalent to a gamma distribution that is parameterized by the average length of streams in each Strahler order.

The method starts with a dense stream network that is classified by Strahler (1957) ordering scheme. Headwater streams are considered first order streams. When streams of the same order merge the resulting stream is one order higher. If streams of different orders merge the resulting stream maintains the order of the highest order stream. The networks used for this method are considered zero order networks because they extend up the hillslope well past the terminus of blue line streams. Networks classified by Strahler order exhibit strong scaling properties and are considered to be self-similar objects with fractal geometry. Geometric laws such as Horton laws (1945) have been used to describe

the scaling and organization of networks as well as to demonstrate the self-similar properties of networks.

Cudennec *et al.* (2004) and Fleurant *et al.* (2006) use a statistical physics reasoning that treats the network as a self-similar object with fractal geometry. Several assumptions must be met to use this reasoning:

- The system must be homogeneous, for example, the basin must share the same geology.
- Individual component lengths of streams are independent from the lengths of other component lengths.
- Stream component distribution is isotropic.

These assumptions are held for the pdf of stream lengths as well as the mean length of components.

These assumptions allow for the introduction of a scaling term called the component length ratio, $rl=rl_i/rl_{i-1}$. This term states that the average length of streams of order i, is on average, rl times larger than the average length of streams of order $i-1$. Average lengths are used because a water drop may enter the stream at any point along the stream segment and may not necessarily traverse the whole length of the network. The component length also takes into account if a first order stream were to flow into a third order stream, the length of the second order would be zero. For a given basin, the component length ratio remains fairly constant across Strahler orders of self-similar networks.

To synthesis the GIUH, all possible flow paths are considered by obtaining the pdf of component lengths for each Strahler order. The pdf, or response function for each order is calculated by:

$$pdf\left(l_k\right) = \frac{1}{\sqrt{2\pi\,\bar{l}_k}}\,\frac{1}{\sqrt{l_k}}\,e^{-l_k/2\bar{l}_k} \qquad \textit{Equation 2}$$

where l_k is the length of streams in order k, and $\bar{l}_k$ is the mean length of streams in order k. Figure 4.1 shows the observed probability density distribution of stream lengths and the theoretical pdf calculated from Equation 2. Equation 2 is a rapidly decreasing and convex gamma law with the parameters:

$$\alpha = ½, \text{ and } \beta = \frac{1}{2\bar{l}_k}.$$

This produces the pdf for each Strahler order; the pdf, or response function of the basin is equal to the convolution of the pdfs from each order:

$$pdf\left(L\right) = pdf\left(l_1\right) * pdf\left(l_2\right) * \ldots * pdf\left(l_n\right) \qquad \textit{Equation 3}$$

where * is the convolution operator. The pdf of path lengths is related to travel time by dividing the pdf by the mean streamflow velocity. This produces a pdf of travel times that is analogous to the GIUH and describes runoff from one unit of rainfall that is applied instantaneously and uniformly across the basin.

The GIUH is then used to calculate the unit hydrograph. This describes runoff from rainfall that occurs at a constant rate over a specified duration of time. Two GIUHs are lagged by the duration of time, the average of the two GIUHs result in the unit hydrograph. The unit hydrograph is then used in conjunction with rainfall excess to estimate storm hydrographs.

Rainfall Excess

Storm runoff is modeled from the unit response function and the volume of runoff. The volume of runoff is usually calculated from the area of the watershed and by estimating

rainfall excess, or the amount of rainfall that turns into surface runoff. Rainfall excess is difficult to estimate and there are no robust methods in which to do so.

Rainfall is assumed to fall uniformly across the watershed, however, not all rainfall turns into runoff; most rainfall infiltrates into the soil, evaporates, or is transpired. The rain that falls onto saturated areas of the watershed will be converted directly into surface runoff. The saturated areas that produce overland flow are assumed to be the stream channels and the areas adjacent to the channels that become saturated. These areas become saturated because the soil can no longer transmit the water flowing through it, therefore, the watertable rises to the surface (Hewlett and Hibbert 1967). Some of the saturated flow is return flow that has previously infiltrated and returns to the surface in saturated areas. It is assumed that all of the rain falling on stream channels and saturated areas is converted into runoff. A simple estimation of surface runoff is then obtained by multiplying rainfall by the saturated area over which it falls.

Factors that effect the extent of these saturated or contributing areas include antecedent moisture conditions, seasonality, rainfall intensity, duration, and storm magnitude. Under wet conditions and large storms these areas will expand further up the hillslope while under dry conditions and small storms only the stream channels will contribute. Dunne *et. al.* (1975) found that contributing areas are quite variable and during very large storms can account for greater than 50% of the watershed.

Estimating the extent of the stream channels and saturated areas is problematic. The stream channels and saturated areas can be estimated from high resolution topography using the procedures in Appendix A and B. However, the problem is determining the density of the network and how far it and the saturated areas extend up the hillslope.

Moreover, the extent of the network and saturated areas change from storm to storm and through-out the course of a storm.

Contributing areas are be back-calculated from observed rainfall and runoff data at Panola. The back-calculated areas for a storm are compared to the storm return periods and used to estimate return periods for contributing areas. The areas are also distributed over stream networks to estimate the density of the network for a given return period. It is assumed that the precipitation falling on contributing areas is converted into runoff, therefore, if the contributing area can be back-calculated or estimated, the equation for storm runoff becomes:

$$Q(t)=\int_0^t a(\tau)\,p(\tau)\,u(t-\tau)\,d\tau\,. \qquad \textit{Equation 4}$$

Where $a(\tau)$ is now contributing area, and $p(\tau)$ is precipitation.

The volume of runoff produced at each time step is estimated by multiplying the contributing area by the rainfall rate. This runoff is distributed by multiplying it by the unit hydrograph. This process is done to produce a hydrograph for each time step of a storm. The final storm hydrograph is equal to convolution of hydrographs from each time step.

Methods

The previous manuscript and Appendix A describe how dense stream networks are extracted from high resolution topography derived from LiDAR. The networks were classified by Strahler order and show to be self-similar in terms of bifurcation, stream lengths, and contributing area. The stream networks are used in the following procedures which are implemented in the computer program "R", the complete code is found in Appendix C.

First, stream lengths and mean stream lengths are found for each Strahler order. Equation 2 is used to calculate the pdf of stream lengths for each Strahler order. An example of observed and calculated pdfs of stream lengths is seen in Figure 4.1. Each pdf is divided by an average velocity that is estimated for each Strahler order using Manning's (1891) equation (Manning's procedures are found in Appendix B). Equation 3 is then used to take the convolution of the pdfs of each order. The result provides the shape of the basin GIUH.

The GIUH is scaled so that the length is equal to the time of concentration and the volume is equal to one. The time of concentration at Panola is measured from observed storm hydrographs as the time difference between when the largest contributing area occurs and the time when surface runoff stops. The time of concentration at Coweeta is estimated using the Soil Conservation Service (SCS) method (Kent 1973) and found to be around 12 hours. The top of Figure 4.2 shows the instantaneous unit hydrograph resulting from the convolution of each order's pdf and scaling.

The GIUH is used to calculate the fifteen minute unit hydrograph. The unit hydrograph is produced by lagging the GIUH by fifteen minutes and then averaging the two

GIUHs. The fifteen minute unit hydrograph of Coweeta is seen in the bottom Figure 4.2. The fifteen minute unit hydrograph is then used to calculate a storm hydrograph. A unit hydrograph is produced for each fifteen minute time step of a storm and then scaled by multiplying it by the runoff which is equal to the precipitation rate multiplied by the contributing area.

For storms at Panola the contributing area for each time step is back-calculated by dividing the storm runoff by the precipitation rate. The back-calculated contributing area is compared to storm return periods in Figure 4.3. Return periods are calculated using the Generalized Extreme Value distribution and the Generalized Pareto distribution for both the cumulative precipitation and peak discharge (Gilleland 2006).

For storms at Coweeta it is assumed that the contributing area is not known. A maximum contributing area must be assumed and is set to 33% of the watershed. There was no relationship between contributing area and return period of the rainfall at Panola, therefore, there is no adequate way to estimate the maximum contributing area based on rainfall.

During the course of a storm the contributing area changes. To estimate this change, the rainfall rate is multiplied by the cumulative rainfall for each time step. These values are scaled so that the maximum value is equal to 33% of the watershed's area. The resulting distribution is similar to the back-calculated contributing areas and provides a simple estimation of contributing area. An example from Panola storm 87 is seen in Figure 4.4.

The contributing areas and precipitation rates are multiplied for each time step to obtain runoff volumes which are then multiplied by the unit hydrograph for each time step. The convolution of the scaled and successively lagged hydrographs produces the storm

hydrograph. An example of the lagged and scaled hydrographs is seen in Figure 4.5; the resulting storm hydrograph is seen in Figure 4.6.

The modeled storm hydrographs are compared to observed storm runoff. Observed storm runoff is obtained by separating baseflow from total streamflow, the remaining flow is considered stormflow. Stormflow at Panola has been separated using geochemical separation completed by Cary (2011). Stormflow on Coweeta was separated using several digital filters including Lyne and Hollick (1979), Chapman (1991), and Eckhardt (2005)

The log of observed and modeled stormflows are compared with the Nash-Sutcliffe (1970) efficiency coefficient (NSE) which is equal to:

$$NSE = 1 - \frac{\sum (Q_O - Q_M)^2}{\sum (Q_O - \bar{Q}_O)^2} \qquad \textit{Equation 5}$$

Where Q_O is observed discharge and Q_M is modeled discharge. A NSE coefficient equal to one represents a perfect match of observed and modeled discharge. If the NSE is less than zero than the observed mean is a better predictor than the model. The log of modeled and observed peak discharges were also compared.

These procedures were first implemented for Panola Mountain Research Watershed where the model was fit to observed storms. Observed stormflow was previously separated from total flow by geochemical separation completed by Cary (2011). The observed stormflow data was used to back-calculate the contributing areas by dividing the observed stormflow by the precipitation rate. These areas were used to calculate surface runoff and to scale the modeled hydrograph. Fitting the model to observed data reveals how well the model is able fit observed storms.

The model is then used to predict stormflow at Coweeta. A maximum contributing area of a third of the watershed is assumed and set to vary based on the precipitation rate and cumulative precipitation. Observed stormflow is estimated by using digital filters to separate baseflow. Precipitation and discharge data for Coweeta are in hourly time steps. The hourly data is disaggregated to fifteen minute data assuming a uniform precipitation rate and discharge over a given hour. Comparisons of the modeled stormflow to observed storms show how well the model is able to predict stormflow. The code for implementing these procedures in "R" is given in Appendix C.

Results and Discussion

Several assumptions are made in order to run this model. First, the watersheds are assumed to be homogeneous. Small scale variations in soil type, geology, and vegetation are unavoidable, however, the watersheds used for this study are relatively small and undisturbed and therefore assumed to behave in a homogenous way. Rainfall rates are also assumed to be the same across the watershed where in reality they are quite variable especially at Coweeta where there is an orographic effect. The stream networks were previously shown to be self-similar and therefore meet the assumptions of independent component lengths and isotropic distribution of streams (Cudennec *et al.* 2004).

Figure 4.1 is a good indicator of the model's applicability. The solid lines in Figure 4.1 depict the observed probability density distribution of stream lengths for a D_8 network at Coweeta; the dashed lines are the theoretical pdfs calculated with Equation 2. The observed lengths are quite variable, although, the theoretical pdfs describe the mean of the observed lengths. The observed lengths of D_∞ networks are less variable but are also

described by the theoretical pdfs. This indicates that Equation 2 is a representation of the pdf of stream lengths.

The convolution of each Strahler order's pdf produces the pdf and GIUH of the basin. Figure 4.2 shows that GIUHs synthesized from D_8 networks have distinctively different shapes from GIUHs synthesized from D_∞ networks. The D_8 GIUHs have sharp peaks that occur almost instantaneously and then decrease rapidly. The D_∞ GIUHs also peak almost instantaneously however, the peak is not as sharp and the recession is not as rapid which produces a broader curve. These differences are due to the different structuring patterns of the networks.

The shape of the GIUH is insensitive to the parameters of Manning's equation, although it is more sensitive to the time of concentration. The time of concentration stretches the hydrograph and raises and lowers the peak, but the general shape remains the same. The time of concentration is calculated from the observed discharge and rainfall for Panola storms and ranges from five hours to over two days, the median time of concentration at Panola is 16 hours. Time of concentration at Coweeta is estimated using the SCS method (Kent, 1973) and found to be about 12 hours. The effect that time of concentration has on the modeled storm hydrographs is demonstrated in Figure 4.7. Longer times of concentration result in lower peaks and broader hydrographs while shorter times result in higher peaks and narrower hydrographs.

The 15 minute unit hydrograph, seen at the bottom of Figure 4.2, is produced by taking the average of two GIUHs, one of which has been lagged by fifteen minutes. The process of averaging produces a lower and more delayed peak than the GIUH. The

difference between D_8 and D_∞ derived unit hydrographs is less pronounced than the GIUH, although, the D_∞ unit hydrograph is broader and has a lower peak.

A unit hydrograph is produced for each time step of a storm and multiplied by the precipitation and the contributing area. Contributing areas are back-calculated for Panola storms and used to scale the unit hydrographs. Figure 4.3 shows contributing areas for Panola storms plotted against the return period for both precipitation and discharge. There is no relationship between the return period of the precipitation and contributing area. The largest contributing areas accounted for over 50% of the watershed, however, they are associated with fairly low return periods while some storms with higher return periods have smaller contributing areas. The factors that effect contributing area are complex and need to be explored more in order to predict contributing area.

The scaled and lagged unit hydrographs are convoluted to produce storm hydrographs. Figure 4.6 shows modeled and observed hydrographs for Panola storm 44. The observed hydrographs tend to have fairly sharp peaks that recede quickly. The modeled Panola hydrographs tend to over estimate the recession tail of the hydrograph. The shape of the unit hydrographs do not recede quickly enough, resulting in over-estimation of the recession tail. Peters *et al.* (2003) notes that Panola is a flashy watershed due to the underlying shallow bedrock and large rock outcrop which would cause the recession tail of the hydrograph to drop rapidly. Results are variable for Panola storms; the model tends to under-estimate peaks of small storms and over-estimate the peaks of larger and medium sized storms. Hydrographs of all the modeled storms are found in Appendix D.

Nash-Sutcliffe efficiency (NSE) coefficients were calculated from the log of flows for each modeled storm to assess the effect that different networks have on the final

hydrograph. NSE values closer to one indicate that the model better matches the observed hydrograph. Figure 4.8 shows boxplots of NSE coefficients for Panola storms modeled with D_8, D_8PD, D_∞, and D_∞DP networks. D_8 and D_8PD networks have slightly higher NSE coefficients indicating a better fit to the observed hydrographs, although, means of the different networks were not statistically different. D_8 and D_8PD networks were shown to display a slightly higher degree of self-similarity which may account for their better performance. The D_8 GIUHs also recede quicker than the D_∞ GIUHs and therefore better match the quickly receding Panola hydrographs.

Networks were extracted at different thresholds. Figure 4.9 displays boxplots of NSE coefficients for Panola storms modeled with D_8 networks of different thresholds. The threshold does not change model performance significantly. Different thresholds were also examined for D_8PD, D_∞, and D_∞PD networks, however, they also did not change the model's performance.

The log of modeled and observed peak discharges were also compared. Figure 4.10 shows peak discharges for Panola storms. The dashed line represents the one to one line where modeled and observed peaks are equal. For small storms, the model tends to under-estimate peak discharges. For the larger storms, the model tended to over-estimate peak discharge. The different types of networks fit the peaks equally well with D_8 networks performing better for some storms and D_∞ networks performing better for other storms.

Stormflow was predicted for storms at Coweeta by estimating contributing areas. First, observed stormflow was defined by separating baseflow using several digital filters including Lyne and Hollick (1979), Chapman (1991), and Eckhardt (2005). Modeled

storms were compared to stormflow defined by each of the filters. Figure 4.11 shows boxplots of NSE coefficients resulting from comparisons to the different filters.

The Lyne and Hollick filter produced significantly better results than the Eckhardt and Chapman filters. This is because the Lyne and Hollick filter does not account for recession and continues to define baseflow until the baseflow hydrograph intersects the discharge hydrograph. This results in less stormflow on the recession tail of the hydrograph. The Eckhardt and Chapman filters account for recession and result in excess stormflow volume on the recession tail of the hydrograph. The modeled storms have quickly receding recession tails that better match results from the Lyne and Hollick filter.

Contributing areas for Coweeta storms were estimated to reach a maximum of 33% of the watershed. Over the course of as storm, the area was estimated to fluctuate based on the precipitation rate and cumulative precipitation allowing for a dynamic area to be estimated. The model using dynamic area was compared to using a constant area of 33% of the watershed. Figure 4.12 shows boxplots of modified NSE coefficients for storms modeled using constant and dynamic areas. The dynamic area slightly improves model results for most storms, although, the improvement is not statistically significant. Models using a constant area tend to over-predict stormflow at the beginning of the storm because the watershed is not yet wetted up and contributing areas are smaller. This method could still be improved by estimating a storm specific maximum contributing area.

Different types of networks were also compared at Coweeta. Figure 4.13 shows boxplots of NSE coefficients for D_8, D_8PD, D_∞, and D_∞PD networks. All networks produced similar results and did not improve model performance.

Observed and modeled peak discharges were also compared and are seen in Figure 4.14. The dashed line represents the one to one line where observed and modeled peaks are equal. The model performed well for all storms except for storm number 404 which has been excluded from Figure 4.14. This storm had a long duration with several peaks which made it hard to model. For small storms the model both under-predicted and over-predicted peaks, however, for larger storms the model tended to under-predict the peaks. Hydrographs, NSE coefficients, and modeled and observed peak discharges are found for each storm in Appendix D.

Conclusion

Dense stream networks were used to synthesize the geomorphologic instantaneous unit hydrograph and to predict storm runoff. The mean length of streams in each Strahler order is used to obtain the pdf of path lengths which is used to calculate the GIUH for the basin. Unit hydrographs are calculated and scaled by precipitation and contributing areas for each time step, the convolution of unit hydrographs from each time step produces storm hydrographs.

Storm hydrographs are fit to observed storms at Panola Mountain Research Watershed. The modeled storm results at Panola are variable but tend to over-estimate the recession tail of the hydrograph. The model also tends to under-estimate peak discharge for small storms and over-estimate peak discharge for larger storms. The type of network used for the model did not have significant effect on the model results.

Hydrographs are predicted for storms at Coweeta Hydrologic Laboratory based solely on the topography and precipitation. A constant maximum contributing area is assumed and estimated to fluctuate through-out a storm based on precipitation rate and

cumulative precipitation. A method of predicting the maximum contributing area is needed to improve model performance.

The observed runoff at Coweeta is estimated by using digital filters which tend to over estimate runoff at the end of storms which explains the model's under estimation of runoff. The Lyne and Hollick (1979) filter produces the best results, although, theoretically this filter is not ideal because it does not account for recession.

The model was able to model storm runoff at two locations and therefore provides a good estimation of storm runoff based solely on precipitation and the topography making this model ideal for use in ungauged basins.

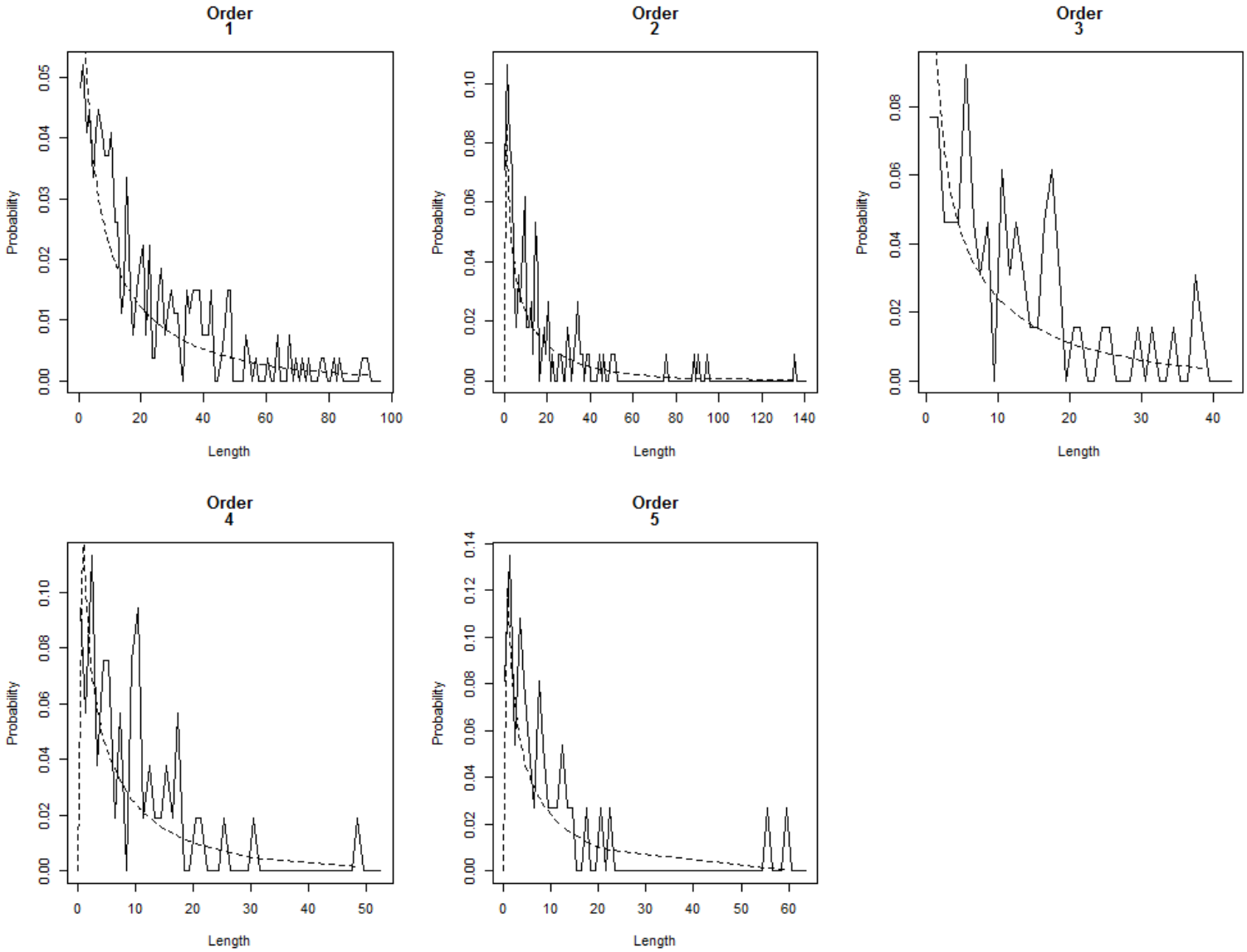

Figure 4.1: Probability density functions of stream lengths by Strahler order. Solid lines are observed lengths. Dashed lines are theoretical lengths calculated with Equation 2.

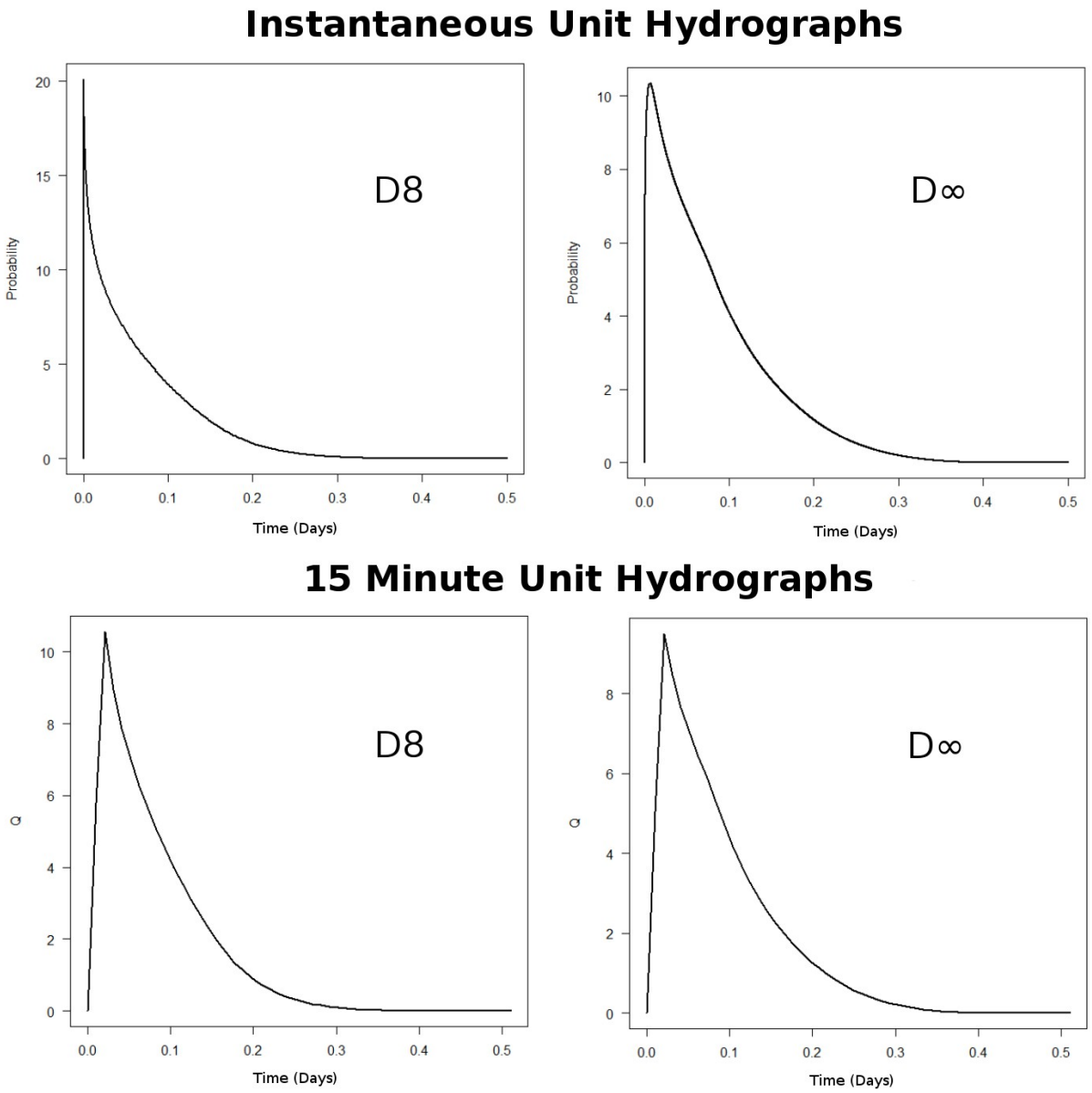

Figure 4.2: D_8 and D_∞ instantaneous unit hydrographs at Coweeta (top). 15 minute unit hydrographs at Coweeta (bottom).

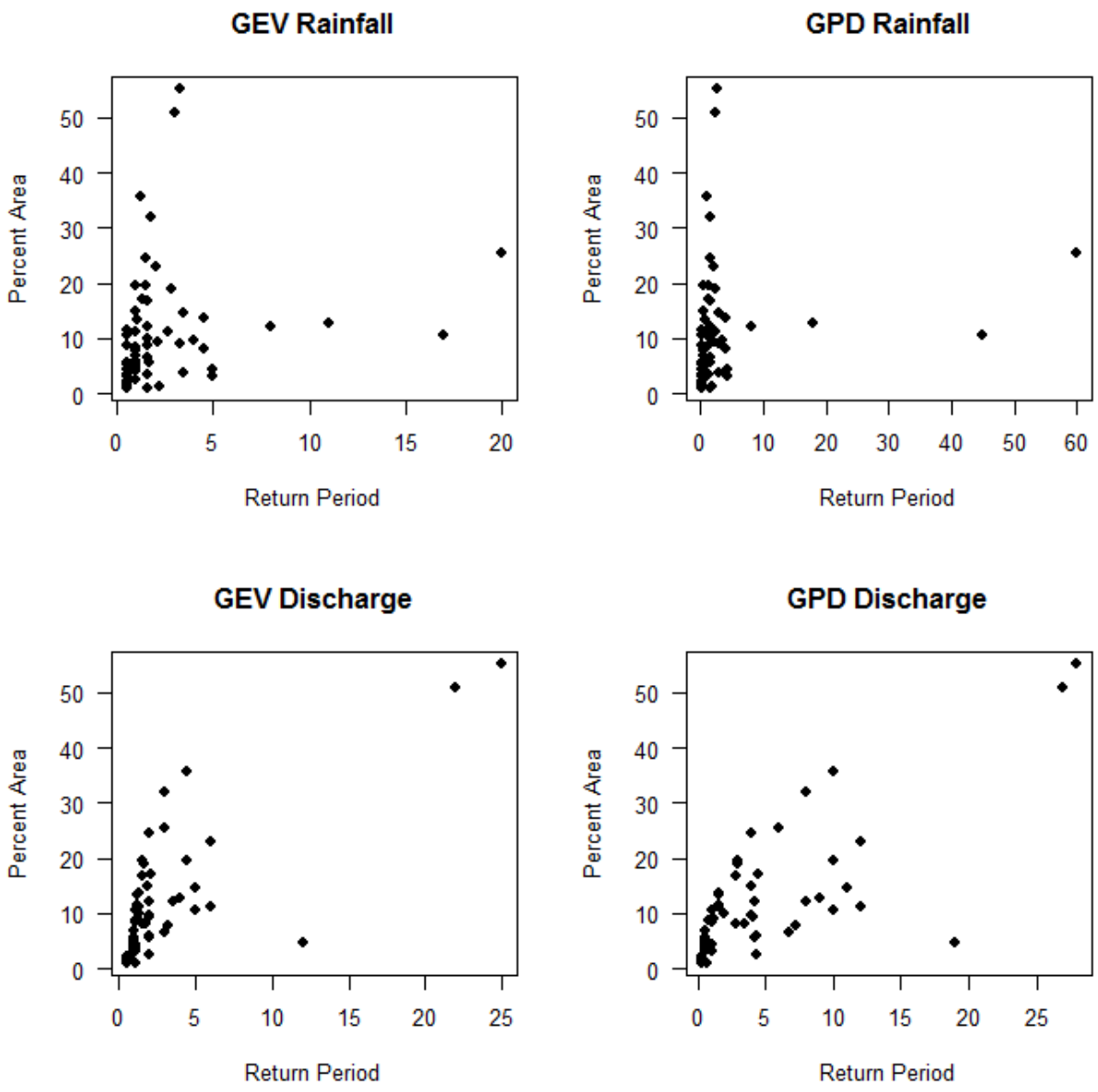

Figure 4.3: Return periods (years) of Panola storms. Return periods were calculated using the Generalized Extreme Value distribution and the Generalized Pareto distribution for both total precipitation and peak discharge.

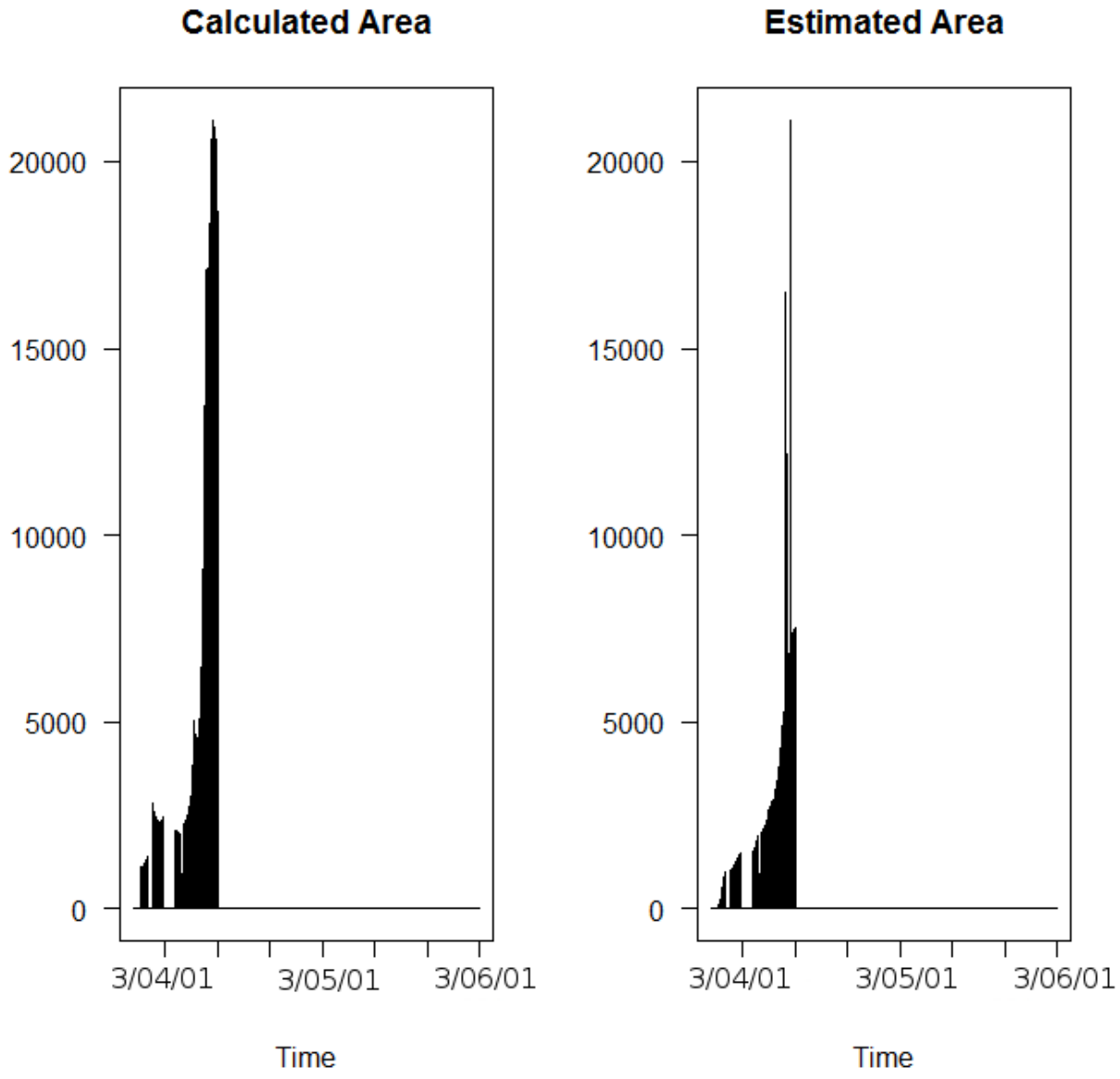

Figure 4.4: Back-calculated area and estimated area for Panola storm 87.

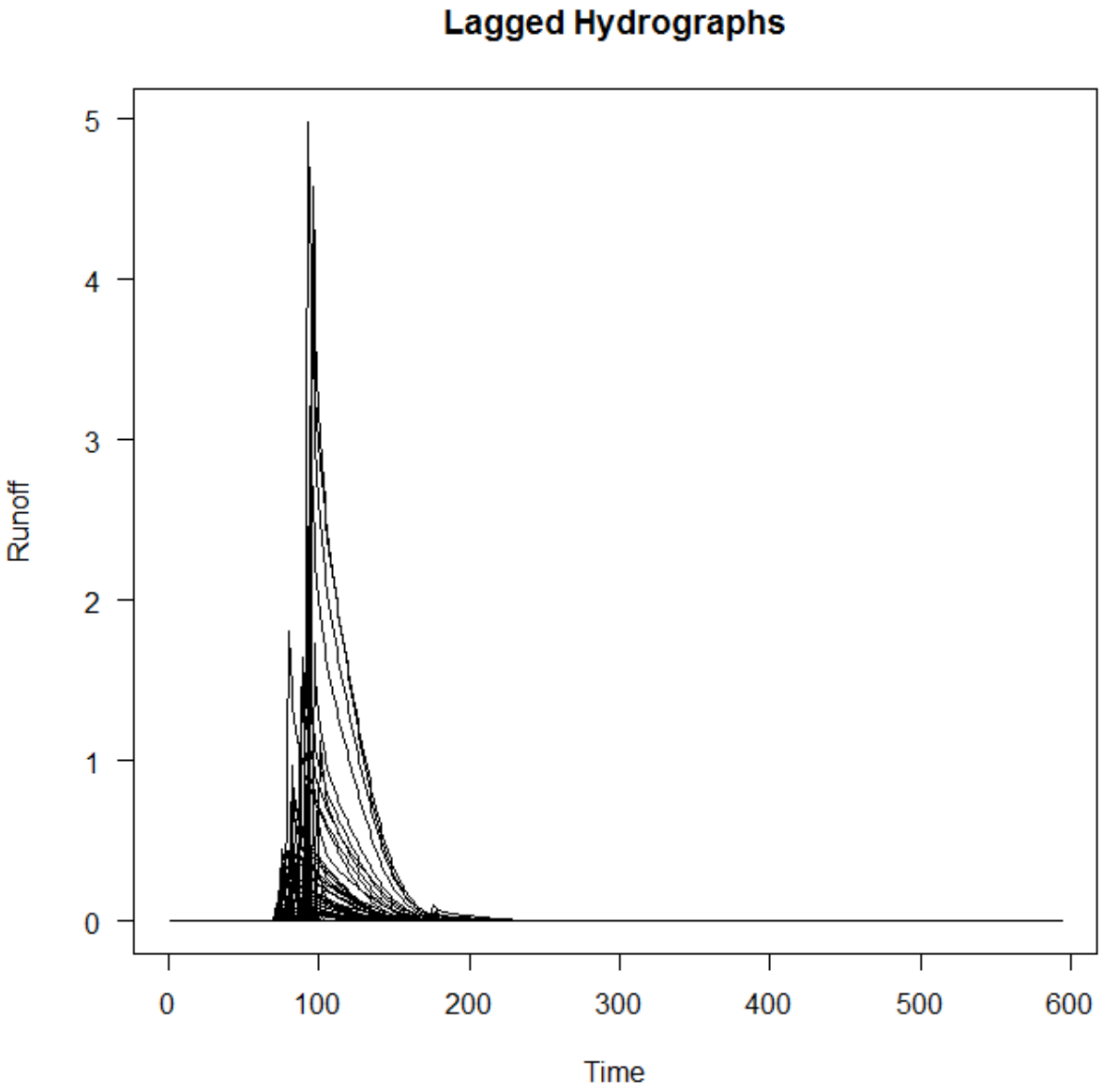

Figure 4.5: Lagged and scaled unit hydrographs for Panola storm 44.

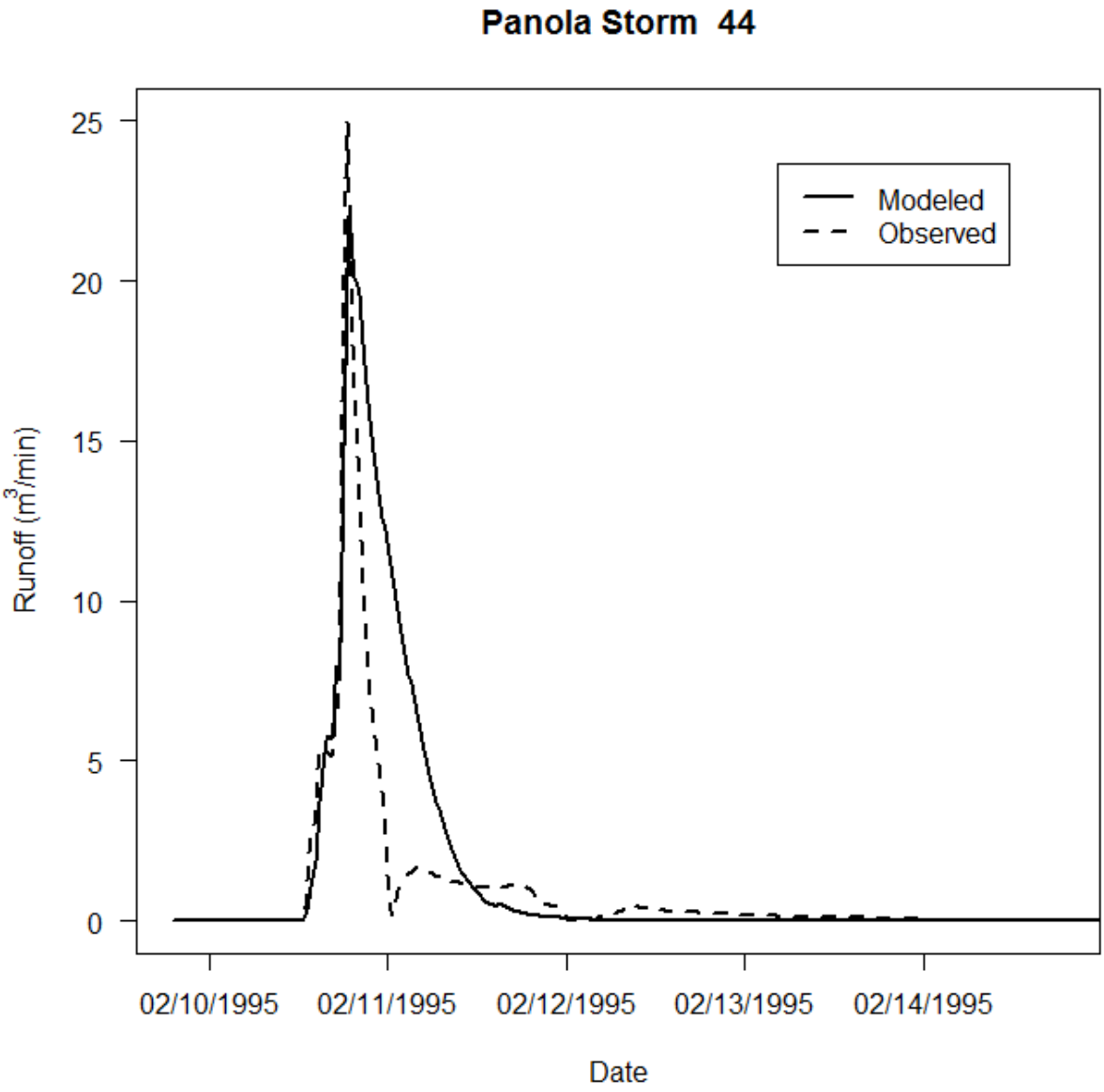

Date	02/11/95	Nash-Sutcliffe	0.62
Time of Concentration	28 hrs	Modified Nash-Sutcliffe	0.54
Contributing Area	99,007 m^2	Observed Peak	24.98
Precipitation	85.1 mm	Modeled Peak	22.04

Figure 4.6: Panola storm 44 storm hydrograph resulting from the convolution of the lagged and scaled unit hydrographs.

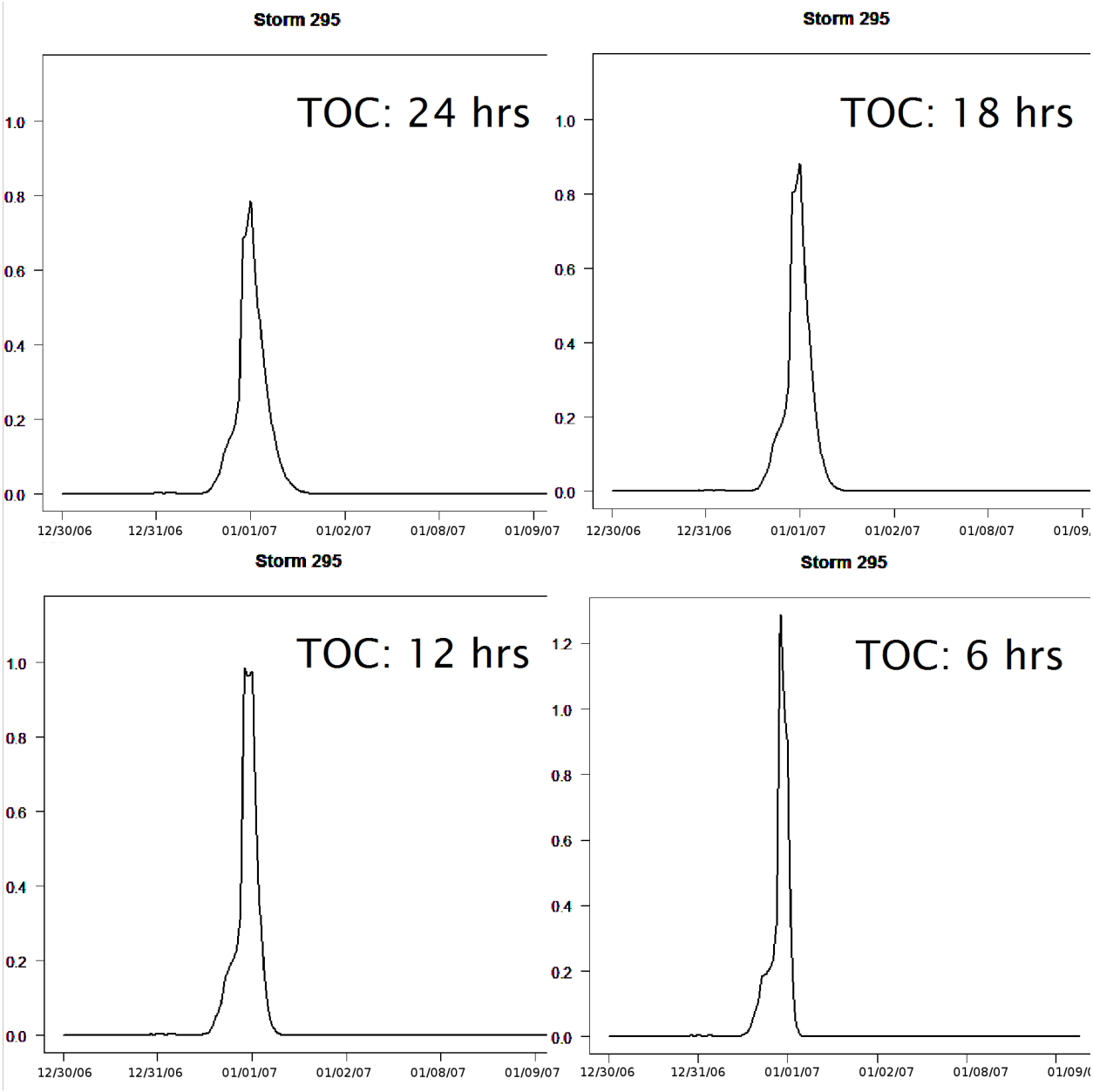

Figure 4.7: Coweeta storm 295 modeled using different times of concentration.

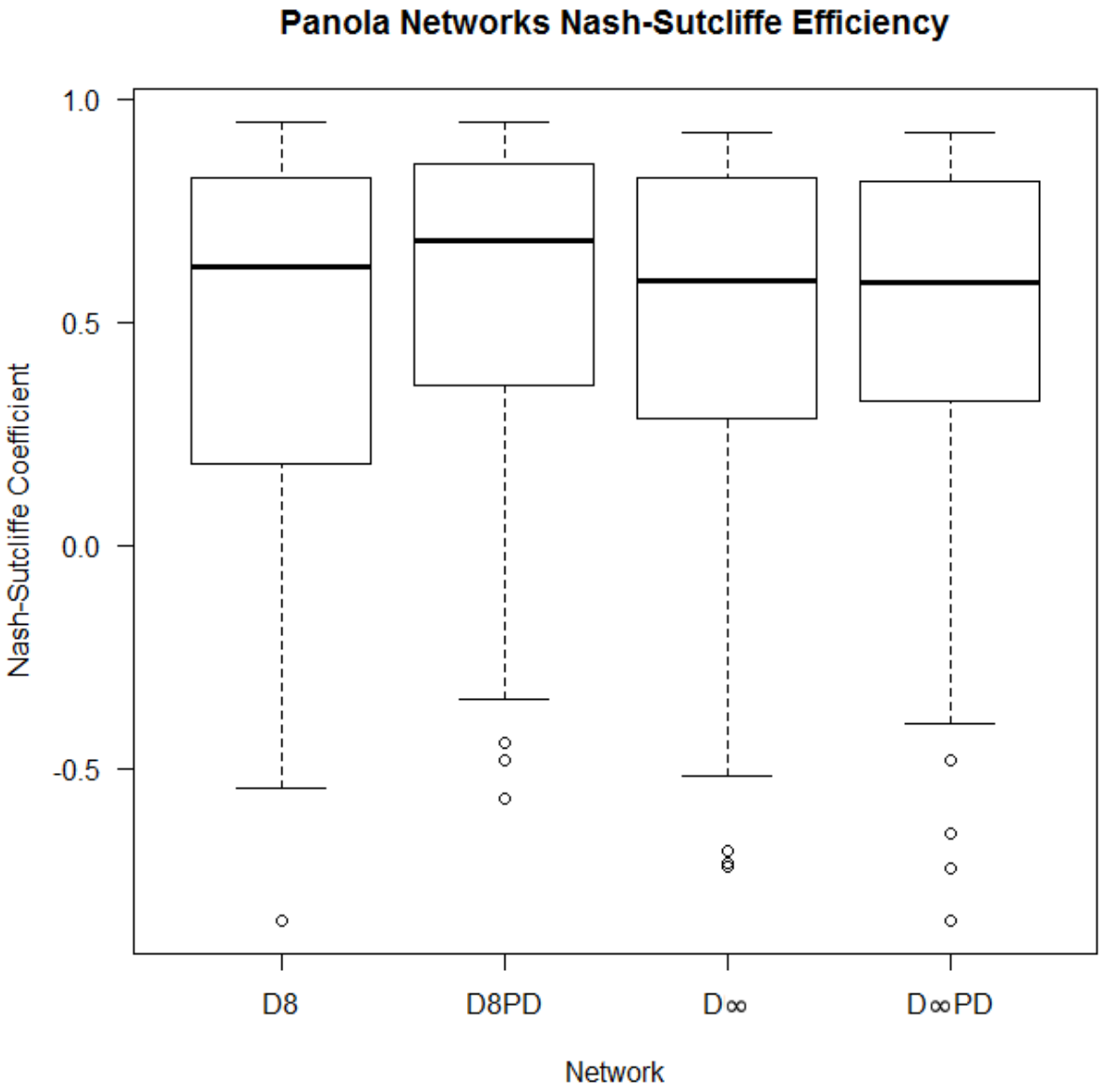

Figure 4.8: Panola storms Nash-Sutcliffe coefficients resulting from each type of network.

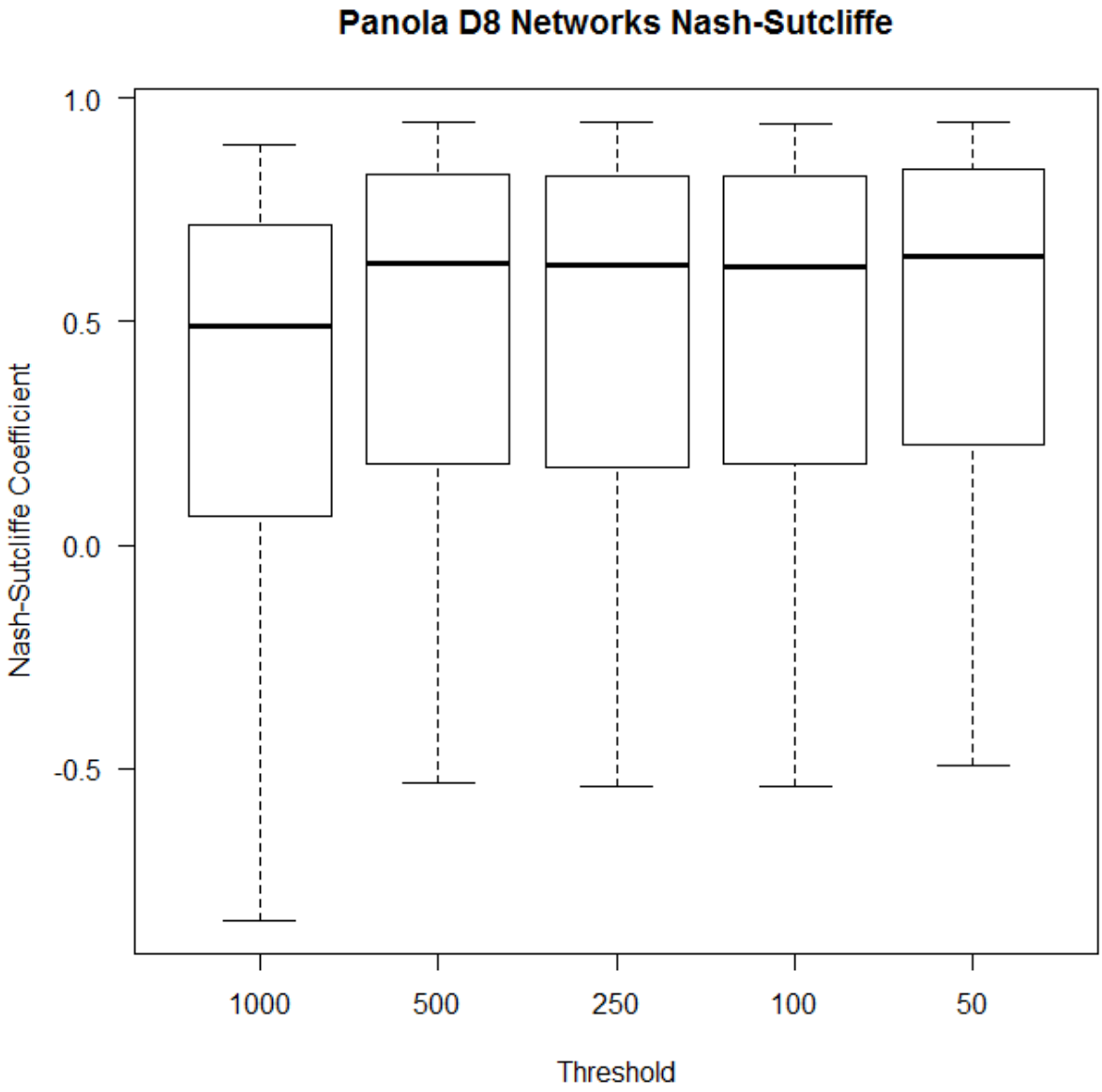

Figure 4.9: Panola storms Nash-Sutcliffe coefficients resulting from different thresholds of D_8 networks.

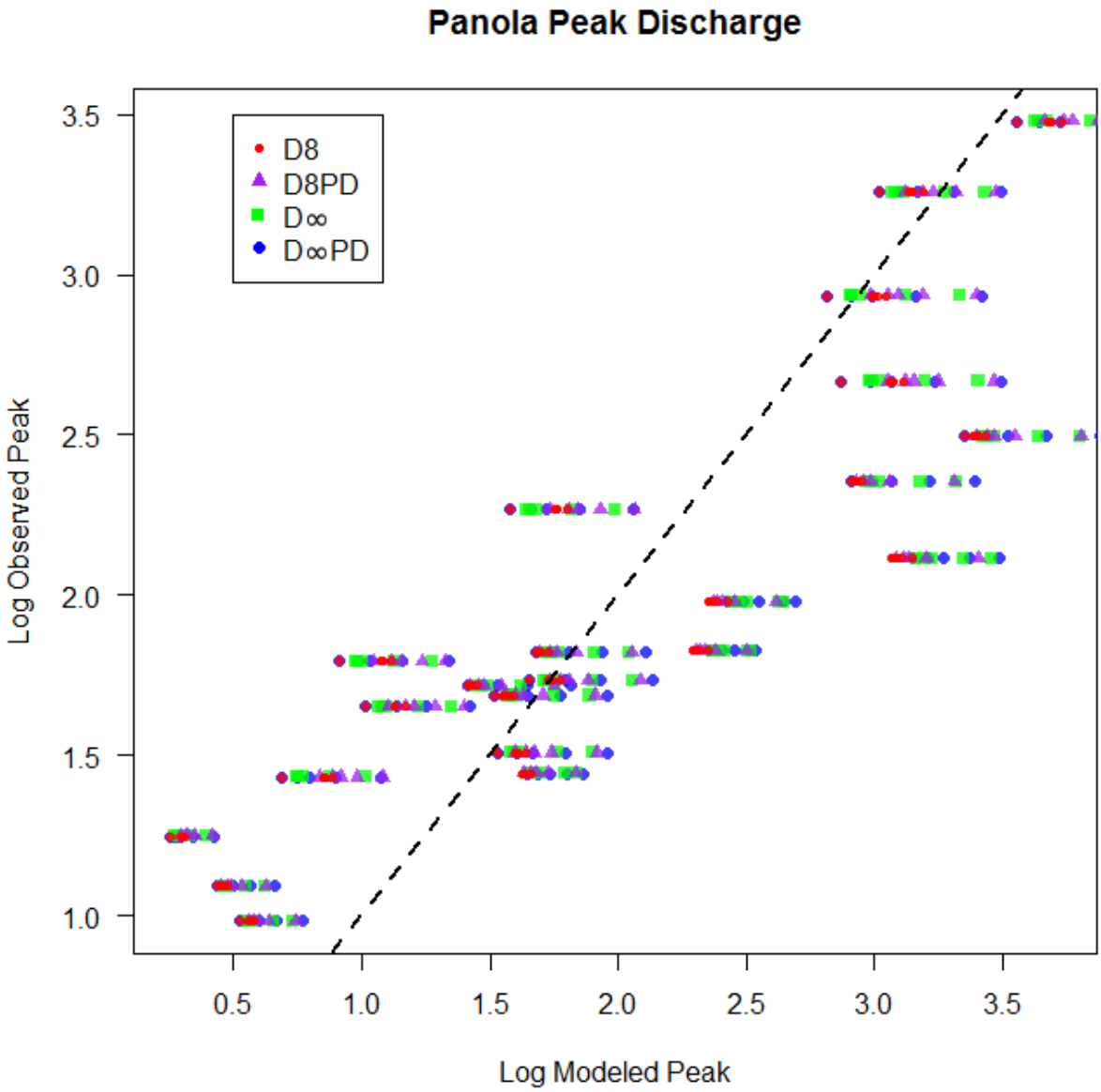

Figure 4.10: Panola storms observed and modeled log of peak discharges. Colors and shapes correspond to the type of network. The dashed line with a slope of one represents where the modeled and observed peaks are equal.

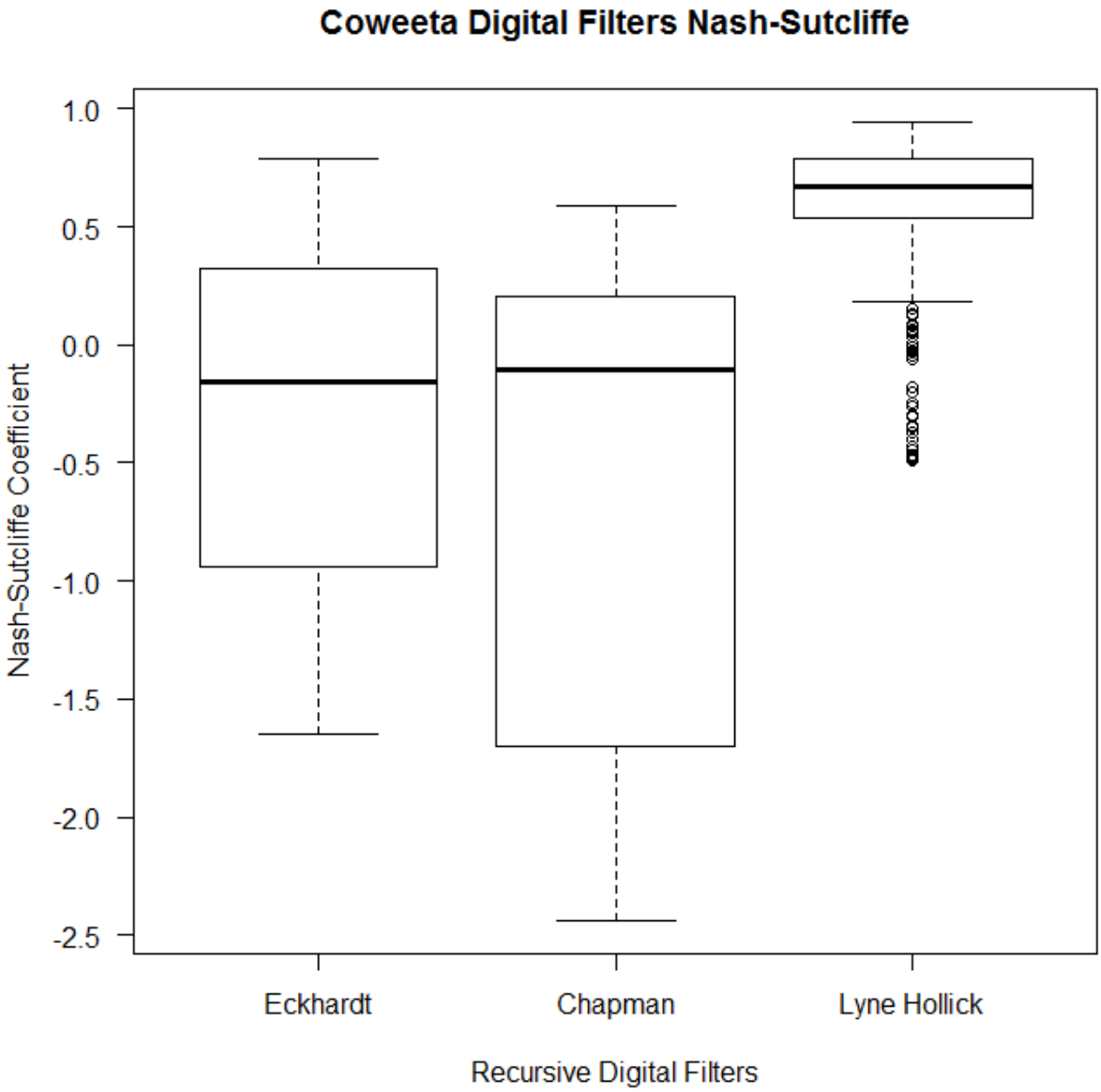

Figure 4.11: Coweeta storms Nash-Sutcliffe coefficients resulting from the different recursive digital filters.

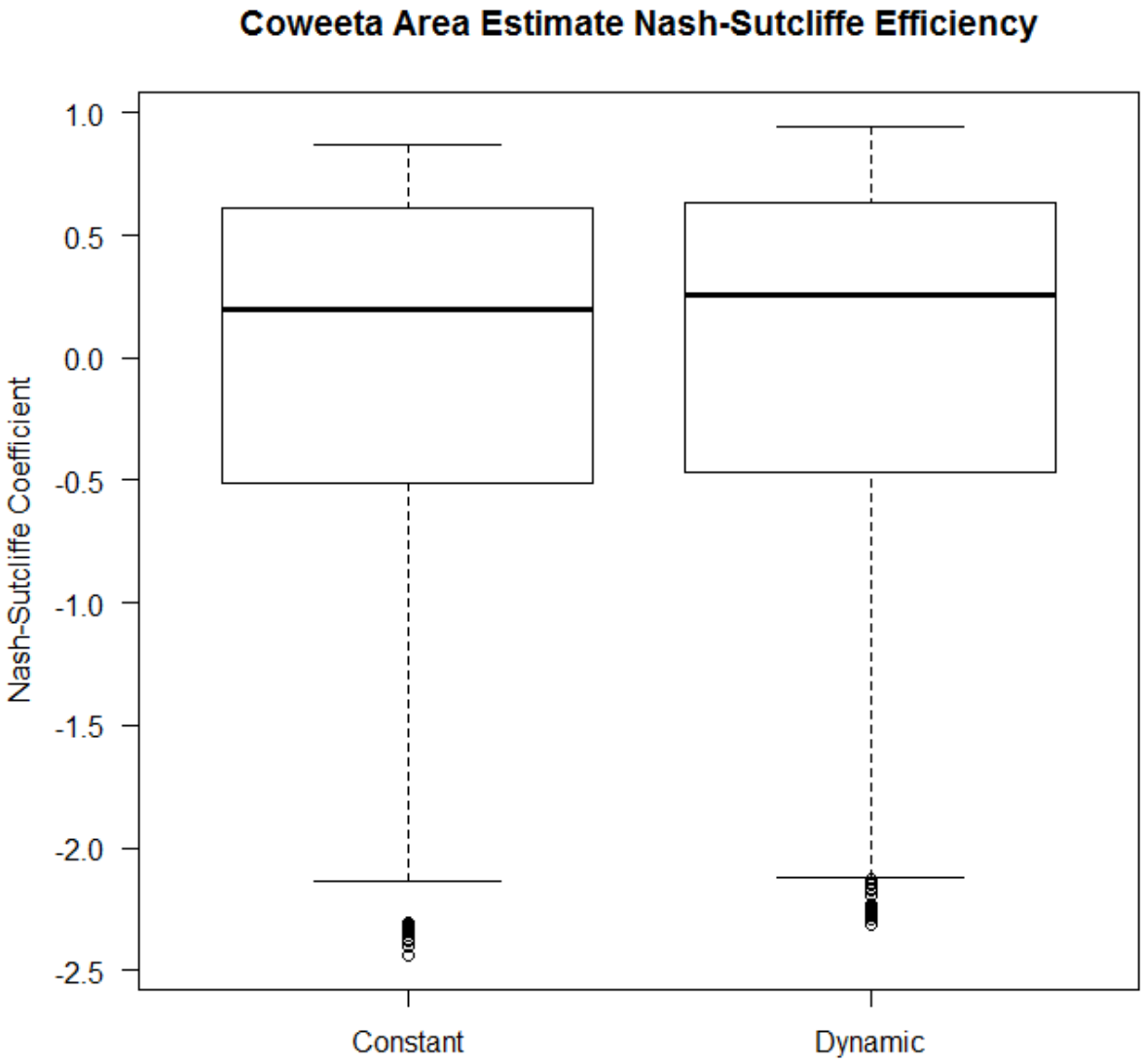

Figure 4.12: Coweeta storms modified Nash-Sutcliffe coefficients resulting from using a constant area and dynamic areas.

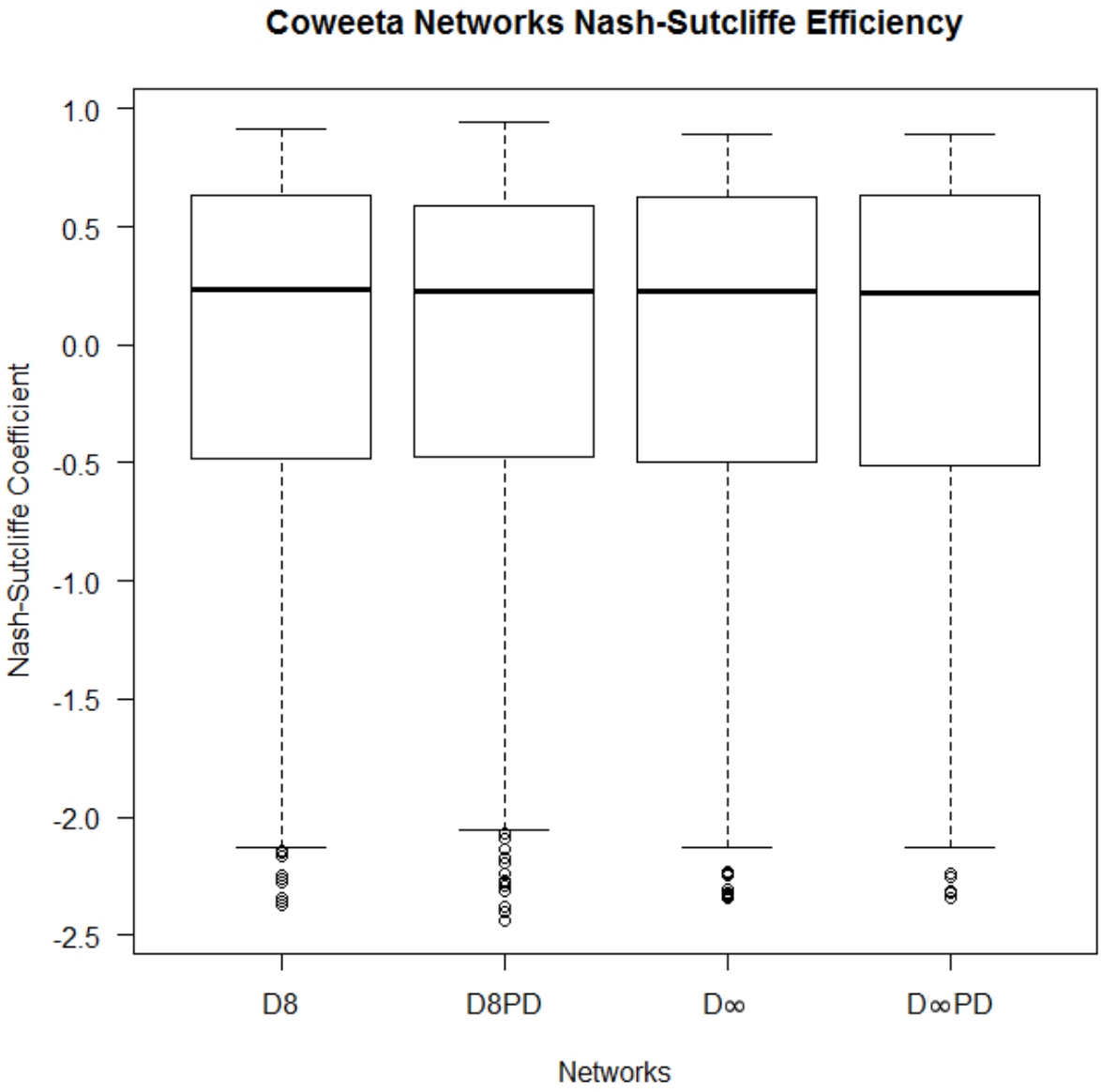

Figure 4.13: Coweeta storms Nash-Sutcliffe coefficients resulting from different types of networks.

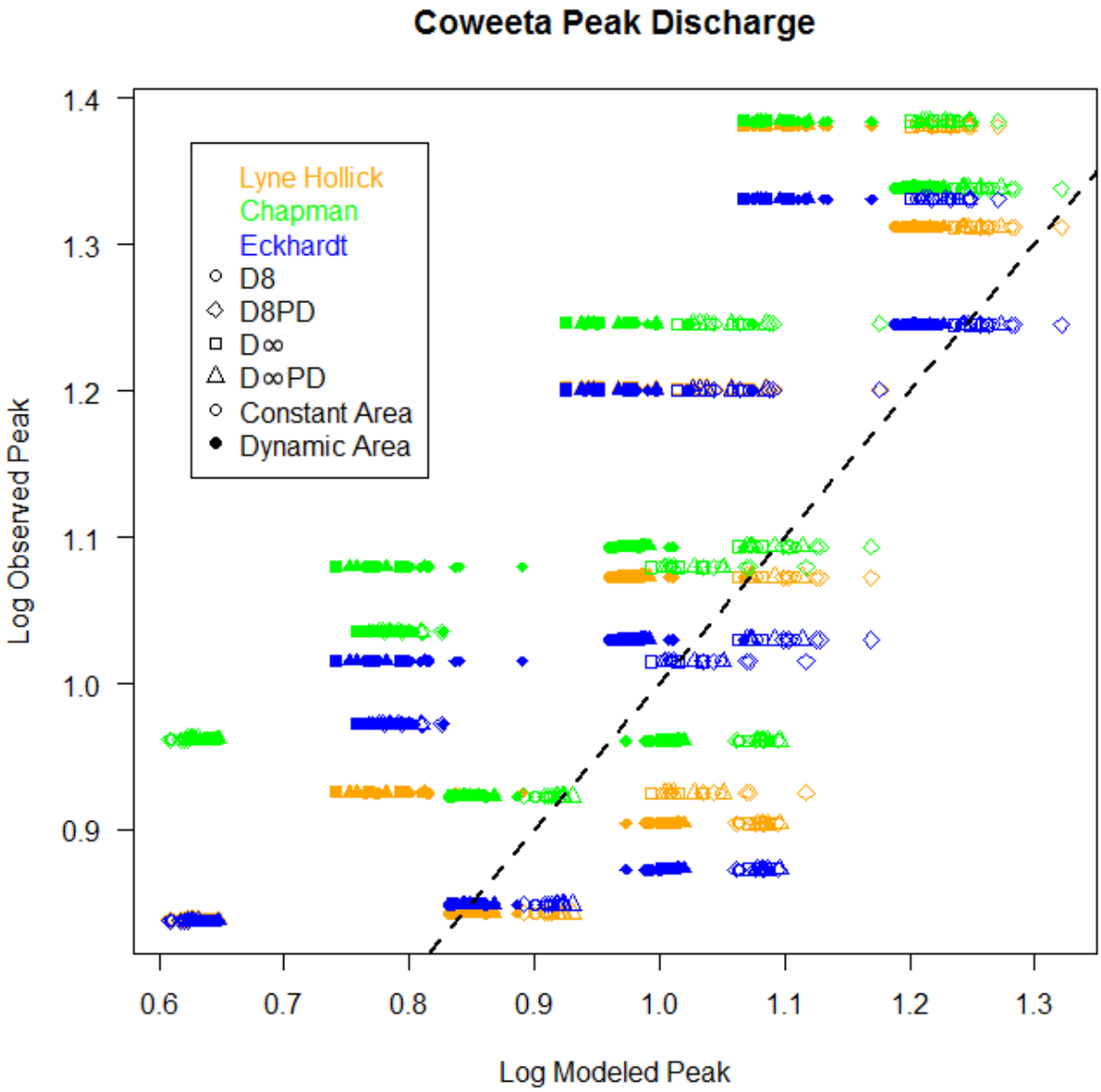

Figure 4.14: Coweeta storms observed and modeled log of peak discharge. Colors correspond to the digital filter type, shapes correspond to the network type, and solid shapes are dynamic areas while hollow shapes are constant areas.

Literature Cited

Cary R. 2011. Dynamic EMMA: Investigating watershed flow pathways using geochemistry and timing at Panola Mountain Research Watershed, Georgia. Thesis University of Georgia, Athens, Georgia.

Chapman T. 1991. Evaluation of automated techniques for base-flow and recession analyses – COMMENT. *Water Resour. Res.* **27**(7): 1783–1784.

Clark CO. 1945. Storage and the unit hydrograph. *Transactions, American Society of Civil Engineers* **10**: 1419-1446.

Cudennec C, Fouad Y, Sumarjo Gatot I, Duchesne J. 2004. A geomorphological explanation of the unit hydrograph concept. *Hydrol. Process.* **18**(4): 603–621.

Dunne T, Taylor CH, Moore TR. 1975. Recognition and prediction of runoff-producing zones in humid regions. Hydrological Sciences – *Bulletin* **3**: 305–327.

Eckhardt K. 2005. How to construct recursive digital filters for baseflow separation. *Hydrological Processes* **19**(2): 507–515.

Fleurant C, Kartiwa B. Roland B. 2006. Analytical model for a geomorphological instantaneous unit hydrograph. *Hydrol. Process.* **20**(18): 3879–3895.

Gilleland E, Katz RW. 2006. Analyzing seasonal to interannual extreme weather and climate variability with the extremes toolkit (extRemes). *Preprints: 18th Conference on Climate Variability and Change, 86th American Meteorological Society (AMS) Annual Meeting* **29**: 2006, Atlanta, Georgia. P2.15.

Kent KM. 1973. A method for estimating volume and rate of runoff in small watersheds. *U.S. Soil Conservation Service.* SCS-TP-149.

Kumar R, Chatterjee C, Singh RD, Lohani AK. Kumar S. 2007. Runoff estimation for an ungauged catchment using geomorphological instantaneous unit hydrograph (GIUH) models. *Hydrological Processes* **21**(14): 1829–1840.

Lyne V, Hollick M. 1979. Stochastic Time variable rainfall runoff modelling. Hydrology and Water Resources Symposium, Institute of Engineers Australia, Perth; 89-92.

Nash J. 1957. The form of the instantaneous unit hydrograph. *International Association of Science and Hydrology* **45**(3): 114:121.

Nash J, Sutcliffe J. 1970. River flow forecasting through conceptual models: 1. Discussion and principles. *Journal of Hydrology* **10**: 282-290.

Peters N, Freer J, Aulenbach B. 2003. Hydrologic dynamics of the Panola Mountain Research Watershed, Georgia, USA. *Ground Water* **41**(7): 973–988.

Rodriguez-Iturbe I, Valdes J. 1979. The geomorphologic structure of hydrologic response. *Water Resources Research* **15**(6): 1409-1420.

Strahler AN. 1957. Quantitative analysis of watershed geomorphology. *American Geophysical Union Transactions* **38**(6): 913-920.

CHAPTER 5

CONCLUSIONS

This thesis presents a comprehensive model that uses the topography and precipitation to predict stormflow based on runoff flow pathways. This model can be applied to ungauged basins because it is based on the topography and does not rely on historical discharge data. The model is fit to storms at Panola Mountain Research Watershed and used to predict storm runoff at Coweeta Hydrologic Laboratory, Watershed 18.

The model is presented in a series of three manuscripts. In the first manuscript, hydrograph separation using recursive digital filters is compared to geochemical hydrograph separation to determine the flow paths that the digital filters define as baseflow and to determine if the filters can be used in ungauged basins. The second manuscript describes the process of extracted dense surface runoff networks from high resolution topography. The self-similar nature of these networks is examined with Horton ratios. The last manuscript uses the extracted networks to calculate the geomorphologic instantaneous unit hydrograph and to model storm runoff. Storms are modeled and compared to observed storms at Panola and Coweeta.

In the first manuscript, independent storms are defined using methods of Restrepo-Posada and Eagleson (1982). Independent storms were found to be separated by six to eight dry hours at Coweeta and Panola. Stormflow and baseflow were defined at Panola

with geochemical hydrograph separation completed by Cary (2011). Recursive digital filters were compared and calibrated to the geochemical separation in order to be used at Coweeta and in ungauged basins. The Lyne and Hollick (1979) and Eckhardt (2005) digital filters produced results that were statistically similar to the geochemically derived baseflows and were found to be estimating shallow groundwater and deep hillslope pathways. The alpha parameter is easily estimated and an independent or regional estimate of the baseflow index is needed to parameterize BFI_{Max}. Nevertheless, the filters do not respond quickly enough to rainfall resulting in delayed peaks and smoother shapes.

In the second manuscript, dense drainage networks are extracted from high resolution topography derived from LiDAR. Four extraction techniques with different assumptions were used to extract networks. The D_8 method assumes single flow directions. The D_8PD method assumes single flow directions and weight concave topography. D_∞ networks assume multiple flow directions. D_∞PD networks assume multiple flow directions and weight concave topography. These methods were used to calculate flow directions for each cell in the watershed. Based on the flow directions, runoff was routed and accumulated to the basin outlet producing flow accumulation maps. These maps were used to extract networks by designating a threshold upstream area at which overland flow occurs.

The networks are used to predict runoff flow paths and the spatial distribution of contributing areas. The self-similar nature and the fractal geometry of the networks were assessed using Horton ratios. In general, the networks were found to be self-similar in terms of bifurcation, stream length, and contributing area. Although, the Coweeta networks were slightly less self-similar, and the Panola networks that were extracted from D_∞ flow

directions were not self-similar in terms of stream lengths. Self-similarity also increases with the density of the network.

The third manuscript derives the geomorphologic instantaneous unit hydrograph (GIUH) from the mean lengths of streams in each Strahler order. The GIUH is used to calculate the unit hydrograph which is scaled by precipitation and contributing area for each time step of a storm. The convolution of hydrographs from each time step produces a final storm hydrograph. The modeled storm hydrographs are compared to observed storms.

The model was fit to storms at Panola by back-calculating the contributing area from observed discharge data. The model performed well in most cases but tended to over-estimate the recession tail of the hydrographs at Panola. The model also tended to under-estimate peak discharge of small storms and over-estimate peak discharge of larger storms at Panola. The type of network did not change model results significantly.

The model was used to predict storms at Coweeta by using digital filters to define stormflow and estimating the contributing areas. A constant area and a dynamic area estimate were used at Coweeta, however, neither significantly improved the model results. Digital filters were used to define observed stormflow and often resulted in large amounts of observed stormflow on the recession tail which the model under-predicted. The Lyne and Hollick filter produced significantly better results than the other filters, although, it is not theoretically the best filter because it does not account for recession. This highlights the need for a digital filter that better matches the observed baseflow at Panola.

Future Research

The results from this thesis show that these methods can be used to predict runoff in ungauged basins. These results also offer insight into how the model can be improved. Comparison of digital filters to geochemical separation reveals that digital filters need to respond quicker to rainfall and have sharper peaks that more closely resemble the discharge hydrograph. The synthesis of a new digital filter that behaves in such a way will improve model results.

An inverse digital filter could also be used to predict total streamflow. The modeled stormflow would be inversely digitally filtered so that the digital filter would be predicting baseflow based on the stormflow. The combination of modeled stormflow and inversely filtered baseflow would then provide an estimate of total streamflow.

The extracted stream networks provide a good estimation of flow paths. However, the initiation points of active streams are not fully understood and change during a storm event. Field observations during storm events would be a useful in determining which parts of the network are active during a storm and how the network changes during a storm. This will also provide insight on how contributing areas change during a storm, which if better understood would further improve model results. Contributing area estimations are paramount to stormflow modeling and often overlooked. An improvement of contributing area estimation would improve model results and be an insight in the field of hydrology.

Different resolution DEMs and different methods of producing DEMs, such as tinning, should be examined to determine how this effects the resulting networks.

There are many different methods of predicting stormflow and unit hydrographs. Different methods of producing instantaneous unit hydrographs should be explored to see how they compare to the methods of Cudennec *et al.* and Fleurant *et al.* Clark's (1945) time-area method is one method that should be explored that might also provide insight to predicting contributing areas.

This model could also be applied to larger watersheds and watersheds of different land use including urban areas. Flow paths would have to be adjusted for areas where the topography does not describe the flow of water, such as through culverts and storm drains. Applying this model to karstic terrain would cause similar problems where the topography does not necessarily describe runoff.

This thesis presents a comprehensive model for predicting storm runoff and contributing areas based on the topography and precipitation. The model performed well given the simplicity of parameters, although, estimates of contributing area would improve results. Nevertheless, the model offers insight into runoff flow pathways and contributing areas by using the topography and structure of the stream network to model storm flow. The model presents a foundation for making predictions in ungauged basins.

LITERATURE CITED

Adams RK, Spotila JA. 2005. The form and function of headwater streams based on field and modeling investigations in the southern Appalachian Mountains. *Earth Surface Processes and Landforms* **30**(12): 1521–1546.

Cary R. 2011. Dynamic EMMA: Investigating watershed flow pathways using geochemistry and timing at Panola Mountain Research Watershed, Georgia. Thesis University of Georgia, Athens, Georgia.

Chapman T. 1991. Evaluation of automated techniques for base-flow and recession analyses – COMMENT. *Water Resour. Res.* **27**(7): 1783–1784.

Clark CO. 1945. Storage and the unit hydrograph. *Transactions, American Society of Civil Engineers* **10**: 1419-1446.

Cudennec C, Fouad Y, Sumarjo Gatot I, Duchesne J. 2004. A geomorphological explanation of the unit hydrograph concept. *Hydrol. Process.* **18**(4): 603–621.

Eckhardt K. 2005. How to construct recursive digital filters for baseflow separation. *Hydrological Processes* **19**(2): 507–515.

Eckhardt K. 2008. A comparison of baseflow indices, which were calculated with seven different baseflow separation methods. *Journal of Hydrology* **352**(1-2): 168–173.

Fleurant C, Kartiwa B. Roland B. 2006. Analytical model for a geomorphological instantaneous unit hydrograph. *Hydrol. Process.* **20**(18): 3879–3895.

Higgins MW, Atkins RL, Crawford TJ, Crawford RF, Brooks R, Cook RB. 1988. The structure, stratigraphy, tectonostratigraphy, and evolution of the southernmost part of the Appalachian Orogen (No. 1044-9612). United States: U. S. Geological Survey: Reston, VA.

Kokkonen TS, Jakeman AJ, Young PC, Koivusalo HJ. 2003. Predicting daily flows in ungauged catchments: model regionalization from catchment descriptors at the Coweeta Hydrologic Laboratory, North Carolina. *Hydrological Processes* **17**(11): 2219–2238.

Kumar R, Chatterjee C, Singh RD, Lohani AK. Kumar S. 2007. Runoff estimation for an ungauged catchment using geomorphological instantaneous unit hydrograph (GIUH) models. *Hydrological Processes* **21**(14): 1829–1840.

Lyne V, Hollick M. 1979. Stochastic Time variable rainfall runoff modelling. Hydrology and Water Resources Symposium, Institute of Engineers Australia, Perth; 89-92.

Peters N, Freer J, Aulenbach B. 2003. Hydrologic dynamics of the Panola Mountain Research Watershed, Georgia, USA. *Ground Water* **41**(7): 973–988.

Restrepo-Posada PJ, Eagleson PS. 1982. Identification of independent rainstorms. *Journal of Hydrology* **55**(1-4): 303–319.

Swank WT, Crossley Jr. DA. 1988. Forest hydrology and ecology at Coweeta. *Ecological Studies* **66**. Springer- Verlag: New York, NY.

Tarboton D. 2012. Terrain Analysis Using Digital Elevation Models (TauDEM). Utah State University. *Available at*: http://hydrology.usu.edu/taudem/taudem5.0/. *Accessed in* January 2013.

APPENDIX A

STREAM NETWORK EXTRACTION

This appendix details the procedures for extracting dense stream networks and estimating contributing area from bare earth LiDAR. The program *Terrain Analysis Using Digital Elevation Models* (TAUDEM)[1] and ESRI's ArcGIS 10.1 are used for these processes. The TauDEM toolbox is used inside of ArcGIS. All raster files must be saved as *.tif* files in order to be used by TauDEM. The process starts with LiDAR in *las* format.

Digital Elevation Models

- **LAS to Multipoint**
    - The raw *las* file is the input.
    - Points have already been classified. Class 2 (ground) is chosen to select only bare earth points.
    - **Point File Information** is run to obtain the average point spacing of the *las* file.
    - The output is a point shapefile.

The point shapefile is then interpolated into a digital elevation model (DEM).

1 http://hydrology.usu.edu/taudem/taudem5.1/index.html

- Natural Neighbors

- The point shapefile is the input.

- Cell size is set to 1 for a one meter DEM.

- Output is a one meter DEM saved as a *.tif* file

Stream Network Extraction

The following processes use the TauDEM toolbox to extract stream networks from the DEM. First, the DEM needs to be hydrologically conditioned so that all cells drain to the outlet.

-Pit Remove

- Inputs the DEM and fills pits so that all cells drain.

The conditioned DEM is used to calculate flow directions from every cell using two methods, D_8 and D_∞.

- D_8 Flow Directions

- Drainage from each cell flows to one of the eight surrounding cells in the direction of steepest downward slope.

- D_∞ Flow Directions

- The angle of steepest slope is found based on a triangular facet. If this occurs between cells the flow will be proportioned between the two adjacent cells based on angle.

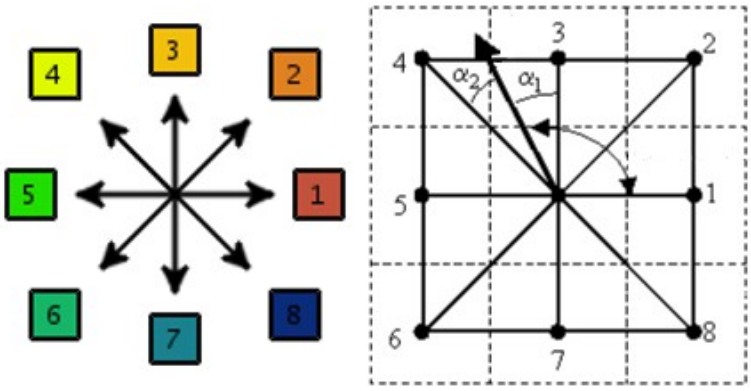

Figure A.1: D8 (left) and D∞ (right) flow directions.

Concave topography concentrates runoff. From the DEM, concave cells are flagged to weight runoff production.

- Peucker Douglas

-Examines all quadrants of four cells, the highest cell is flagged.

The entire DEM is processed, the remaining cells are considered concave.

Flow accumulation maps are produced using a combination of techniques. Each cell yields one unit of runoff which is routed to the basin outlet based on flow directions. A flow accumulation map gives the number of upstream cells flowing through each cell. Versions of these maps are produced using both D_8 and D_∞ flow directions. Versions are also produced by only allowing the concave cells to produce runoff.

- D_8 Contributing Area

- Inputs are D_8 flow directions and a shapefile of the weir or watershed outlet. Only cells upstream of this location are evaluated, this also delineates the watershed.

- Peucker Douglas is input as a weight grid.

- D_∞ Contributing Area

- Inputs are D_∞ flow directions and a shapefile of the weir or watershed outlet. Only cells upstream of this location are evaluated, this also delineates the watershed.
- Peucker Douglas is input as a weight grid.

A stream network is then extracted based on a threshold flow accumulation. Cells greater than the threshold are assigned 1 and less than are assigned to 0.

-**Stream Definition by Threshold**

- Flow accumulation map is the input.
- Threshold is arbitrarily determined. The Threshold can be varied to change the density of the network.

This network is a raster file. It needs to be converted into a polyline shapefile.

-Stream Reach and Watershed

- Inputs include: DEM, D_8 flow direction, flow accumulation map (D_8 or D_∞), weir shapefile, and the stream raster file.
- A polyline shapefile of the network is the output. Several attributes are automatically calculated for each arc in the network including: Strahler order, length, slope, drop, and upstream area.

Networks made from D_∞ flow directions will have segments of the network that do not connect and do not drain to the outlet. This is because D_∞ flow directions allow for divergent flow. The unconnected stream links need to be deleted. The network shapefile is

put into a geodatabase where it is converted to a geometric network. This network is tested for connectivity and the unconnected segments are deleted.

- Create File GDB

- Create Feature Dataset

- Feature Class to Geodatabase

- D_∞ stream network and the weir shapefile are the inputs.

- Create Geometric Network

- The weir is set to a sink.

- Trace Geometric Network

- The task type is set to find disconnected.

- Delete Features

- The input is the traced geometric network, where the disconnected links have been selected and will be deleted.

- Export as Shapefile

Estimating Contributing Area

Contributing area is estimated from the stream network and the surrounding topography. The **Viewshed** function in ArcMap is used to look upslope of the network and flag cells within a certain slope of the network. Before the Viewshed function can be used a few attributes must be added to the stream network shapefile. The first attribute to be added is "OFFSETTA". This is the height of the vantage point above the network and is set to 0.1 meters. "VERT1" is set to 0, this is the angle above horizontal that is examined. "VERT2" is set to -90 and is the angle below horizontal that is examined. "RADIUS" is the radius around each vantage point on the network that is examined and is set to 5 meters. These parameters can be varied but these values produced adequate results.

The network shapefile with the added attributes and the DEM are input into the **Viewshed** function. The output is a raster of the cells that were visible and the number of times that they were visible. This raster is a spatial representation of contributing area based on the topography. The number of visible cells are counted using the **RECLASS** function. The number of cells are equivalent to contributing area in square meters.

This procedure is implemented for various networks of different density to estimate the areas contributing runoff. The Viewshed function, however, is computationally expensive and takes time to run, especially for dense networks.

APPENDIX B:

TRAVEL TIMES

This appendix gives the procedures for applying Manning's equation to a stream network and using it to produce an isochrone map for a watershed. The procedure starts with a stream network produced by the procedures in Appendix A. The network is read into the computer program "R" where Manning's equation is applied and travel times are computed. The "R" package *shapefiles* must be installed in order to read the network file. A matrix of parameters must be input for Manning's equation. A Manning's roughness coefficient, and a stream depth must be input for each Strahler order. The following is the "R" code used in this procedure.

```
library(shapefiles)

dbf <- read.dbf(         "NETWORK.dbf"       , header = TRUE)
#dbf$dbf$Order <- dbf$dbf$Order_
max(dbf$dbf$Order)

#----- INPUT PARAMETERS from 1st Strahler order to Last

parameters <- matrix(c(
     c(0.9, 0.51, 0.3, 0.17, 0.096, 0.055, 0.03),      # N
     c(1, 1, 1, 1, 1, 1, 1),                           #
     c(0.003, 0.006, 0.0125, 0.025, 0.05, 0.1, 0.2)), # Depth
          nrow = 7, ncol = 3, byrow = FALSE)
          colnames(parameters) <- c("N", "Width Parameter",
          "Depth")
```

```
#--------------     MANNING   ----------------

Manning <- function(dbf, parameters) {

#----  GRAB Parameters and Network DATA

N_P            <- parameters[ , "N"]
WIDTH_PARAMETER <- parameters[ , "Width Parameter"]
DEPTH_P        <- parameters[ , "Depth"]
LINKNO         <- dbf$dbf$LINKNO
DSLINKNO  <- dbf$dbf$DSLINKNO
ORDER          <- dbf$dbf$Order
LENGTH         <- dbf$dbf$Length
LENGTH [which(LENGTH == 0)] <- 1
DS_CONT_AR     <- dbf$dbf$DS_Cont_Ar
US_CONT_AR     <- dbf$dbf$US_Cont_Ar
SLOPE          <- dbf$dbf$Slope
SLOPE [which(SLOPE == 0)] <- 0.001


#-------- Generate parameters for each link  ---------

i    <- array(c(1:max(ORDER)))
N    <- c()
N_F  <- function(i) {
          N [ which(ORDER == i)] <<- N_P[i]
                    }
     apply(i, 1, N_F)
WIDTH_P   <- c()
WIDTH_F   <- function(i) {
          WIDTH_P [ which(ORDER == i)] <<- WIDTH_PARAMETER[i]
                         }
     apply(i, 1, WIDTH_F)
DEPTH          <- c()
DEPTH_F   <- function(i) {
          DEPTH [ which(ORDER == i)] <<- DEPTH_P[i]
                         }
     apply(i, 1, DEPTH_F)

#--------  CALCULATE WIDTH    ---------

US_CONT_AR_N <- (US_CONT_AR / max(US_CONT_AR)) * 2
WIDTH <- (((2- US_CONT_AR_N) / WIDTH_P) + 1) * US_CONT_AR_N

#plot(WIDTH~ORDER)
```

```
#mean(WIDTH[which(ORDER== 1)])

#----------    CALCULATE HYDRAULIC RADIUS
HR <- (WIDTH * DEPTH) / (WIDTH + 2*DEPTH)

#----------    CALCULATE VELOCITY
VELOCITY <- (1/N) * HR^(2/3) * SLOPE^(1/2)

#----------    CALCULATE TIME IN LINK (MINUTES)
ARC_TIME <- (LENGTH / VELOCITY) /60

#---------- ACCUMULATED TIME TO OUTLET (MINUTES)
Accumulator <- function(x) {
     sum <- 0
     DSLINK <- 1
     index <- x
path <- function() {
          if(DSLINK > 0) {
               sum <<- sum + ARC_TIME[index]
               DSLINK <<- DSLINKNO[index]
               index <<- which(LINKNO == DSLINK)
               path()
                    }    }
path()
ACCUM_TIME[x] <<- sum
                         }
ACCUM_TIME <- c()
x <- array(c(1:length(LINKNO)))
apply(x, 1, Accumulator)

#---------- BUILD MATRIX ---------

data <-   matrix(c(LINKNO, DSLINKNO, ORDER, LENGTH, DS_CONT_AR,
     US_CONT_AR, SLOPE, WIDTH_P, DEPTH, WIDTH, HR, N, VELOCITY,
     ARC_TIME, ACCUM_TIME),
          nrow = length(LINKNO), ncol = 15, byrow = FALSE)
          colnames(data) <- c("LINKNO", "DSLINKNO", "ORDER",
               "LENGTH", "DS_CONT_AR", "US_CONT_AR", "SLOPE",
               "WIDTH_P", "DEPTH", "WIDTH", "HR", "N",
               "VELOCITY", "ARC_TIME", "ACCUM_TIME")

parameters <- matrix(c(N_P, WIDTH_PARAMETER, DEPTH_P),
     nrow = max(ORDER), ncol = 3, byrow = FALSE)
     colnames(parameters) <- c("N", "Width Parameter", "Depth")

#----------    WRITE DBF ---------
```

```
dbf$dbf$WIDTH_P <- WIDTH_P
dbf$dbf$DEPTH <- DEPTH
dbf$dbf$WIDTH <- WIDTH
dbf$dbf$HR <- HR
dbf$dbf$N <- N
dbf$dbf$VELOCITY <- VELOCITY
dbf$dbf$ARC_TIME <- ARC_TIME
dbf$dbf$ACCUM_TIME <- ACCUM_TIME
write.dbf(dbf, "network.dbf")

#----------    PLOTS     ---------

windows(height=8, width=10)
par(mfrow=c(2, 2))

#----------    WIDTH
WIDTH_MEAN     <- c()
     for( i in 1:max(ORDER)) {
     WIDTH_MEAN[i] <- mean(WIDTH[ which(ORDER == i)])
                              }
plot( WIDTH ~ ORDER, type = "n",
     main= "Width", xlab= "Order", ylab= "Width (m)", las=1)
     points(WIDTH ~ ORDER)
     points(WIDTH_MEAN, pch=16, col="blue", type= "o")

#-----------   PARAMETERS
x <- seq(from= 0.001, to= 1, by= (1-0.001)/max(ORDER))
plot(x, log="y", type="n", main = "Parameters", xlab="Order",
ylab="", las=1, axes=FALSE)
     axis(2, at= c(0.001, 0.01, 0.1, 1), labels=c("0.001",
"0.01", "0.1", "1"), las=1)
     axis(1, labels=TRUE)
     legend(3, 0.005, c("Depth", "N"), col= c("red", "orange"),
pch= c(16, 15))
     points(DEPTH_P, pch=16, col="red", type="o")
     points(N_P, pch=15, col="orange", type="o")
     #points(WIDTH_PARAMETER, pch=17, col="blue", type="o")

#----------    VELOCITY
VELOCITY_MEAN  <- c()
     for( i in 1:max(ORDER)) {
     VELOCITY_MEAN[i] <- mean(VELOCITY[ which(ORDER == i)])
                              }

plot(VELOCITY~ORDER, type ="n", main="Velocity", xlab="Order",
ylab="Velocity (m/s)", las=1)
points(VELOCITY~ORDER)
```

```
points(VELOCITY_MEAN, pch=16, las=1, type="o")

#----------    TIME
ACCUM_TIME_MEAN     <- c()
     for( i in 1:max(ORDER)) {
     ACCUM_TIME_MEAN[i] <- mean(ACCUM_TIME[ which(ORDER == i)])
                                }
ACCUM_TIME_MAX      <- c()
     for( i in 1:max(ORDER)) {
     ACCUM_TIME_MAX[i] <- max(ACCUM_TIME[ which(ORDER == i)])
                                }
plot(ACCUM_TIME_MAX, type="n", las=1, main="Time to Outlet",
xlab="Order", ylab="Time (min)")
     points(ACCUM_TIME ~ ORDER, col="grey50")
     points(ACCUM_TIME_MEAN, pch=16, col="blue", type="o")
     points(ACCUM_TIME_MAX, pch=17, col="red", type= "o")
     legend(5, 225, c("Mean", "Max"), col= c("blue", "red"), pch=
     c(16, 17))

#--------- Time of Concentration  ---------

TOC <- max(ACCUM_TIME)
Lag.Time <- mean(ACCUM_TIME)

return(c(TOC, Lag.Time))
}
MANNING <- Manning(dbf, parameters)
```

This “R” function will rewrite the database file of the network shapefile and add a field entitled “ACCUM_TIME”. This is the travel time to the basin outlet for each link in the network. These travel time values are interpolated across the watershed to produce an isochrone map. First, The network shapefile with the updated database file is read into ArcGIS and converted to a point file.

-Polyline to Raster

- Network shapefile is the input and “Accum_Time” field is selected.

- Raster To Point

The point values are then interpolated with the **Natural Neighbors** function using a cell size of one. The result is an isochrone map of the watershed. A dense network that covers most of the watershed needs to be used for better interpolation. The parameters used for Manning's equation will determine the distribution of travel times.

APPENDIX C:

GEOMORPHOLOGIC INSTANTANEOUS UNIT HYDROGRAPH

Introduction

This appendix presents the methods calculating the geomorphological instantaneous unit hydrograph (GIUH) from a stream network. The GIUH is then used to derive the 15 minute unit hydrograph. The unit hydrograph is scaled by the precipitation and contributing area then lagged and summed to produce storm hydrographs. The modeled hydrographs are then compared to observed hydrographs by comparing Nash-Sutcliffe and modified Nash-Sutcliffe coefficients, peak discharge, and volume.

This procedure is implemented in "R" using the following code. A stream network shapefile produced from procedures in Appendix A and Appendix B is one of the inputs. The other input is a storm *csv* file. These files contain columns for the date, time, precipitation, discharge and baseflow. For Panola storms this file also contains runoff from each source water.

The code for analyzing Coweeta storms differs slightly from the code for Panola storms. The differences include that the Panola data is in minute steps while the Coweeta data is in hourly steps. The Panola data is accumulated into 15 minute time steps while the Coweeta data is disaggregated to 15 minute time steps. For Panola storms the time of concentration is measured from the observed hydrograph and used as a model parameter. For Coweeta storms the time of concentration is set to 0.5 days or 12 hours. The Panola

model calculates the contributing area by dividing the observed runoff by the precipitation rate. This area is used to scale the unit hydrograph and create storm hydrographs. The Coweeta model estimates how the contributing area changes during a storm by multiplying the precipitation rate by the cumulative storm precipitation for each time step. This distribution is scaled so that the maximum is equal to the area of the watershed.

Coweeta

```
storm<-   read.csv("storm.csv", header= TRUE, sep=",")

COWEETA_GIUH <- function(storm) {

#----------    Runoff    ---------
#-----    Convert to CFS from CSM
storm$Q <- storm$Q * 0.0468923002
storm$BK <- storm$BK * 0.0468923002
Runoff <- storm$Q - storm$BK
storm$Runoff <- Runoff
#-----    Cumulative runoff
runoff.cum <- cumsum(Runoff)


#----------    Precipitation  ---------
precip <- storm$Precip
precip <- precip - min(precip)
storm$Precip <- precip
#------   Precipitation rate in minutes
     rate <- diff(storm$Precip, 1, 1)
     Precip.Rate <- c()
     Precip.Rate[1] <- storm$Precip[1]
     Precip.Rate[2:(length(rate)+1)] <- rate
     Precip.Rate <- Precip.Rate
     storm$Precip.Rate <- Precip.Rate
#cum.p <- cumsum(storm$Precip.Rate)
#storm$Precip - storm$Precip.Rate
#diff.p <- storm$Precip - cum.p
#max(diff.p)

#----------  Area in minute steps  ---------
     Area <- storm$Runoff / storm$Precip.Rate
     Area[which(is.nan(Area))] <- 0
```

```
     Area[which(is.infinite(Area))] <- 0
     storm$Area <- Area
     Area.Q <- storm$Q / storm$Precip.Rate
     Area.Q[which(is.nan(Area.Q))] <- 0
     Area.Q[which(is.infinite(Area.Q))] <- 0
     storm$Area.Q <- Area.Q

#----------    Convert to 15 minute data    ----------
storms <- storm
L <- 1:length(storms$Runoff)
runoff <- storms$Runoff
ro <- c()
FIFTEEN_R <- function(x){
     ro <<- c(ro, rep(runoff[x], 4))
                         }
RO <- sapply(L, FIFTEEN_R)
RO <- RO[[length(runoff)]]
precip.rate <- storms$Precip.Rate / 4
pr <- c()
FIFTEEN_PR <- function(x){
     pr <<- c(pr, rep(precip.rate[x], 4))
                         }
PR <- sapply(L, FIFTEEN_PR)
PR <- PR[[length(precip.rate)]]
P <- cumsum(PR)
l <- length(RO)
TI <- seq(from= storms$Time[1], by= 1/24/4, length.out= l)
fifteen <- data.frame(TI=TI, RO=RO, PR=PR, P=P)

#---------- GIUH ----------

library(shapefiles)

toc <- 0.5

     dbf <- read.dbf("network.dbf", header = TRUE)
     stream <- dbf$dbf
     K <- max(stream["Order"])
     k <- c()
     k <- 1:K
     K.less <- K-1
     c <- c(1:K.less)

#----------    Find mean lengths of each Order    --------
#----------    Calculate PDF of each Order        --------
strahler.lengths <-  function(x){
     lk <- c()
```

```
     meanlk <- c()
     pdf_l <- c()
     lk <- (stream$Length [ which(stream$Order == x)])
     lk <- sort(lk, decreasing=FALSE)
     meanlk <- mean(stream$Length [ which(stream$Order == x)])
     pdf_l <- (1/sqrt(2*pi*meanlk)) * (1/sqrt(lk)) * exp(-lk/
     (2*meanlk))
     max_lk <- max(lk) + 5
     freq <- hist(lk, breaks = seq(from=0, to=max_lk, by=1),
     plot=FALSE)
     title <- c("Order", x)
     pdf.exp <- freq$density
     mid.exp <- freq$mids
     pdf_l[is.infinite(pdf_l)] <- 0
     return(list(pdf_l=pdf_l, lk=lk, pdf.exp=pdf.exp,
     mid.exp=mid.exp))
                                    }
pdfs <<- sapply(k, strahler.lengths)

#----------    Convolutions   ---------
#----------    Grab PDFs
x <- c(1)
conv1 <- pdfs[["pdf_l", 1]]
conv1 <- conv1 / (mean(stream$VELOCITY[which(stream$Order == 1)])
* 3.28084)
conv3 <- pdfs[["lk", 1]]
conv2 <- pdfs[["pdf.exp", 1]]
conv2 <- conv2 / (mean(stream$VELOCITY[which(stream$Order == 1)])
* 3.28084)
conv4 <- pdfs[["mid.exp", 1]]

H.K <- (K/2)
     if(is.integer(H.K) == FALSE){
     H.K <- H.K + 0.5}
     #windows(height=10, width=13)
     #par(mfrow=c(2, H.K))

conv <-  function (x){
     x <- c(x + 1)
     pdf.1 <- c()
     pdf.1 <- conv1
     pdf.b <- pdfs["pdf_l", x]
     pdf.2 <- c()
     pdf.2 <- pdf.b[[1]]
     pdf.2 <- pdf.2 / (mean(stream$VELOCITY[which(stream$Order ==
     x)]) * 3.28084)
     lk.1 <- c()
```

```
     lk.1 <- conv3
     lk.1 <- sort(lk.1, decreasing = TRUE)
     length.b <- pdfs["lk", x]
     lk.2 <- c()
     lk.2 <- length.b[[1]]
     lk.2 <- sort(lk.2, decreasing = TRUE)
     pdf.3 <- c()
     pdf.3 <- conv2
     pdf.d <- pdfs["pdf.exp", x]
     pdf.4 <- c()
     pdf.4 <- pdf.d[[1]]
     pdf.4 <- pdf.4 / (mean(stream$VELOCITY[which(stream$Order ==
     x)]) * 3.28084)
     mid.1 <- c()
     mid.1 <- conv4
     mid.1 <- sort(mid.1, decreasing = TRUE)
     mid.b <- pdfs["mid.exp", x]
     mid.2 <- c()
     mid.2 <- mid.b[[1]]
     mid.2 <- sort(mid.2, decreasing = TRUE)

#----------    Convolution    ---------
          conv1 <<- c()
          conv1 <<- convolve(pdf.1, rev(pdf.2), type="o")
          conv2 <<- c()
          conv2 <<- convolve(pdf.3, rev(pdf.4), type="o")
          conv3 <<- c()
          conv3 <<- convolve(lk.1, rev(lk.2), type="o")
          conv3 <<- sort(conv3, decreasing=FALSE)
          conv4 <<- c()
          conv4 <<- convolve(mid.1, rev(mid.2), type="o")

#----------    Export    ----------
Title <- c("Order", x)
plot(conv1 ~ conv3, type="l",
     xlab="", ylab="", main=Title, las=1, lwd=2)
convolutions <- list("Theoretical" = conv1, "Experimental" =
conv2, "Time" = conv3, "Mid" = conv4)
     if(x < K){
               conv(get("x"))
               } else{
               return(list("Theoretical" = conv1, "Experimental"
               = conv2, "Time" = conv3, "Mid" = conv4))
               }    }
convolutions <- conv(x)

#----------    Plot PDFs ---------
```

```
order.plots <- function(x) {
     pdf.a <- pdfs["pdf_l", x]
     pdf.1 <- c()
     pdf.1 <- pdf.a[[1]]
     time.a <- pdfs["lk", x]
     lk.1 <- c()
     lk.1 <- time.a[[1]]
     pdf.c <- pdfs["pdf.exp", x]
     df.3 <- c()
     pdf.3 <- pdf.c[[1]]
     mid.a <- pdfs["mid.exp", x]
     mid.1 <- c()
     mid.1 <- mid.a[[1]]
     title <- c("Order", x)
     plot(pdf.3 ~ mid.1, type="n", main=title, xlab="Length",
     ylab="Probability")
     points(pdf.1 ~ lk.1, type="l", lty=2)
     points(pdf.3 ~ mid.1, type="l", lty=1)
                                }
H.K <- (K/2)
if(is.integer(H.K) == FALSE){
     H.K <- H.K + 0.5}
windows(height=10, width=13)
par(mfrow=c(2, H.K))
     sapply(k, order.plots)

#----------    Scale GIUH     ----------
Time <- convolutions$Time
Unit <- convolutions$Theoretical
Times <- (toc / max (Time)) * Time
Times <- c(0, Times)
Unit <- c(0, Unit)

SIMPSON <- function(x){
     a <- x
     b <- x+1
     d <- c()
     d <- (Times[b] - Times[a]) * ((Unit[a] + Unit[b]) /2)
     d
                    }
x <- 1:length(Time)
Simpson <- sapply(x, SIMPSON)
SS <- sum(Simpson)
Unit <- Unit / SS
Simpson <- sapply(x, SIMPSON)
SS <- round(sum(Simpson))
SS
```

```
     if(SS != 1){print("warning: Not Unit Hydrograph")}
#return(list(Unit=Unit, Times=Times))



#-----------   Unit Hydrograph     ---------

Q <- Unit
iTimes <- seq(from=0, to=max(Times), by=(1/24/4))
interp <- approx(Times, Q, iTimes)
iQ <- interp[[2]]
iTimes <- interp[[1]]

#----------    Calculate 15 minute Unit Hydrograph    --------

MT <- max(iTimes)
lagTimes <- c(iTimes, MT + (1/24/4))
Q1 <-  c(iQ, 0)
Q2 <- c(0, iQ)
windows()
plot(Q1 ~ lagTimes, type="n")
points(Q1 ~ lagTimes, type="l", col="blue")
points(Q2 ~ lagTimes, type="l", col="orange")

unithydrograph <- function(x) {
mean(c(Q1[x], Q2[x]))
                                }
x <- c(1:length(Q1))
UH <- sapply(x, unithydrograph)
Time <- lagTimes

plot(UH ~ lagTimes, type="l", lwd=2, las=1,
main="Unit Hydrograph", xlab="Time", ylab="Q")

#----------    Storm Hydrograph    ----------

UH <- list(UH, Time)

x <- 1:length(fifteen[ ,1])
AM <- max(fifteen$P[which(fifteen$PR == max(fifteen$PR))] *
fifteen$PR[which(fifteen$PR == max(fifteen$PR))])
MS <- (max(fifteen$PR) / 12) / AM
UHLAG <-  function(x){
Ascales <- ((fifteen$PR[x]) * (fifteen$P[x]))
uh <- UH[[1]] * (Ascales * MS) # * 40483.5
                      }
uh <- sapply(x, UHLAG)
```

```
LAG <- function(x){
maximum <- length(uh[ , 1]) + length (fifteen$PR)
laguh <- c( rep(0, x-1), uh[ , x])
dif <- (maximum - length(laguh))
LAGUH <- c(laguh, rep(0, dif))
return(LAGUH)
                    }
LAGUH <- sapply(x, LAG)
m <- which(fifteen$PR == max(fifteen$PR))
m <- LAGUH[ , m[1]]
maximum <- c(1:(length(uh[ , 1]) + length (fifteen$PR)))
hydrograph <- rep(0, length(maximum))
SHYDRO <- function(x){
hydrograph <<- LAGUH[ , x] + hydrograph
                    }
hydro <- sapply(x, SHYDRO)
Time <- seq(from= fifteen$TI[1], by= 1/24/4,
length.out=length(maximum))
hydro <- data.frame(hydrograph=hydrograph, Time=Time)

#----------    COMPARE   ---------

library(hydroGOF)

if(length(hydro$Time) > length(fifteen$TI)){
     dif <- length(hydro$Time) - length(fifteen$TI)
     TI <- c(fifteen$TI, seq(from= (max(fifteen$TI) + 1/24/4), by
     = 1/24/4, length.out = dif))
     RO <- c(fifteen$RO, rep(0, dif))
     Time <- hydro$Time
     hydrograph <- hydro$hydrograph
} else{
     dif <- length(fifteen$TI) - length(hydro$Time)
     Time <- c(hydro$Time, seq(from= (max(hydro$Time) + 1/24/4),
     by = 1/24/4, length.out = dif))
     hydrograph <- c(hydro$hydrograph, rep(0, dif))
     TI <- fifteen$TI
     RO <- fifteen$RO
                                              }
NS <- NSE(hydrograph, RO)
MNS <- mNSE(hydrograph, RO)
MPO <- max(fifteen$RO)
MPM <- max(hydrograph)

SIMPSON <- function(x){
     a <- x
     b <- x+1
```

```
     d <- c()
     d <- (TI[b] - TI[a]) * ((RO[a] + RO[b]) / 2)
     d
                    }
x <- which(hydro$hydrograph > 0)
Simpson <- sapply(x, SIMPSON)
SSO <- sum(Simpson)

SIMPSON <- function(x){
     a <- x
     b <- x+1
     d <- c()
     d <- (hydro$Time[b] - hydro$Time[a]) * ((hydro$hydrograph[a]
     + hydro$hydrograph[b]) /2)
     d
                    }
x <- which(hydro$hydrograph > 0)
Simpson <- sapply(x, SIMPSON)
SSM <- sum(Simpson)

compare <- c(NS, MNS, MPO, MPM, SSO, SSM)
names(compare) <- c("Nash Sutcliffe", "Modified Nash Sutcliffe",
"Observed Peak", "Modeled Peak", "Observed Volume", "Modeled
Volume")
return(compare)
}
```

Panola

```
Panola_GIUH <- function(storm){

#-----    Calculate storm water (Event water + Hillslope2)
runoff <- storm$EW + storm$H2
#-----    Divide by 100 -> mm/min
runoff <- runoff / 100
#-----    Divide by 1000 -> meters/min
runoff <- runoff / 1000

#-----    Multiply by watershed area -> m^3/min
watershed <- 415440
runoff <- runoff * watershed
#-----    Cumulative runoff
runoff.cum <- cumsum(runoff)
storm$Runoff <- runoff
storm$Runoff.Cum <- runoff.cum
```

```
#---------------    Discharge ----------
Q <- storm$Q
#-----    Divide by 100 -> mm/min
Q <- Q /100
#-----    Divide by 1000 -> meters/min
Q <- Q /1000
#-----    Multiply by watershed area -> m^3/min
watershed <- 415440
Q <- Q * watershed
#-----    Cumulative runoff
Q.cum <- cumsum(Q)
storm$Q <- Q
storm$Q.Cum <- Q.cum

#----------    Precipitation  ---------
precip <- storm$Precip * 0.001
precip <- precip - min(precip)
storm$Precip <- precip
#-----    Precip rate minutes
     rate.m <- diff(storm$Precip, 1, 1)
     Precip.Rate.m <- c()
     Precip.Rate.m[1] <- storm$Precip[1]
     Precip.Rate.m[2:(length(rate.m)+1)] <- rate.m
     Precip.Rate.m <- Precip.Rate.m
     storm$Precip.Rate <- Precip.Rate.m
#cum.p <- cumsum(storm$Precip.Rate)
#storm$Precip - storm$Precip.Rate
#diff.p <- storm$Precip - cum.p
#max(diff.p)

#----------    Area minutes   ---------
     Area.min <- storm$Runoff / storm$Precip.Rate
     Area.min[which(is.nan(Area.min))] <- 0
     Area.min[which(is.infinite(Area.min))] <- 0
     storm$Area <- Area.min
     Area.Q <- storm$Q / storm$Precip.Rate
     Area.Q[which(is.nan(Area.Q))] <- 0
     Area.Q[which(is.infinite(Area.Q))] <- 0
     storm$Area.Q <- Area.Q

#----------Plot runoff and precip minutes   ---------
windows(height=7, width=13)
par(mfrow=c(2, 2))
par(mar=c(4, 4, 4, 4) + 0.1)
plot(storm$Runoff ~ storm$Time,
```

```
axes=FALSE, ylim=c(0,(max(storm$Runoff))),
xlim=c(min(storm$Time), max(storm$Time)),
xlab="", ylab="", main="Storm Minutes",
type="l",lty=1, lwd=2, col="blue")
axis(2, ylim=c(0,max(storm$Runoff)),lwd=2,line=0, las =1)
mtext(2,text="Runoff (m^3/min)",line=3)
par(new=T)
plot(storm$Precip ~ storm$Time,
axes=FALSE, ylim=c(0, max(storm$Precip)), xlim=c(min(storm$Time),
max(storm$Time)),
xlab="", ylab="", main="", type="l", col="orange" , las = 1)
axis(4, ylim=c(0,max(storm[ , 2])),col="black", lwd=2, line=0)
mtext(4,text="Precipitation (mm)", line=3)
axis(1,pretty(range( storm$Time),5), lwd=2, line=0)
mtext("Time",side=1,col="black",line=3)
plot(storm$Area ~ storm$Time, type="s", main="Contributing Area",
xlab="Time", ylab="Area (m^2)", las=1)
#return(storm)

#-----------   Accumulate to hourly    ----------
Time <- c()
Precip <- c()
Precip.Rate <- c()
Precip__Rate <- c()
Q <- c()
Base <- c()
H1  <- c()
H2 <- c()
EW <- c()
Base.H1 <- c()
Base.H1.H2 <- c()
Runoff <- c()
Runoff.Cum <- c()
AREA <- c()
Precip_Rate <- c()
a <- 1
b <- 15
c <- b-1
x <- 1
z <- c()
L <- length(storm$Time)/15
     for(i in 1:L) {
          Time[x] <- mean(storm$Time[a:b])
          Precip[x] <- storm$Precip[b]
          Precip_Rate[x] <- storm$Precip[b] - storm$Precip[a]
          Precip__Rate[x] <- sum(storm$Precip.Rate[a:b])
          Q[x] <- mean(storm$Q[a:b])
```

```
          Base[x] <- mean(storm$Base[a:b])
          H1[x] <- mean(storm$H1[a:b])
          H2[x] <- mean(storm$H2[a:b])
          EW[x] <- mean(storm$EW[a:b])
          Base.H1[x] <- mean(storm$Base.H1[a:b])
          Base.H1.H2[x] <- mean(storm$Base.H1.H2[a:b])
          Runoff[x] <- mean(storm$Runoff[a:b])
          Runoff.Cum[x] <- mean(storm$Runoff.Cum[a:b])
          z <- storm$Area[a:b]
          #z <- z[which(z != 0)]
          AREA[x] <- mean(z)
          a <- a + 15
          b <- b + 15
          x <- x + 1
                    }

#----------    Precip rate    ----------
     rate <- diff(Precip, 1, 1)
     Precip.Rate <- c()
     Precip.Rate[1] <- Precip[1]
     Precip.Rate[2:(length(rate)+1)] <- rate

#----------    Areas     -----------

Area <- Runoff / Precip_Rate
Area [which(is.infinite(Area))] <- 0
Area [which(is.nan(Area))] <- 0
AREA [which(is.infinite(AREA))] <- 0
AREA [which(is.nan(AREA))] <- 0
#-----------   Write Storm Table   ----------
storms <- matrix(c(
                   Time, Precip, Precip__Rate, Precip.Rate,
                   Q, Base, H1, H2, EW, Base.H1,
                   Base.H1.H2, Runoff, Runoff.Cum, Area, AREA),
                   nrow=length(Time), ncol=15, byrow=FALSE)
                   colnames(storms) <- c("Time", "Precip",
                   "Precip_Rate", "Precip.Rate", "Q", "Base",
                   "H1", "H2", "EW", "Base.H1", "Base.H1.H2",
                   "Runoff", "Runoff.Cum", "Area", "AREA")

#----------    Plot runoff and precip hours  ---------
minx <- min(Time)
maxx <- max(Time)
maxy <- max(Runoff)
par(mar=c(4, 4, 4, 4) + 0.1)
plot(Runoff ~ Time,
axes=FALSE, ylim=c(0,maxy), xlim=c(minx, maxx),
```

```
xlab="", ylab="", main="Storm Hours",
type="l",lty=1, lwd=2, col="blue")
axis(2, ylim=c(0,maxy+5),lwd=2,line=0, las =1)
mtext(2,text="Runoff (m^3/min)",line=3)
maxy <- max(Precip)
par(new=T)
plot(Precip ~ Time,
axes=FALSE, ylim=c(0, maxy), xlim=c(minx, maxx),
xlab="", ylab="", main="", type="l", col="orange", lwd=2 , las =
1)
axis(4, ylim=c(0, maxy+5),col="black", lwd=2, line=0)
mtext(4,text="Precipitation (mm)", line=3)
axis(1,pretty(range(Time),10), lwd=2, line=0)
mtext("Time",side=1,col="black",line=3)
plot(Area ~ Time, type="l", main="Contributing Area")

#---------     Storm Characteristics    ---------
     Max.Area <- max(Area)
     Peak.Area <- Area[which(Runoff== max(Runoff))]
     Peak.Time <- Time[which(Runoff== max(Runoff))]
     Start <- Time[which(Area == max(Area))]
     zeros <- (Runoff[which(Time > Peak.Time)])
     zeros <- zeros[which(zeros < 0.01)]
     End <- Time[which(Runoff == zeros[1])]
     toc <<- c()
     toc <<- (End - Start)

     Peak.Area.min <- storm$Area[which(storm$Runoff==
     max(storm$Runoff, na.rm = TRUE))]
     Peak.Time.min <- storm$Time[which(storm$Runoff==
     max(storm$Runoff, na.rm = TRUE))]
     max.area <- max(storm$Area)
     max.area.q <- max(storm$Area.Q)
     print(c("Maximum Area Hourly", Max.Area))
     print(c("Contributing area at Hourly Peak Discharge:",
     Peak.Area))
     print(c("Time of Hourly Peak Discharge:", Peak.Time))
     print(c("TOC:", toc))
     print(c("Time of Peak Discharge:", Peak.Time.min))
     print(c("Contributing area at Peak Discharge:",
     Peak.Area.min))
     print(c("Maximum Area", max.area))
     print(c("Discharge Area", max.area.q))
     #return(storms)

#----------    GIUH ----------
     library(shapefiles)
```

```
     dbf <- read.dbf("network.dbf", header = TRUE)
     stream <- dbf$dbf
     K <- max(stream["Order"])
     k <- c()
     k <- 1:K
     K.less <- K-1
     c <- c(1:K.less)

#----------    Calculate Strahler lengths and PDF ---------
strahler.lengths <-  function(x){
     lk <- c()
     meanlk <- c()
     pdf_l <- c()
     lk <- (stream$Length [ which(stream$Order == x)])
     lk <- sort(lk, decreasing=FALSE)
     meanlk <- mean(stream$Length [ which(stream$Order == x)])
     pdf_l <- (1/sqrt(2*pi*meanlk)) * (1/sqrt(lk)) * exp(-lk/
     (2*meanlk))
     max_lk <- max(lk) + 5
     freq <- hist(lk, breaks = seq(from=0, to=max_lk, by=1),
     plot=FALSE)
     title <- c("Order", x)
     pdf.exp <- freq$density
     mid.exp <- freq$mids
     pdf_l[is.infinite(pdf_l)] <- 0

     return(list(pdf_l=pdf_l, lk=lk, pdf.exp=pdf.exp,
     mid.exp=mid.exp))
               }
pdfs <<- sapply(k, strahler.lengths)

#----------    Convolutions   ----------
x <- c(1)
conv1 <- pdfs[["pdf_l", 1]]
conv1 <- conv1 / (mean(stream$VELOCITY[which(stream$Order == 1)])
* 60)
conv3 <- pdfs[["lk", 1]]
conv2 <- pdfs[["pdf.exp", 1]]
conv2 <- conv2 / (mean(stream$VELOCITY[which(stream$Order == 1)])
* 60)
conv4 <- pdfs[["mid.exp", 1]]
H.K <- (K/2)
     if(is.integer(H.K) == FALSE){
          H.K <- H.K + 0.5}
          windows(height=10, width=13)
          par(mfrow=c(2, H.K))
     conv <-  function (x){
```

```
          x <- c(x + 1)
#----------    Extract pdfs
pdf.1 <- c()
pdf.1 <- conv1
pdf.b <- pdfs["pdf_l", x]
pdf.2 <- c()
pdf.2 <- pdf.b[[1]]
pdf.2 <- pdf.2 / (mean(stream$VELOCITY[which(stream$Order == x)])
* 60)
lk.1 <- c()
lk.1 <- conv3
lk.1 <- sort(lk.1, decreasing = TRUE)
length.b <- pdfs["lk", x]
lk.2 <- c()
lk.2 <- length.b[[1]]
lk.2 <- sort(lk.2, decreasing = TRUE)
pdf.3 <- c()
pdf.3 <- conv2
pdf.d <- pdfs["pdf.exp", x]
pdf.4 <- c()
pdf.4 <- pdf.d[[1]]
pdf.4 <- pdf.4 / (mean(stream$VELOCITY[which(stream$Order == x)])
* 60)
mid.1 <- c()
mid.1 <- conv4
mid.1 <- sort(mid.1, decreasing = TRUE)
mid.b <- pdfs["mid.exp", x]
mid.2 <- c()
mid.2 <- mid.b[[1]]
mid.2 <- sort(mid.2, decreasing = TRUE)

#----------    Convolution
     conv1 <<- c()
     conv1 <<- convolve(pdf.1, rev(pdf.2), type="o")
     conv2 <<- c()
     conv2 <<- convolve(pdf.3, rev(pdf.4), type="o")
     conv3 <<- c()
     conv3 <<- convolve(lk.1, rev(lk.2), type="o")
     conv3 <<- sort(conv3, decreasing=FALSE)
     conv4 <<- c()
     conv4 <<- convolve(mid.1, rev(mid.2), type="o")

#----------- Export ---------
     Title <- c("Order", x)
     plot(conv1 ~ conv3, type="l",
     xlab="", ylab="", main=Title, las=1, lwd=2)
```

```
     convolutions <- list("Theoretical" = conv1, "Experimental" =
     conv2, "Time" = conv3, "Mid" = conv4)
               if(x < K){
               conv(get("x"))
               } else{
               return(list("Theoretical" = conv1, "Experimental"
               = conv2, "Time" = conv3, "Mid" = conv4))
               }}
     convolutions <- conv(x)

#----------    Plot PDFs ---------
     order.plots <- function(x) {
     pdf.a <- pdfs["pdf_l", x]
     pdf.1 <- c()
     pdf.1 <- pdf.a[[1]]
     time.a <- pdfs["lk", x]
     lk.1 <- c()
     lk.1 <- time.a[[1]]
     pdf.c <- pdfs["pdf.exp", x]
     df.3 <- c()
     pdf.3 <- pdf.c[[1]]
     mid.a <- pdfs["mid.exp", x]
     mid.1 <- c()
     mid.1 <- mid.a[[1]]
     title <- c("Order", x)
     plot(pdf.3 ~ mid.1, type="n", main=title, xlab="Length",
     ylab="Probability")
     points(pdf.1 ~ lk.1, type="l", lty=2)
     points(pdf.3 ~ mid.1, type="l", lty=1)
     }
H.K <- (K/2)
if(is.integer(H.K) == FALSE){
     H.K <- H.K + 0.5}
windows(height=10, width=13)
par(mfrow=c(2, H.K))
sapply(k, order.plots)

#-----------   Scale Instantaneous Unit Hydrograph    ---------
Time <- convolutions$Time
Unit <- convolutions$Theoretical
Times <- (toc / max (Time)) * Time
Times <- c(0, Times)
Unit <- c(0, Unit)

SIMPSON <- function(x){
     a <- x
     b <- x+1
```

```
     d <- c()
     d <- (Times[b] - Times[a]) * ((Unit[a] + Unit[b]) /2)
     d
                    }
x <- 1:length(Time)
Simpson <- sapply(x, SIMPSON)
SS <- sum(Simpson)
Unit <- Unit / SS
Simpson <- sapply(x, SIMPSON)
SS <- round(sum(Simpson))
SS
     if(SS != 1){print("warning: Not Unit Hydrograph")}
     #windows()
     plot(Unit ~ Times, type="l", main="Instantaneous Unit
     Hydrograph",
     xlab="Time", ylab="Probability",
     las=1, lwd=2)
IUH <- (list(Unit=Unit, Times=Times))


#----------    Unit Hydrograph     ---------
Q <- IUH[[1]]
Times <- IUH[[2]]
iTimes <- seq(from=0, to=max(Times), by=(1/24/4))
interp <- approx(Times, Q, iTimes)
iQ <- interp[[2]]
iTimes <- interp[[1]]

#---------- Calculate 15 minute Unit Hydrograph
MT <- max(iTimes)
lagTimes <- c(iTimes, MT + (1/24/4))
Q1 <-  c(iQ, 0)
Q2 <- c(0, iQ)
windows()
     plot(Q1 ~ lagTimes, type="n")
     points(Q1 ~ lagTimes, type="l", col="blue")
     points(Q2 ~ lagTimes, type="l", col="orange")
unithydrograph <- function(x) {
          mean(c(Q1[x], Q2[x]))
                              }
x <- c(1:length(Q1))
UH <- sapply(x, unithydrograph)
plot(UH ~ lagTimes, type="l", lwd=2, las=1,
main="Unit Hydrograph", xlab="Time", ylab="Q")
Time <- lagTimes
UH <- (list(UH=UH, Time=Time))
```

```
#----------    Storm Hydrograph    ---------

x <- 1:length(storms[ ,1])
SPrecip <- storms[ , "Precip.Rate"]
SRunoff <- storms[ , "Runoff"]
STime <- storms[ , "Time"]
SArea <- sqrt(storms[ , "AREA"]) #/ (100 * 2)
UHLAG <-  function(x){
uh <- UH[[1]] * (SPrecip[x] * SArea[x])
                    }
uh <- sapply(x, UHLAG)
LAG <- function(x){
maximum <- length(uh[ , 1]) + length(SPrecip)
laguh <- c( rep(0, x-1), uh[ , x])
dif <- (maximum - length(laguh))
LAGUH <- c(laguh, rep(0, dif))
return(LAGUH)
               }
LAGUH <- sapply(x, LAG)
#----------    PLOT LAGS ---------
m <- which(SPrecip == max(SPrecip))
m <- LAGUH[ , m[1]]
maximum <- c(1:(length(uh[ , 1]) + length (SPrecip)))
windows()
plot(m ~ maximum, type = "n", ylab="", xlab="")
PLOTHYDROG <- function(x){
y <- LAGUH[ ,x]
points(y ~ maximum, type="l")
                         }
sapply(x, PLOTHYDROG)
hydrograph <- rep(0, length(maximum))
SHYDRO <- function(x){
hydrograph <<- LAGUH[ , x] + hydrograph
}
hydro <- sapply(x, SHYDRO)
Time <- seq(from= STime[1], by= 1/24/4,
length.out=length(maximum))
if(max(hydrograph) > max(SRunoff)) {
windows()
plot(hydrograph ~ Time, type="n", las=1,
xlab="Time (days)", ylab="Runoff (m^3/min)", main = snum)
points(hydrograph ~ Time, lwd=2, type="l")
points(SRunoff ~ STime, lwd=2, type="l", lty=2)
} else{
#windows()
plot(SRunoff ~ STime, type="n", las=1,
xlab="Time (days)", ylab="Runoff (m^3/min)", main= snum)
```

```
points(hydrograph ~ Time, lwd=2, type="l")
points(SRunoff ~ STime, lwd=2, type="l", lty=2)
}
hydro <- data.frame(hydrograph=hydrograph, Time=Time)

#---------     Compare   ---------
library(hydroGOF)
if(length(hydro$Time) > length(storms[ , "Time"])){
     dif <- length(hydro$Time) - length(storms[ , "Time"])
          TI <- c(storms[ , "Time"], seq(from= (max(storms[ ,
          "Time"]) + 1/24/4), by = 1/24/4, length.out = dif))
          RO <- c(storms[ , "Runoff"], rep(0, dif))
          Time <- hydro$Time
          hydrograph <- hydro$hydrograph
     } else{
          dif <- length(storms[ , "Time"]) - length(hydro$Time)
          Time <- c(hydro$Time, seq(from= (max(hydro$Time) +
          1/24/4), by = 1/24/4, length.out = dif))
          hydrograph <- c(hydro$hydrograph, rep(0, dif))
          TI <- storms[ , "Time"]
          RO <- storms[ , "Runoff"]
          }
NS <- NSE(hydrograph, RO)
MNS <- mNSE(hydrograph, RO)
MPO <- max(RO)
MPM <- max(hydrograph)
SIMPSON <- function(x){
     a <- x
     b <- x+1
     d <- c()
     d <- (TI[b] - TI[a]) * ((RO[a] + RO[b]) / 2)
     d
                    }
x <- which(hydro$hydrograph > 0)
Simpson <- sapply(x, SIMPSON)
SSO <- sum(Simpson)
SIMPSON <- function(x){
     a <- x
     b <- x+1
     d <- c()
     d <- (hydro$Time[b] - hydro$Time[a]) * ((hydro$hydrograph[a]
     + hydro$hydrograph[b]) /2)
     d
                    }
x <- which(hydro$hydrograph > 0)
Simpson <- sapply(x, SIMPSON)
SSM <- sum(Simpson)
```

```
compare <- c(NS, MNS, MPO, MPM, SSO, SSM, toc)
return(compare)
}
```

The final result of this code is a graph of both the modeled and observed hydrograph for the specified storm. Various comparisons are output from the model including Nash-Sutcliffe and modified Nash-Sutcliffe coefficients, observed and modeled peak discharge and volume.

APPENDIX D: MODELED STORMS

Panola Modeled Storms

This appendix presents the results for the modeled storms. The hydrographs shown in this appendix were modeled using D8 networks with an extraction threshold of 250.

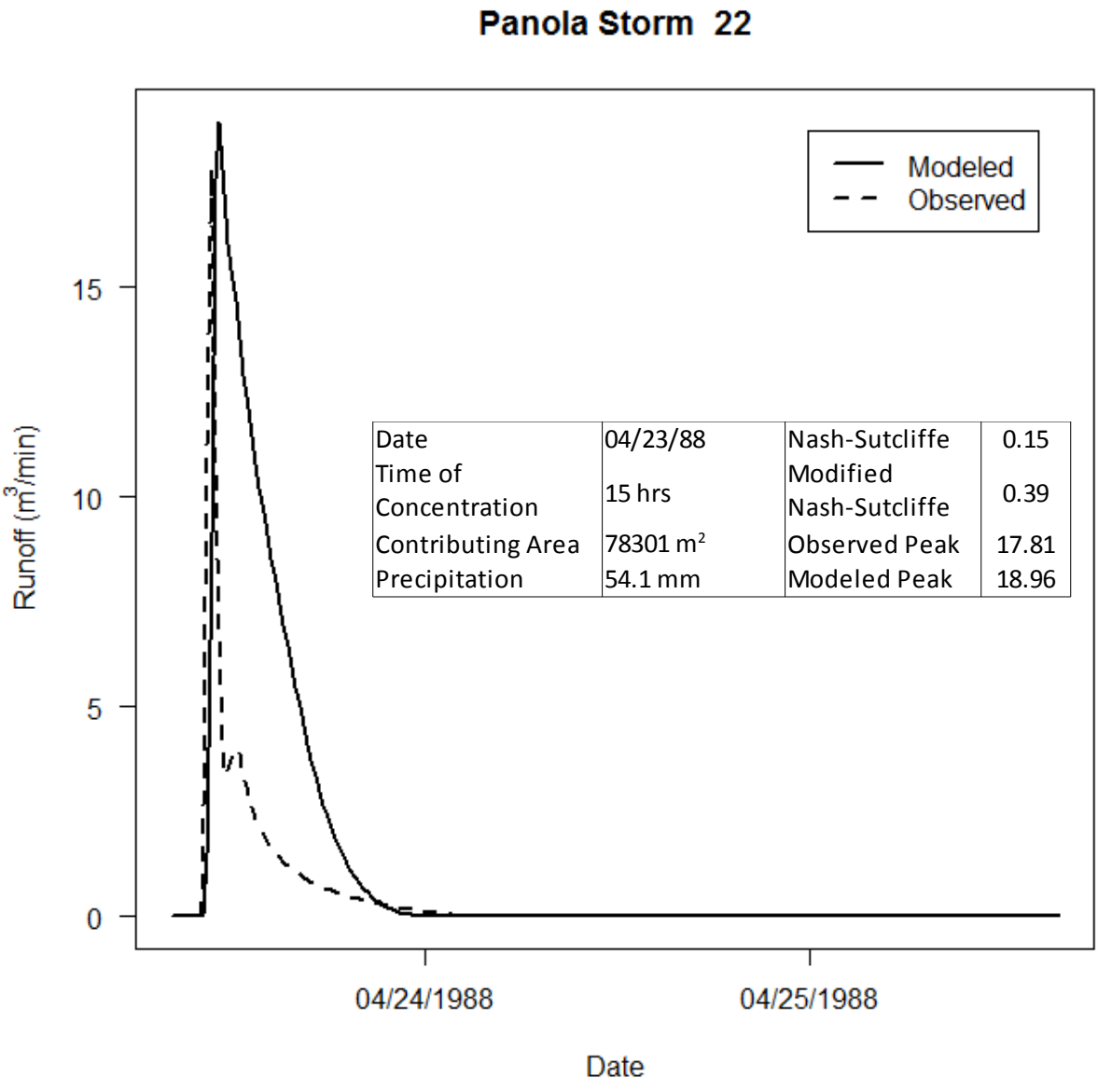

Figure D.1: Panola storm 22.

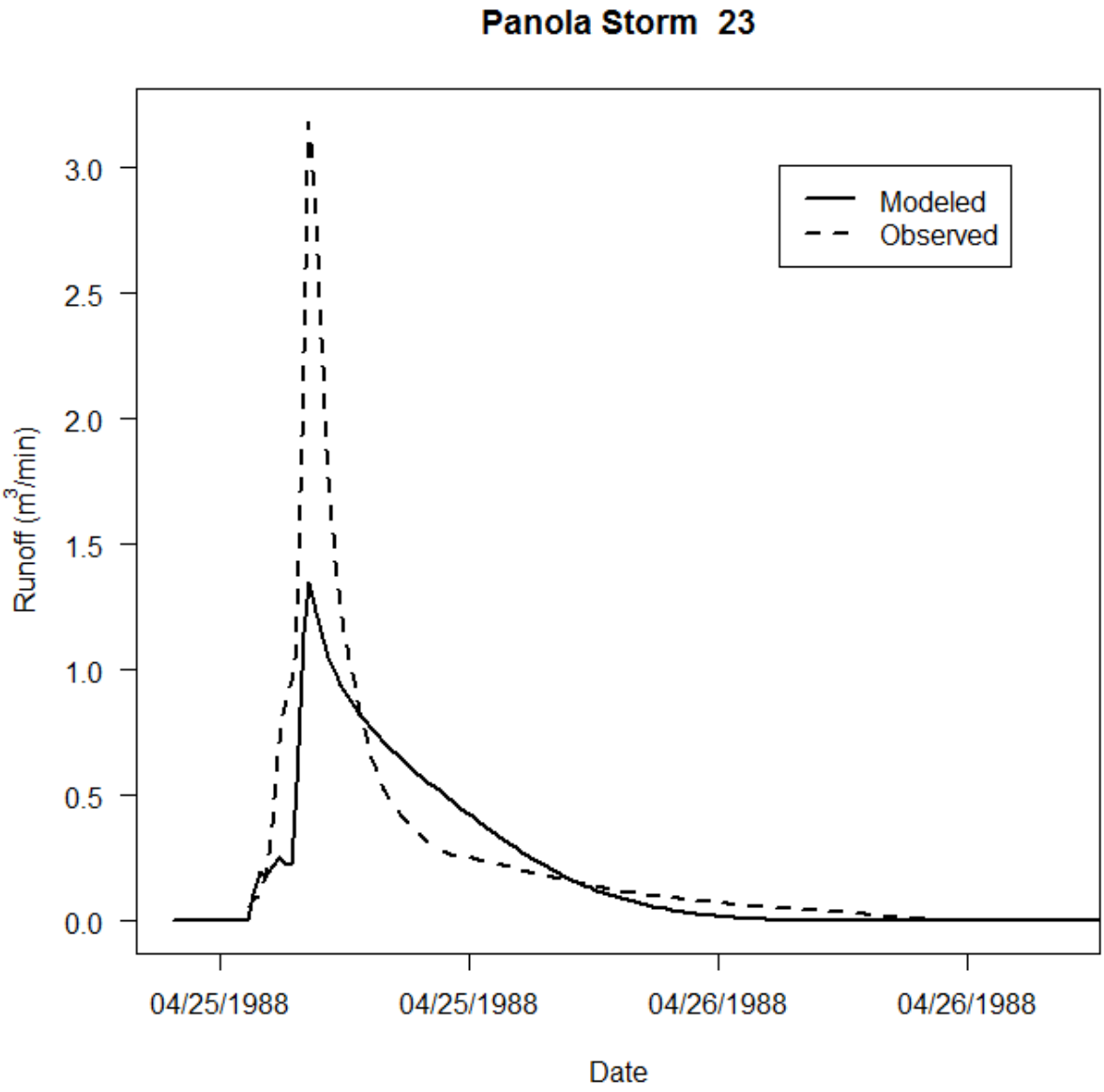

Date	04/25/88	Nash-Sutcliffe	0.82
Time of Concentration	25 hrs	Modified Nash-Sutcliffe	0.71
Contributing Area	7,309 m^2	Observed Peak	3.18
Precipitation	17.3 mm	Modeled Peak	1.34

Figure D.2: Panola storm 23.

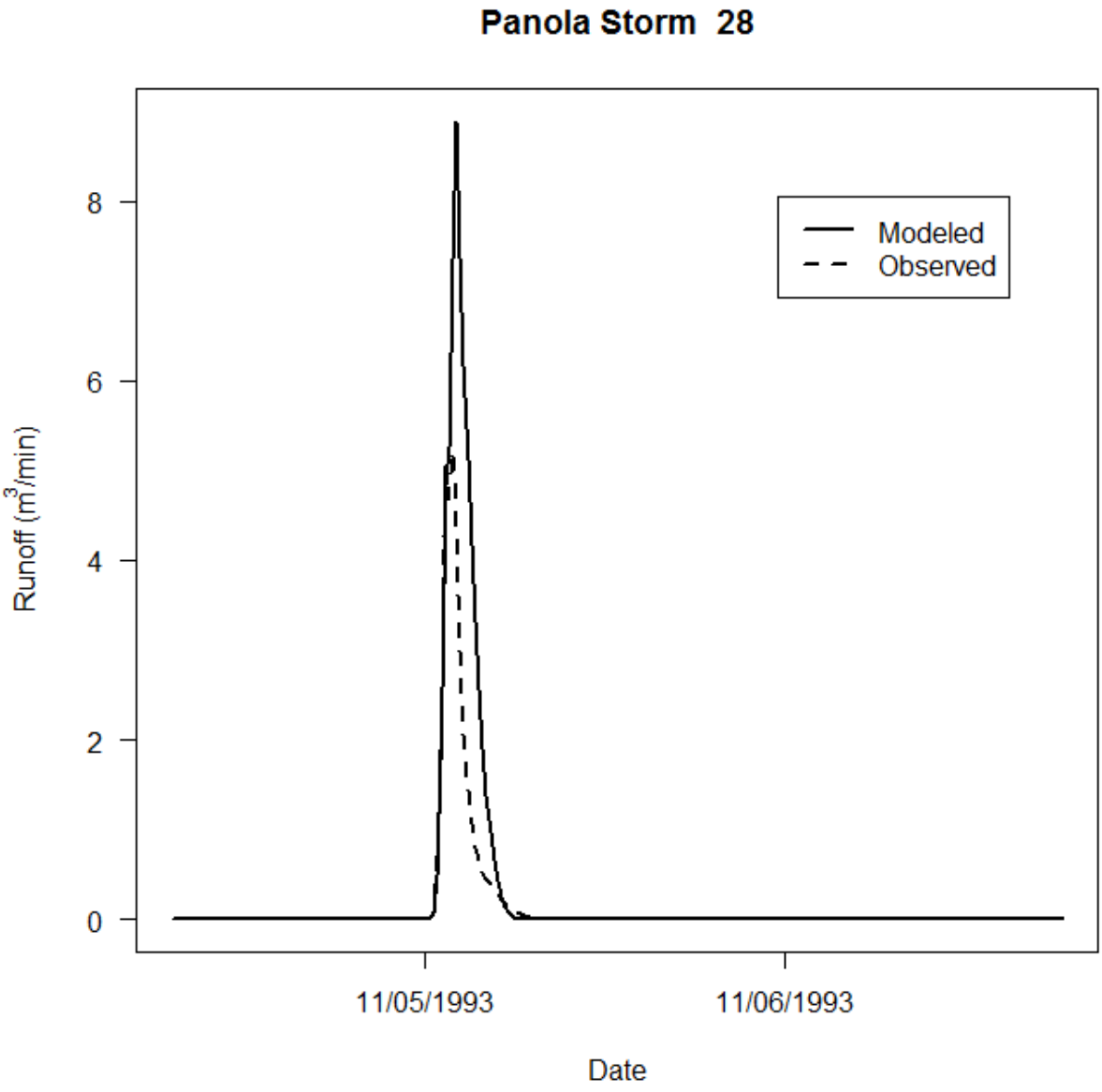

Date	11/05/93	Nash-Sutcliffe	0.71
Time of Concentration	5 hrs	Modified Nash-Sutcliffe	0.71
Contributing Area	20,831 m^2	Observed Peak	5.21
Precipitation	33.5 mm	Modeled Peak	8.89

Figure D.3: Panola storm 28.

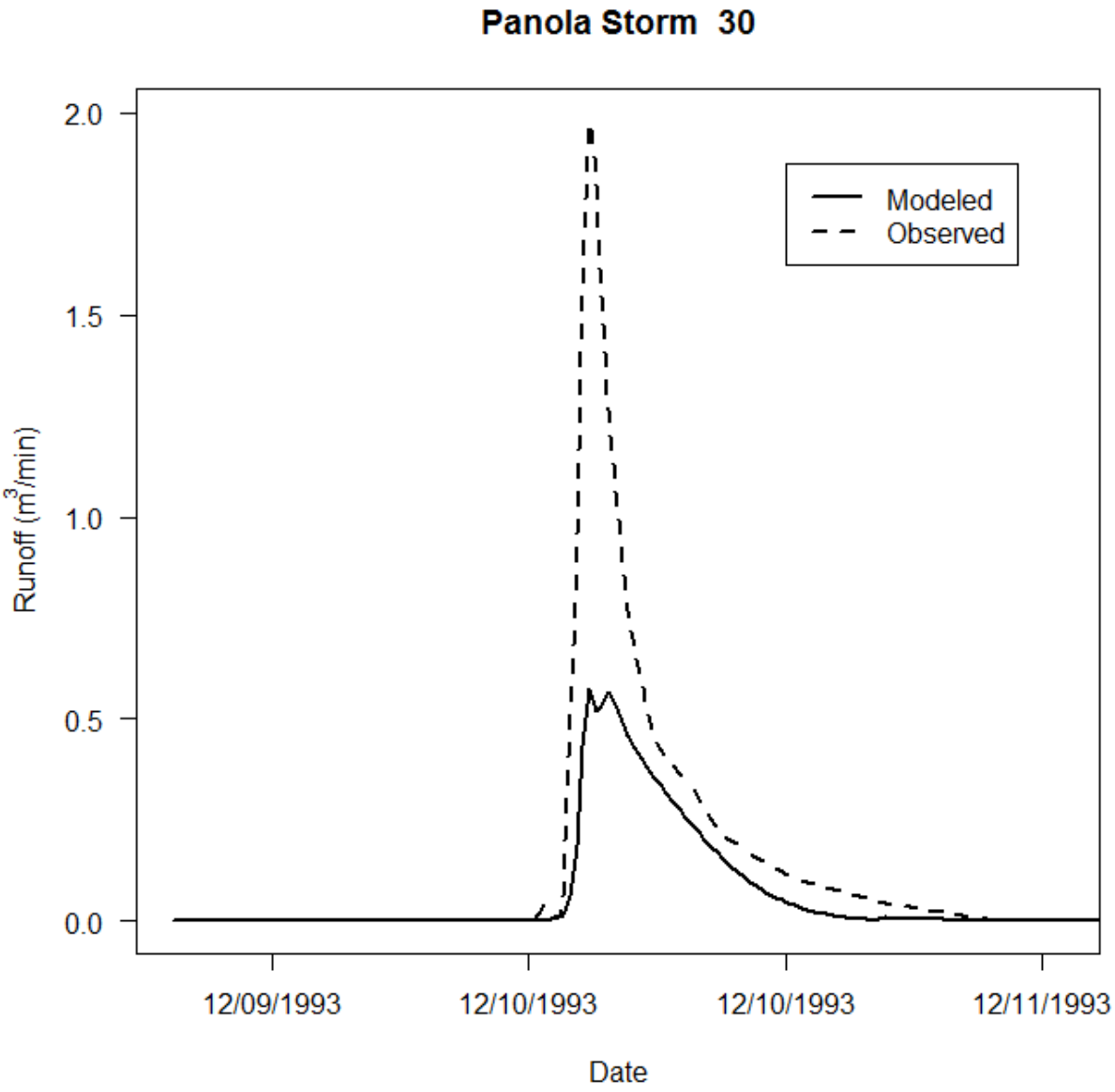

Date	12/10/93	Nash-Sutcliffe	0.69
Time of Concentration	15 hrs	Modified Nash-Sutcliffe	0.68
Contributing Area	9,100 m^2	Observed Peak	1.98
Precipitation	20.1 mm	Modeled Peak	0.57

Figure D.4: Panola storm 30.

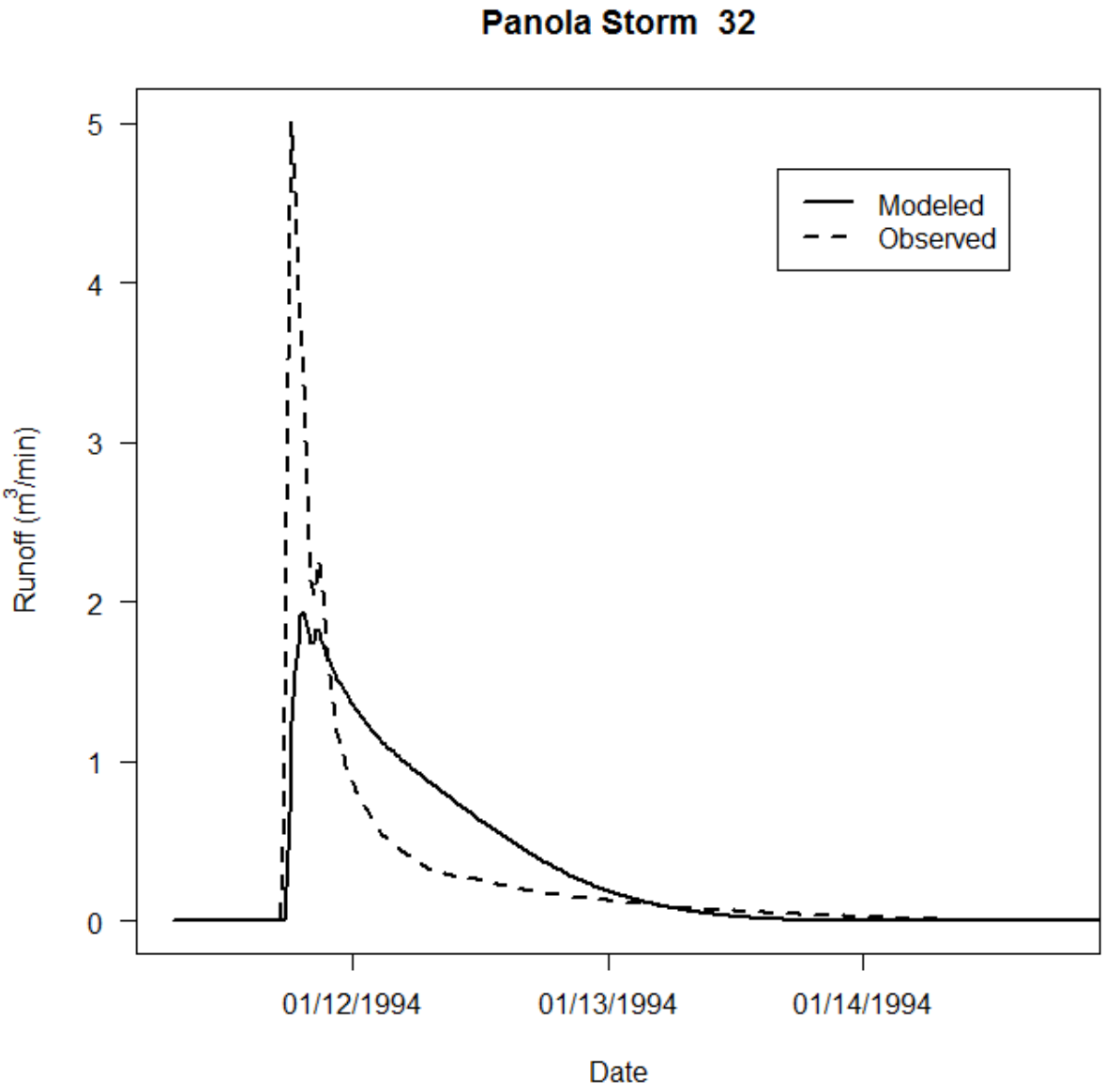

Date	01/12/94	Nash-Sutcliffe	0.70
Time of Concentration	59 hrs	Modified Nash-Sutcliffe	0.58
Contributing Area	20,124 m^2	Observed Peak	5.01
Precipitation	30.5 mm	Modeled Peak	1.98

Figure D.5: Panola storm 32.

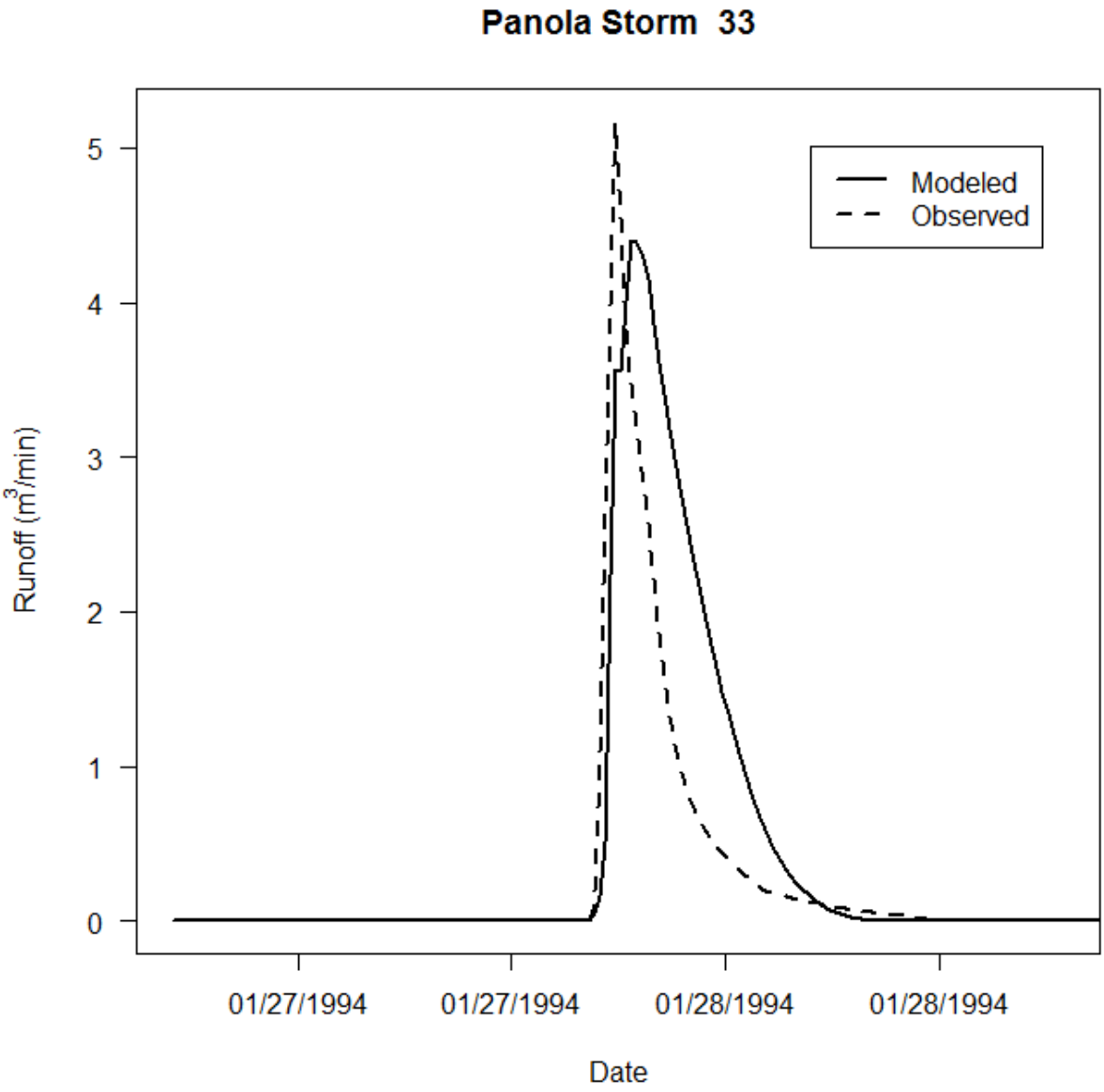

Date	01/28/94	Nash-Sutcliffe	0.69
Time of Concentration	13 hrs	Modified Nash-Sutcliffe	0.62
Contributing Area	20,500 m^2	Observed Peak	5.17
Precipitation	29.5 mm	Modeled Peak	4.40

Figure D.6: Panola storm 33.

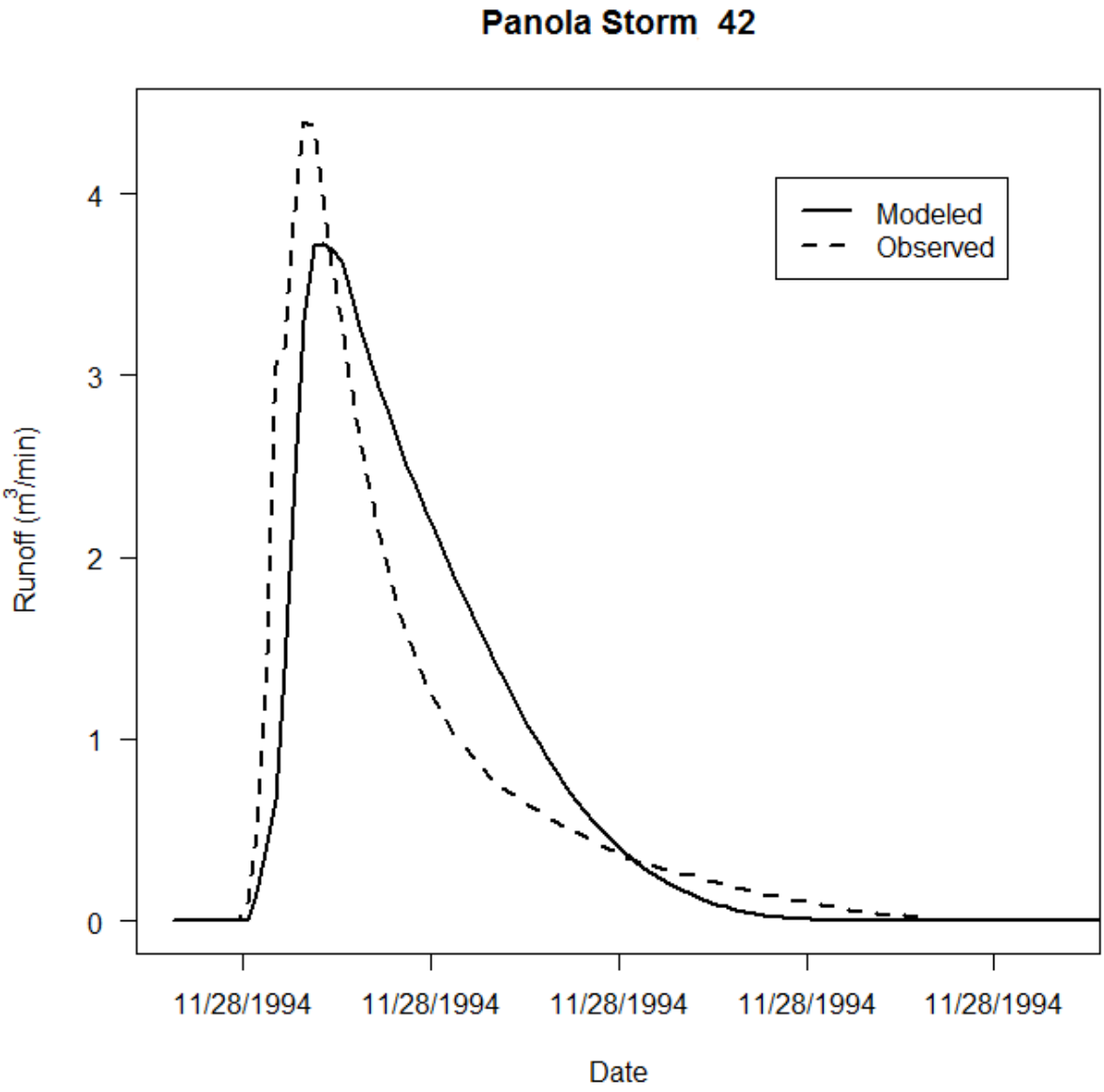

Date	11/28/94	Nash-Sutcliffe	0.87
Time of Concentration	16 hrs	Modified Nash-Sutcliffe	0.76
Contributing Area	17,600 m^2	Observed Peak	4.40
Precipitation	22.6 mm	Modeled Peak	3.73

Figure D.7: Panola storm 42.

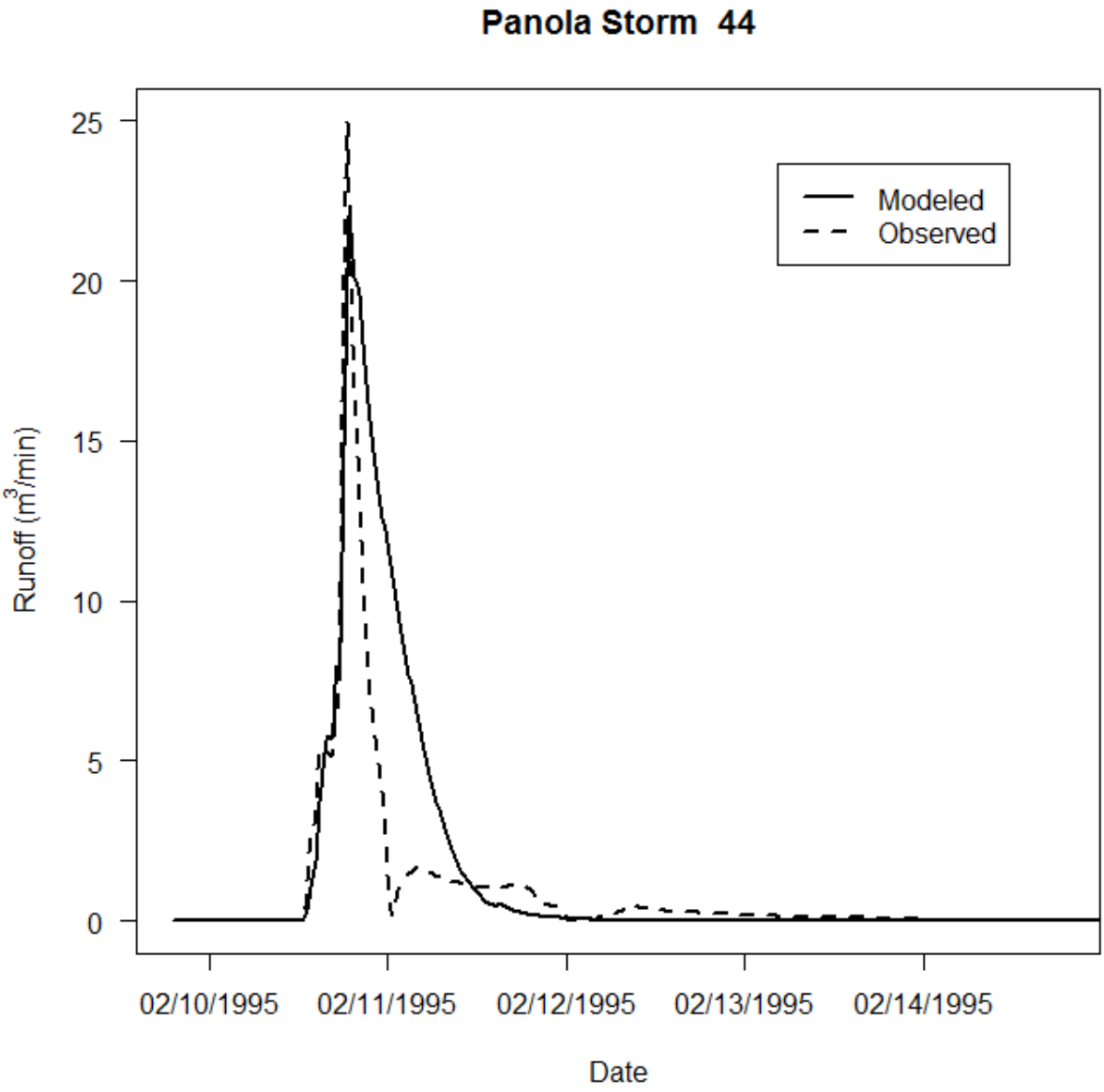

Date	02/11/95	Nash-Sutcliffe	0.62
Time of Concentration	28 hrs	Modified Nash-Sutcliffe	0.54
Contributing Area	99,007 m^2	Observed Peak	24.98
Precipitation	85.1 mm	Modeled Peak	22.04

Figure D.8: Panola storm 44.

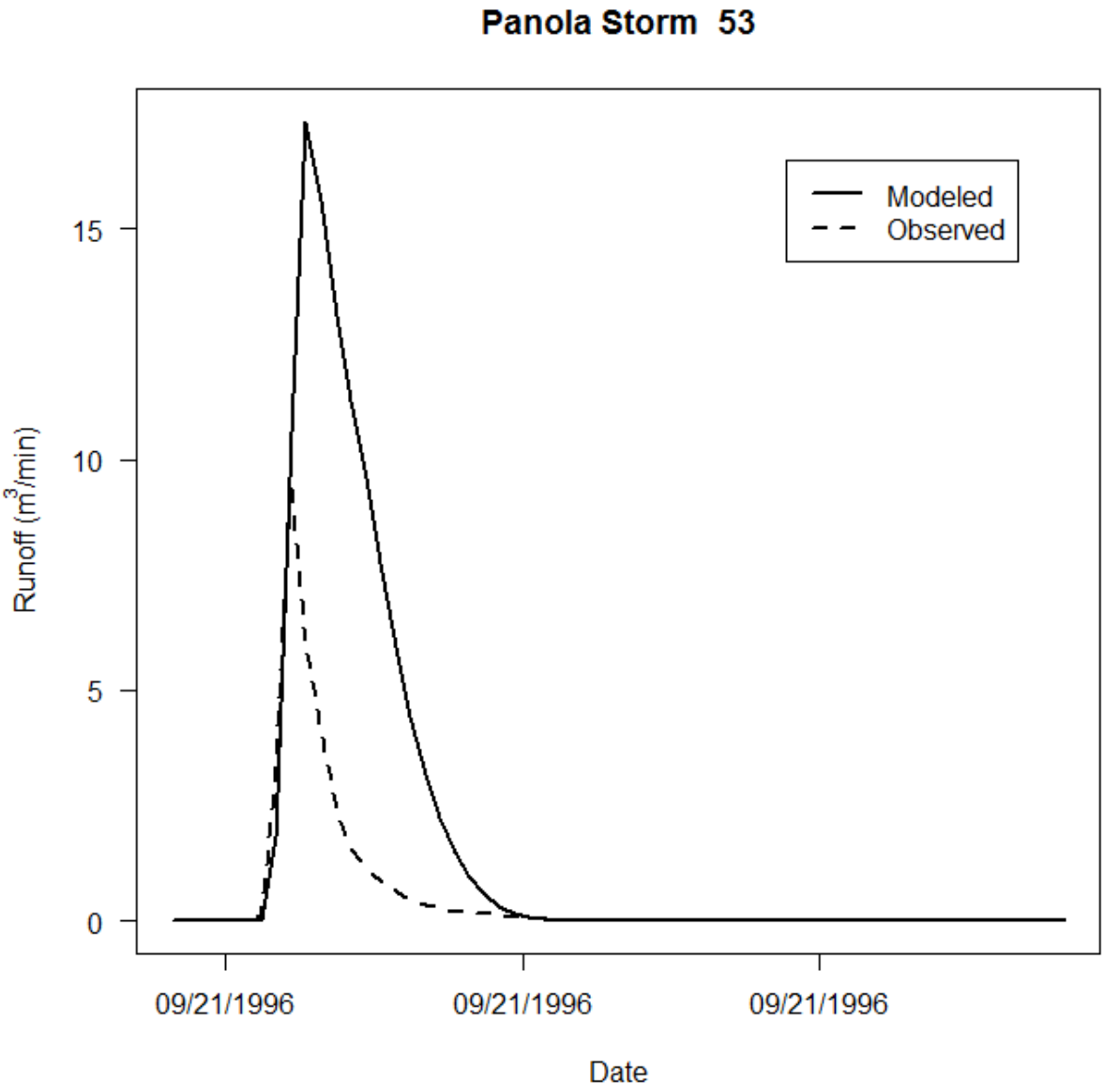

Date	09/21/96	Nash-Sutcliffe	-0.24
Time of Concentration	5 hrs	Modified Nash-Sutcliffe	0.20
Contributing Area	42,333 m^2	Observed Peak	9.53
Precipitation	33.5 mm	Modeled Peak	17.33

Figure D.9: Panola storm 53.

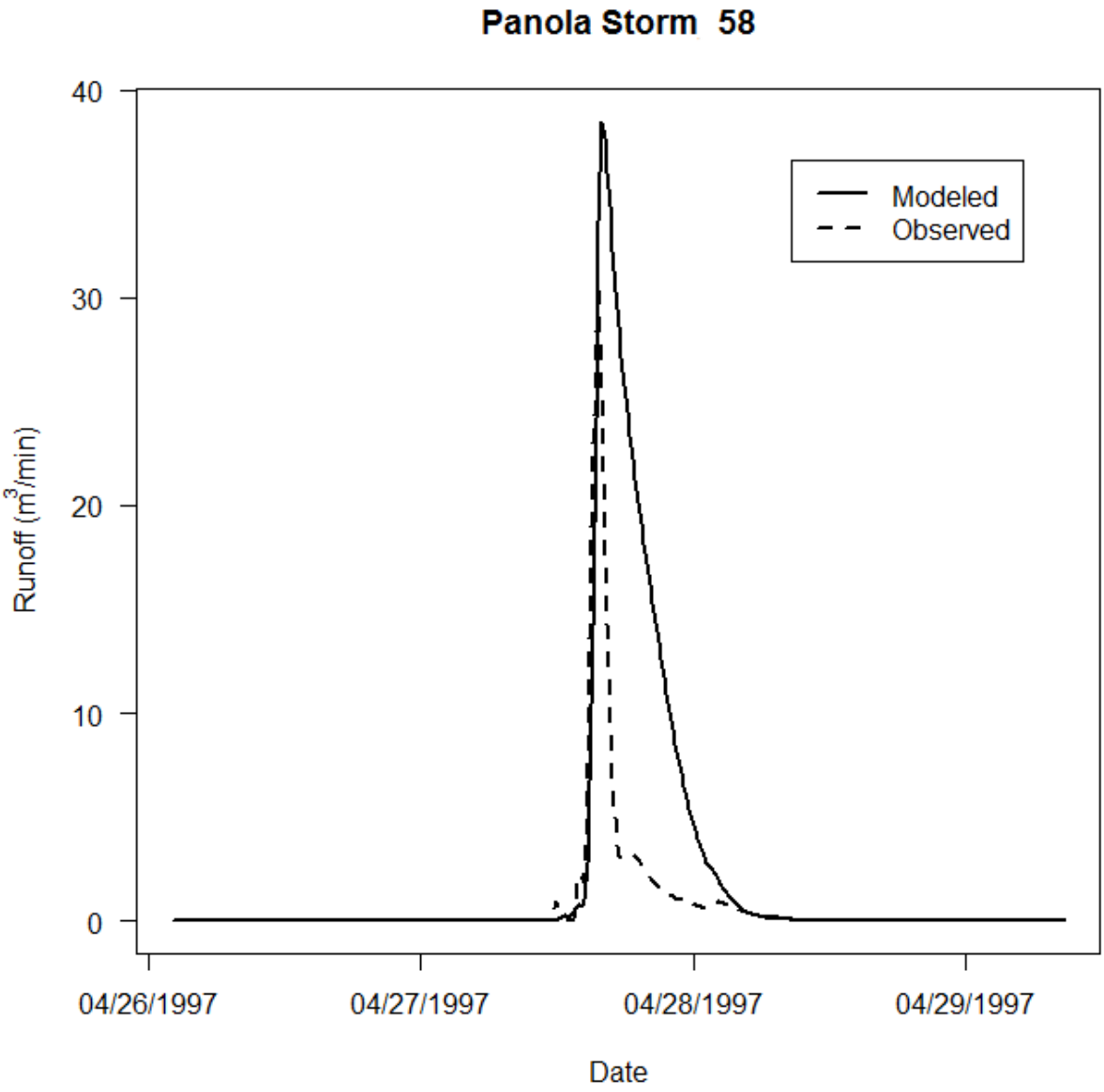

Date	04/27/97	Nash-Sutcliffe	0.17
Time of Concentration	17 hrs	Modified Nash-Sutcliffe	0.44
Contributing Area	126,253 m^2	Observed Peak	31.42
Precipitation	87.6 mm	Modeled Peak	38.49

Figure D.10: Panola storm 58.

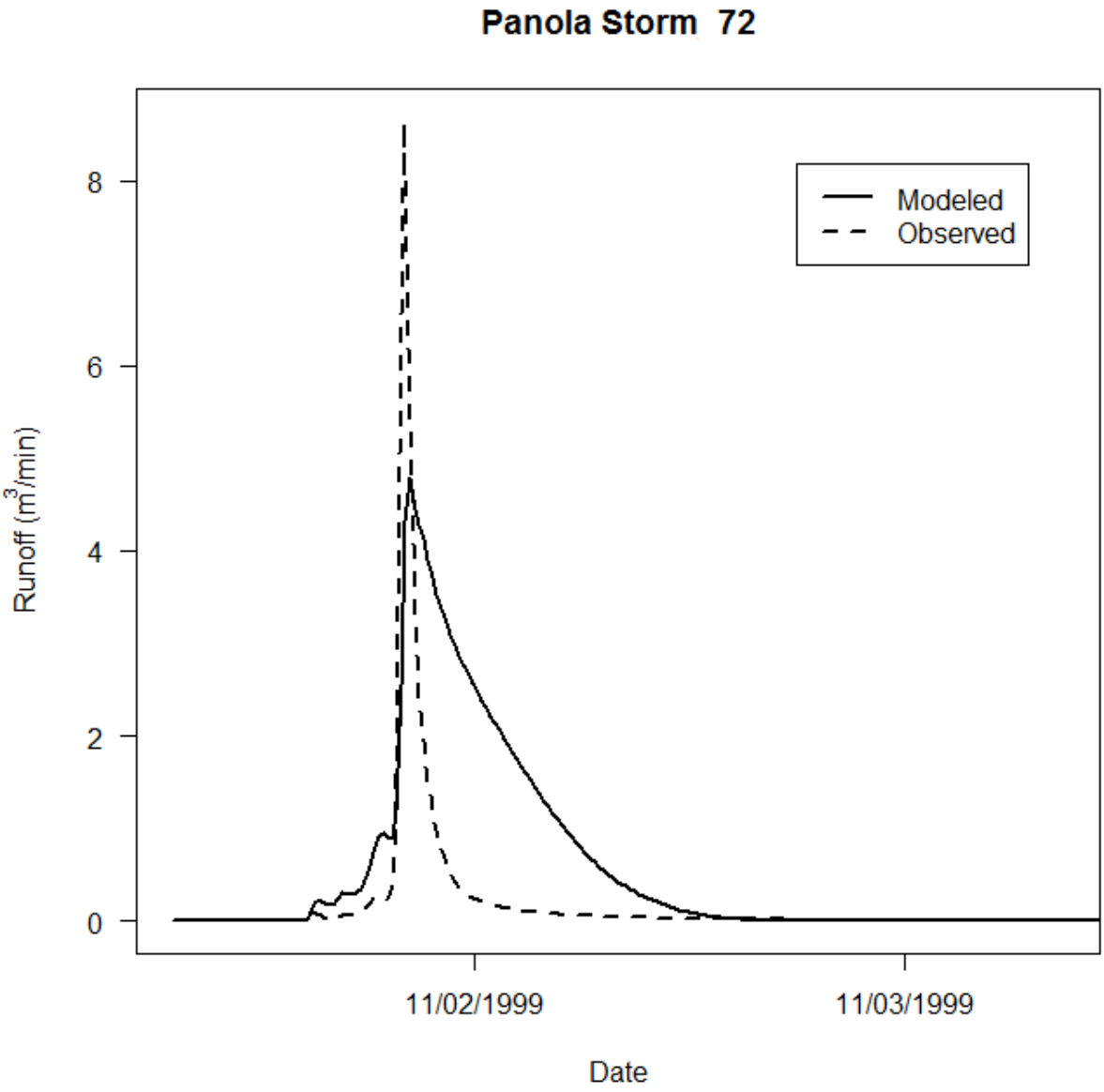

Date	11/02/99	Nash-Sutcliffe	-0.54
Time of Concentration	25 hrs	Modified Nash-Sutcliffe	-0.32
Contributing Area	34,007 m^2	Observed Peak	8.64
Precipitation	52.8 mm	Modeled Peak	4.80

Figure D.11: Panola storm 72.

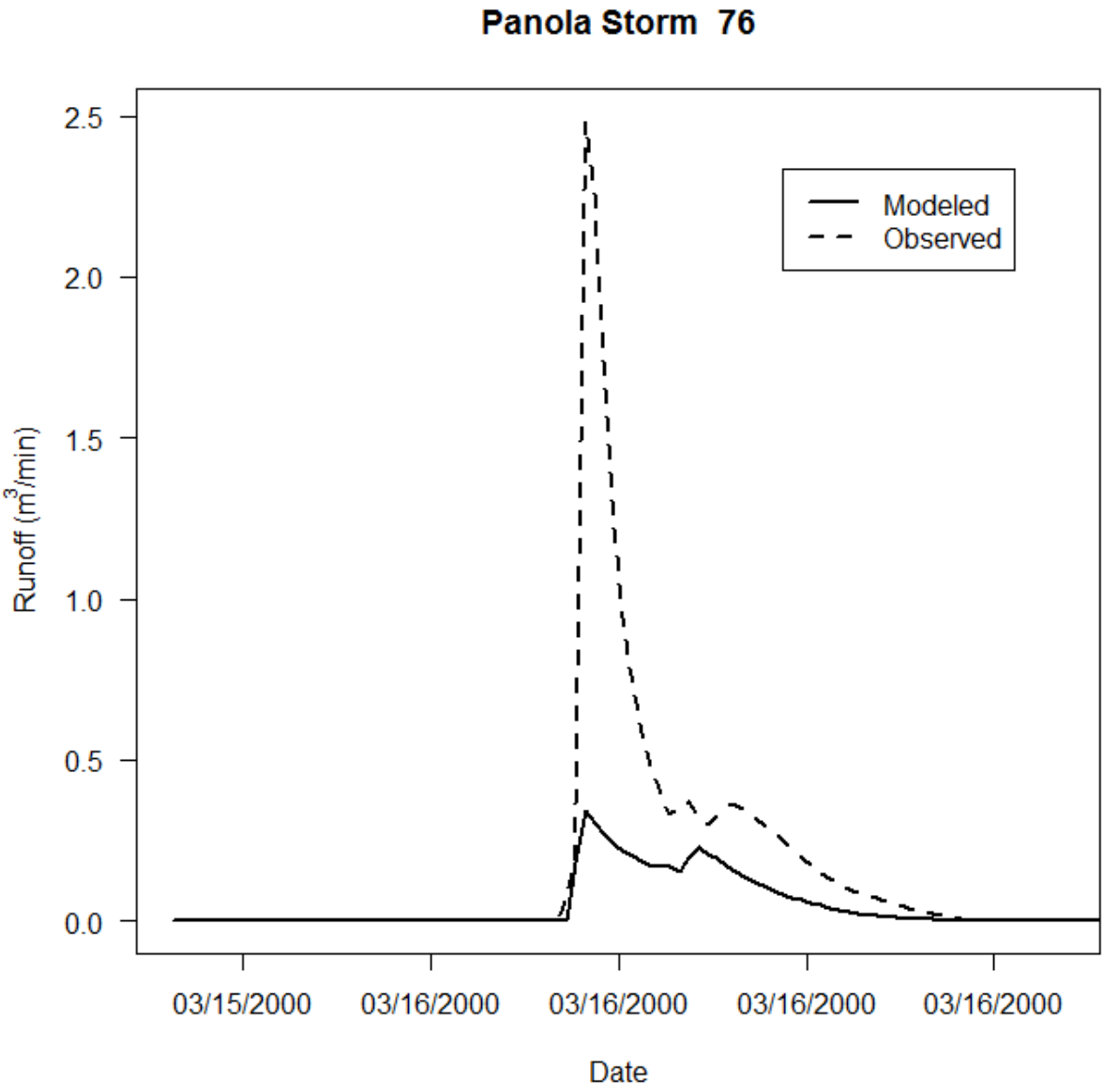

Date	03/16/00	Nash-Sutcliffe	0.41
Time of Concentration	8 hrs	Modified Nash-Sutcliffe	0.57
Contributing Area	3,871 m^2	Observed Peak	2.48
Precipitation	24.4 mm	Modeled Peak	0.34

Figure D.12: Panola storm 76.

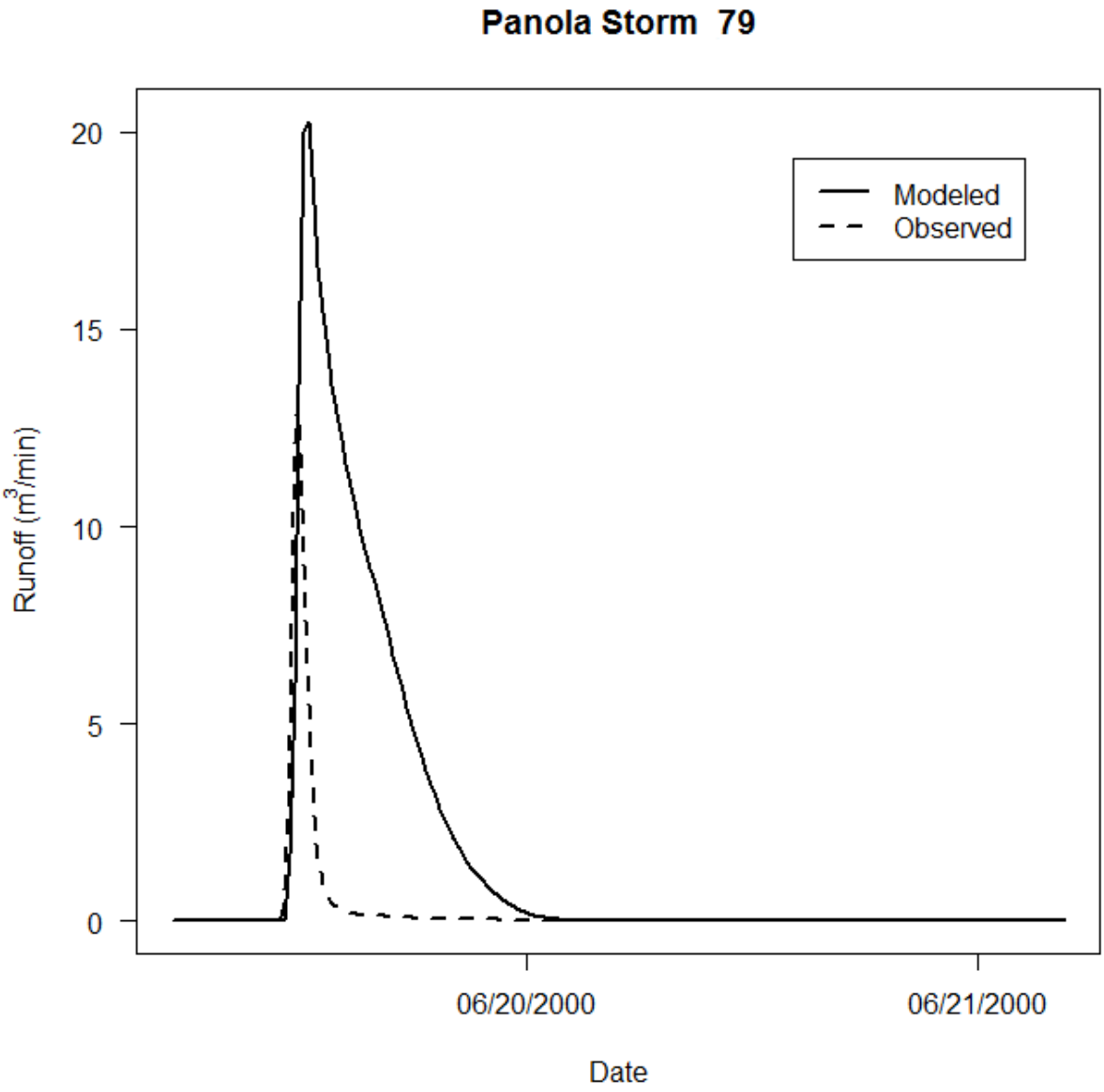

Date	06/19/00	Nash-Sutcliffe	-3.46
Time of Concentration	17 hrs	Modified Nash-Sutcliffe	-1.37
Contributing Area	54,550 m^2	Observed Peak	13.39
Precipitation	72.4 mm	Modeled Peak	20.28

Figure D.13: Panola storm 79.

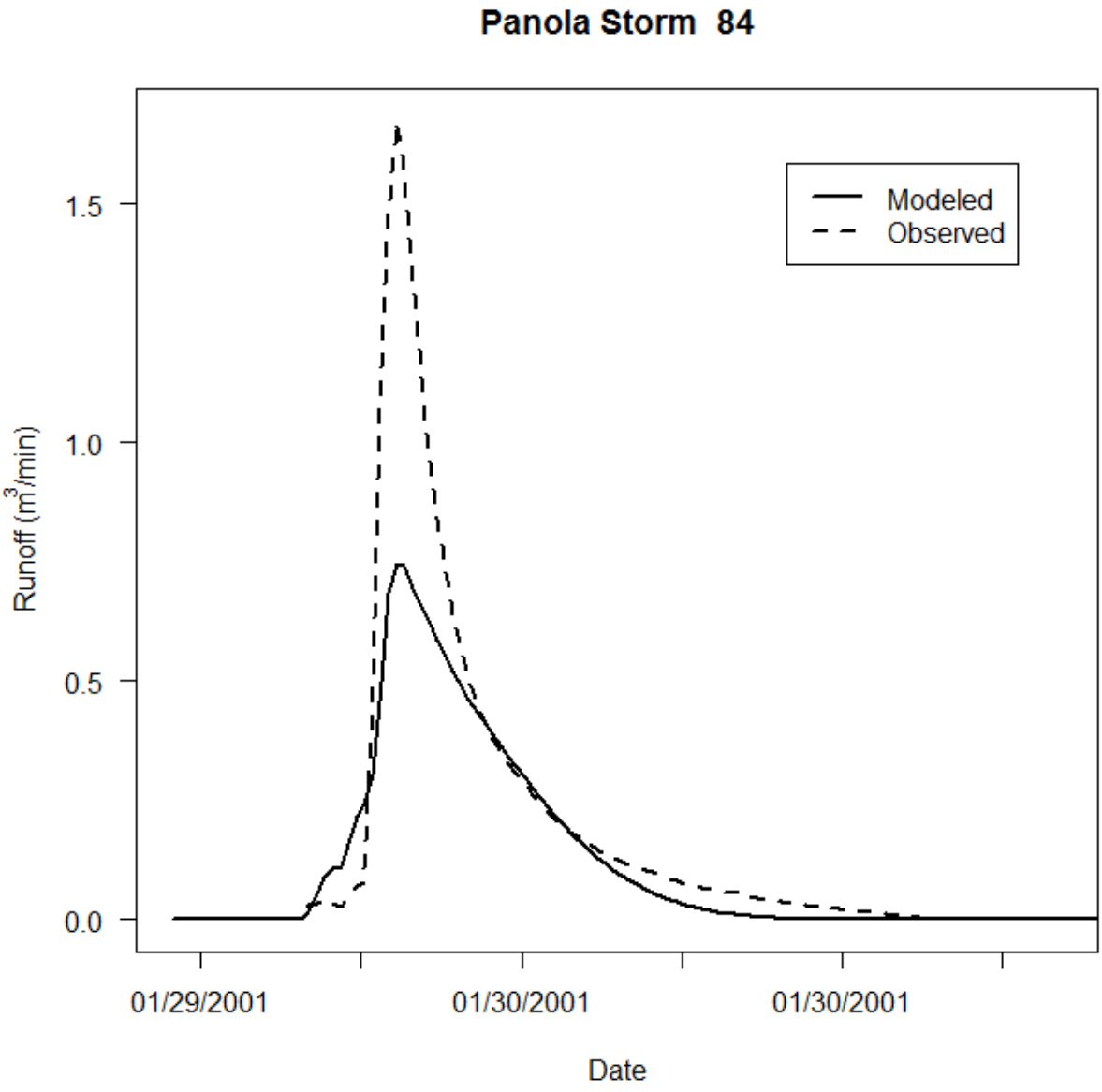

Date	01/30/01	Nash-Sutcliffe	0.85
Time of Concentration	16 hrs	Modified Nash-Sutcliffe	0.77
Contributing Area	7,469 m^2	Observed Peak	1.67
Precipitation	22.4 mm	Modeled Peak	0.74

Figure D.14: Panola storm 84.

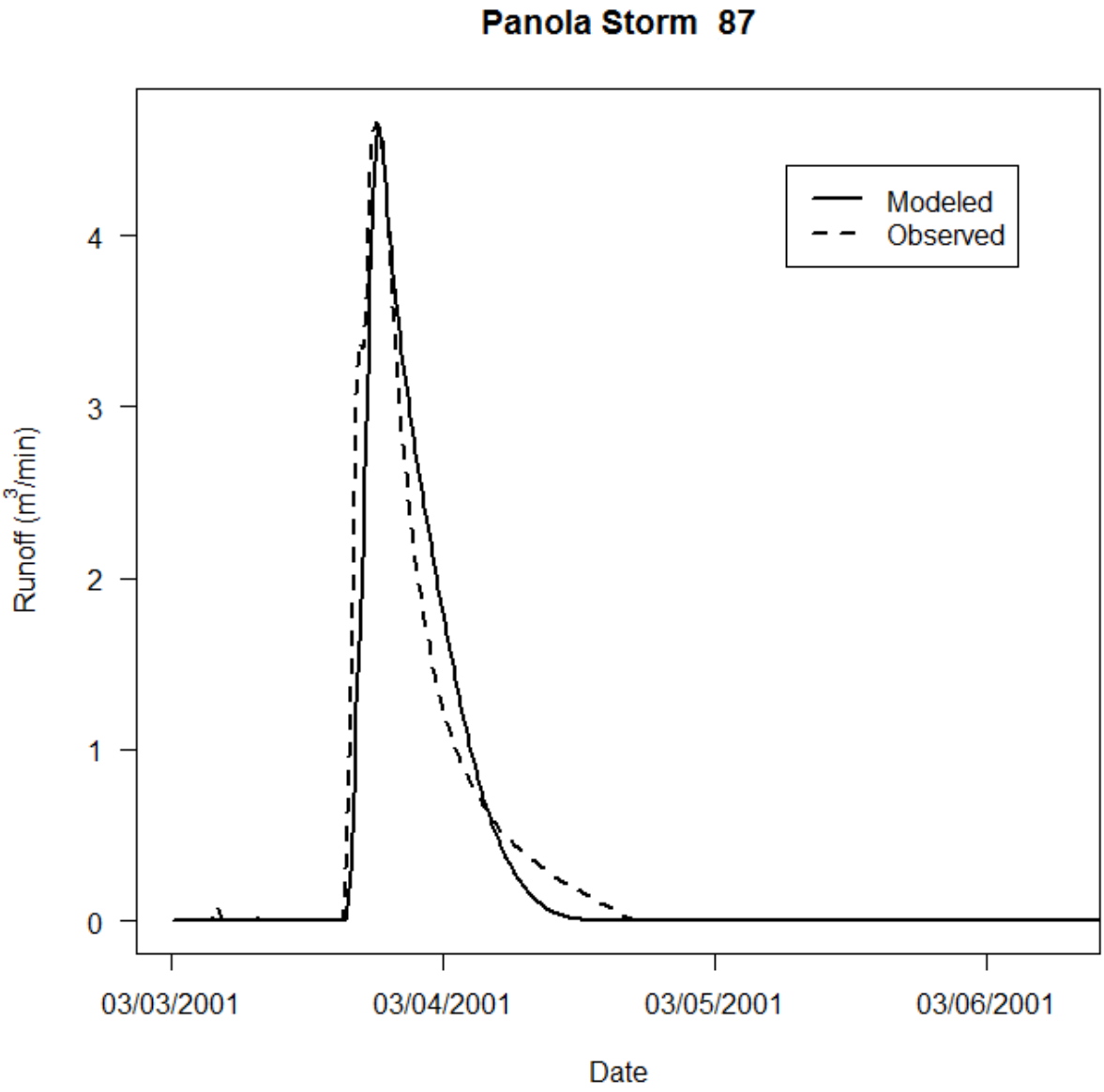

Date	03/03/01	Nash-Sutcliffe	0.94
Time of Concentration	22 hrs	Modified Nash-Sutcliffe	0.85
Contributing Area	16,789 m^2	Observed Peak	4.67
Precipitation	52.5 mm	Modeled Peak	4.64

Figure D.15: Panola storm 87.

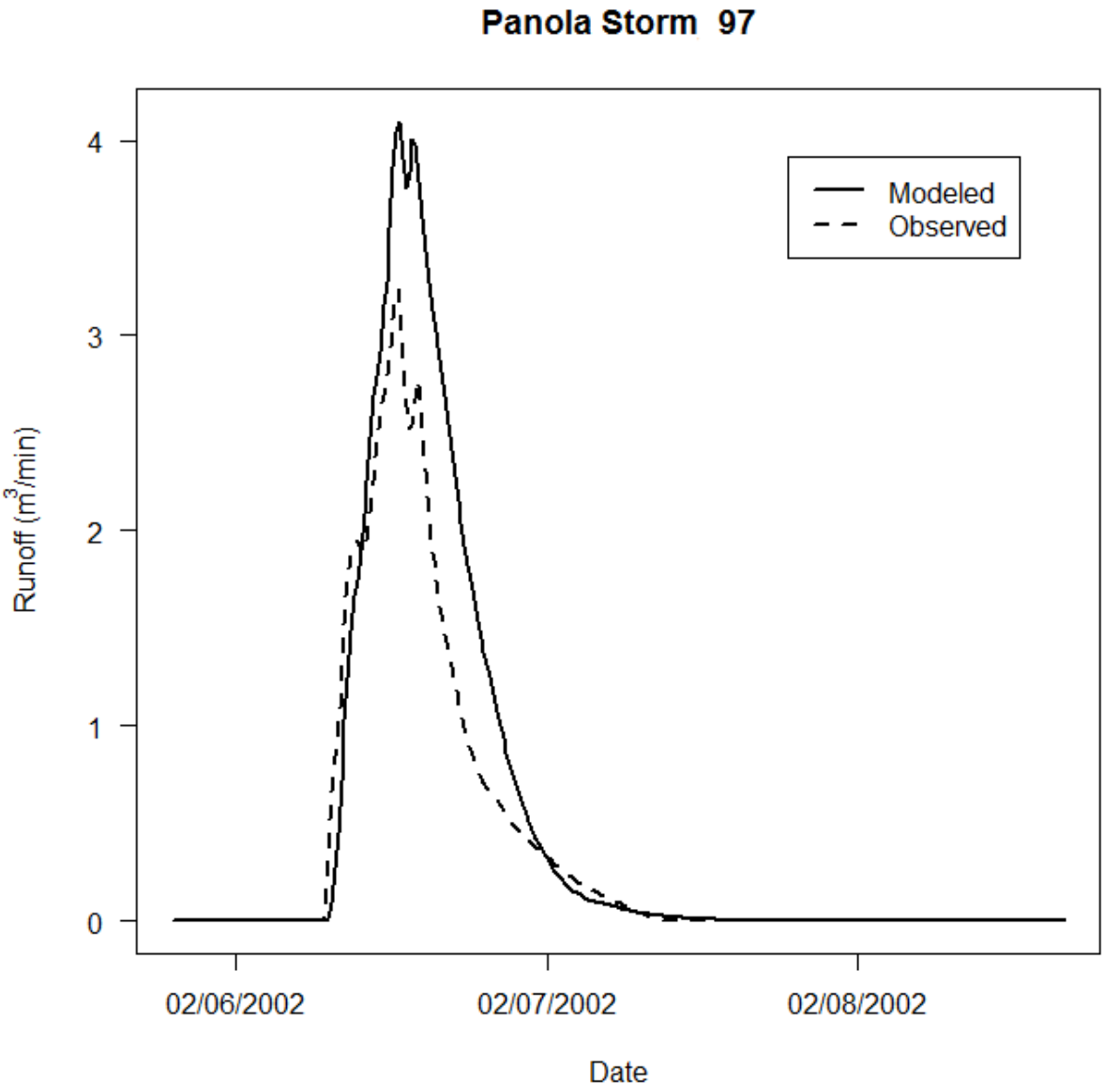

Date	02/06/02	Nash-Sutcliffe	0.89
Time of Concentration	20 hrs	Modified Nash-Sutcliffe	0.80
Contributing Area	16,410 m^2	Observed Peak	3.24
Precipitation	58.9 mm	Modeled Peak	4.10

Figure D.16: Panola storm 97.

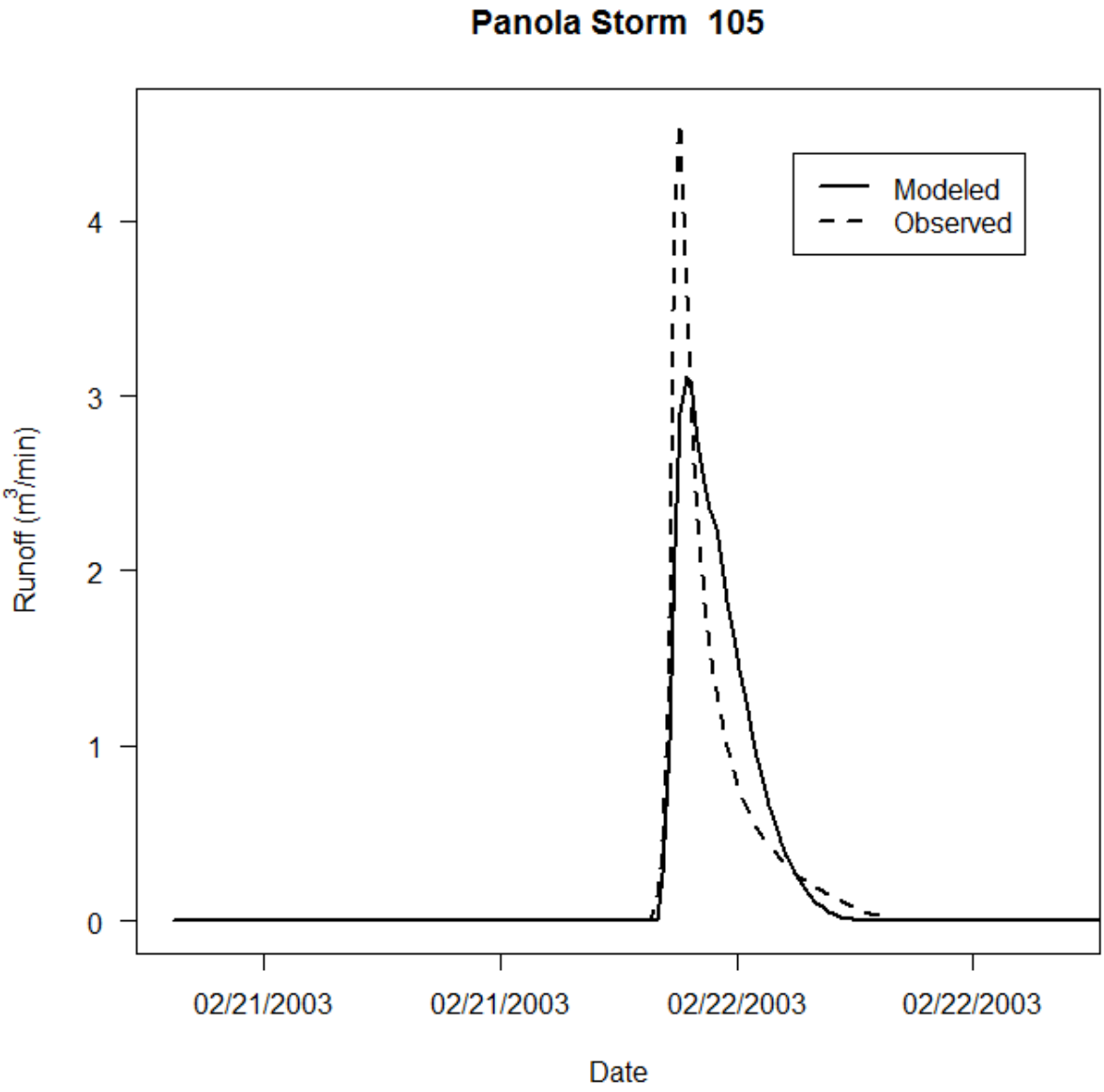

Date	02/22/03	Nash-Sutcliffe	0.91
Time of Concentration	9 hrs	Modified Nash-Sutcliffe	0.81
Contributing Area	21,370 m^2	Observed Peak	4.57
Precipitation	24.6 mm	Modeled Peak	3.11

Figure D.17: Panola storm 105.

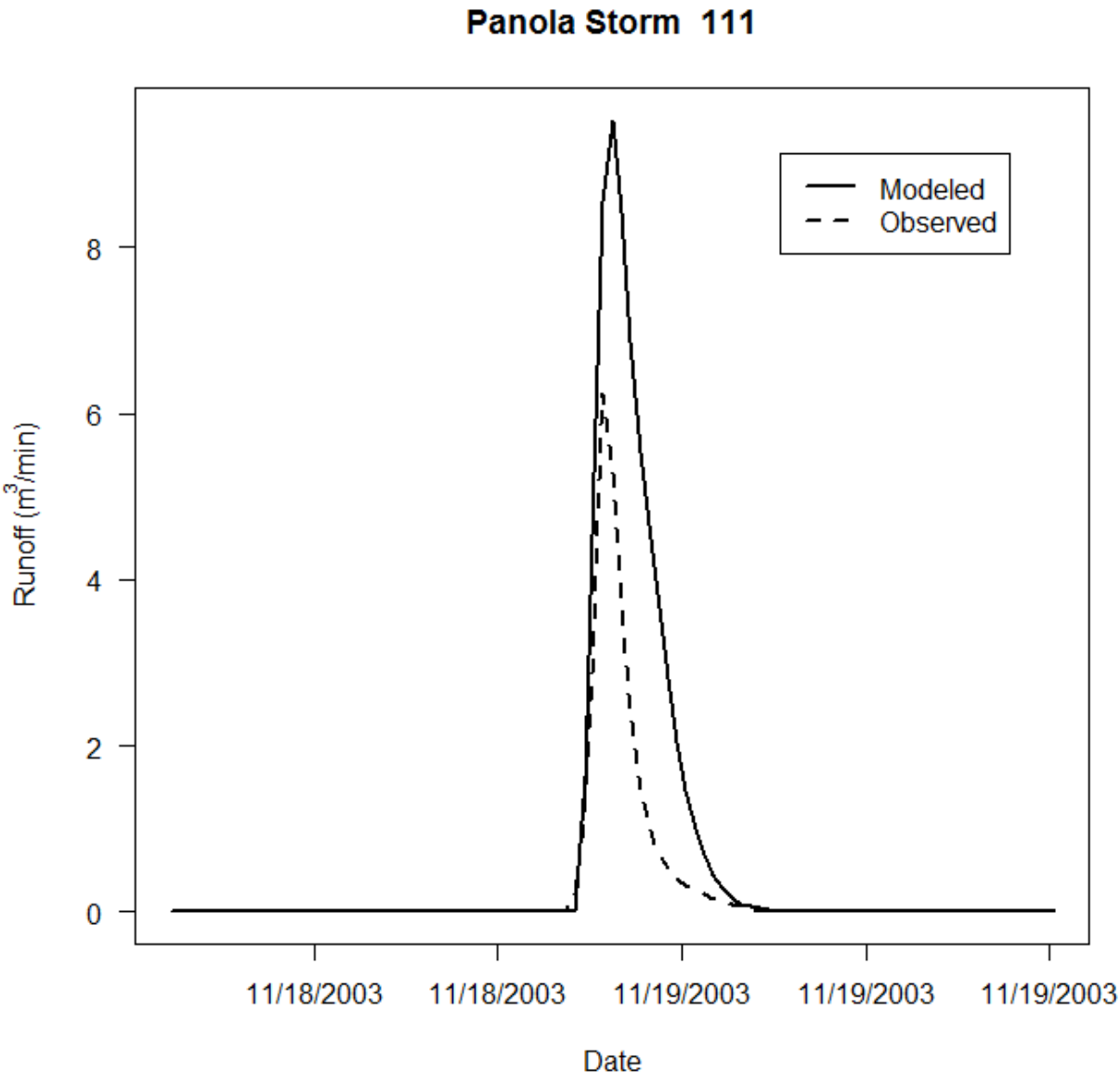

Date	11/19/03	Nash-Sutcliffe	0.51
Time of Concentration	5 hrs	Modified Nash-Sutcliffe	0.54
Contributing Area	13,794 m^2	Observed Peak	6.24
Precipitation	42.4 mm	Modeled Peak	9.53

Figure D.18: Panola storm 111.

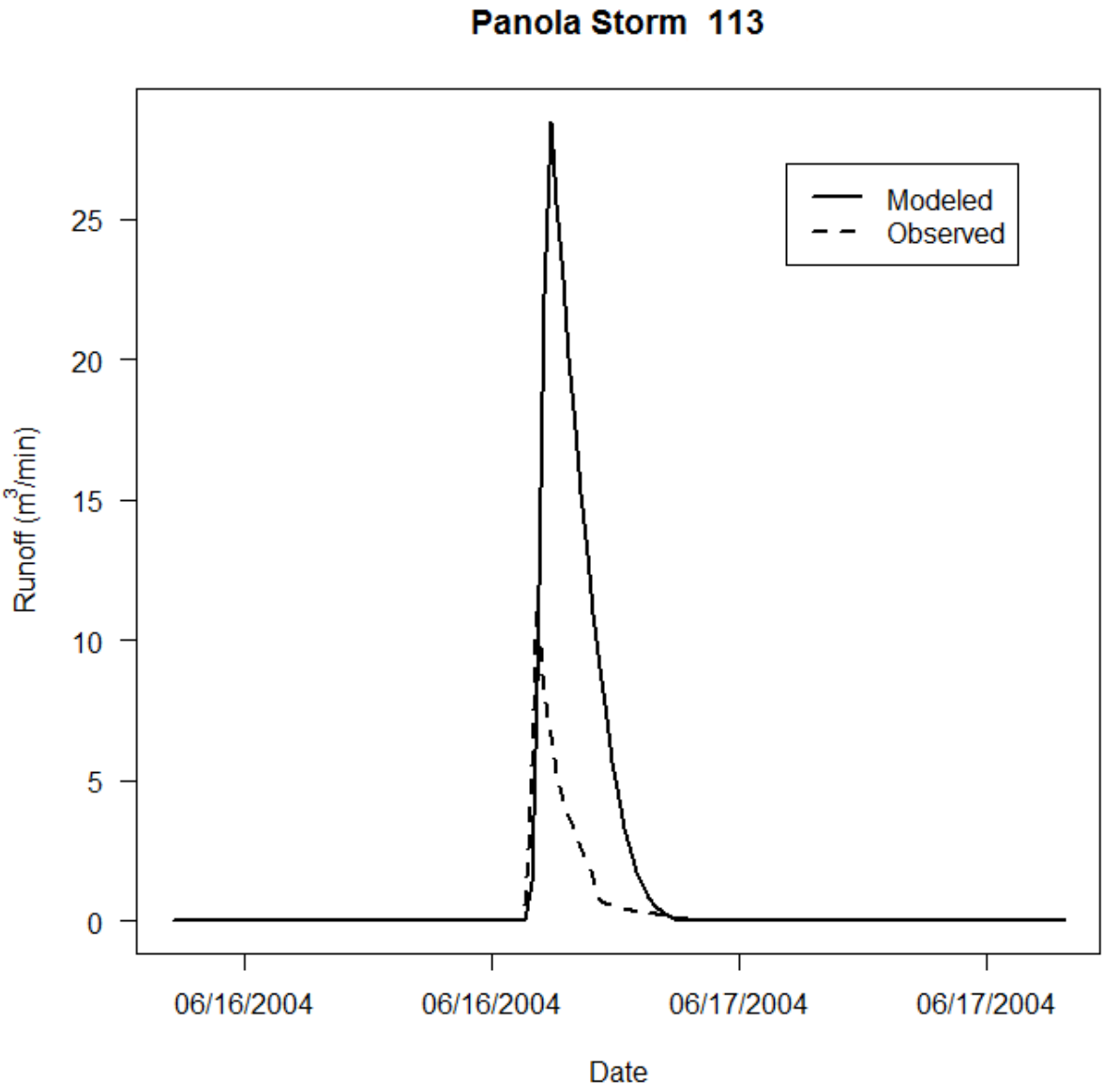

Date	16/16/2004	Nash-Sutcliffe	-0.04
Time of Concentration	5 hrs	Modified Nash-Sutcliffe	0.35
Contributing Area	47,588 m^2	Observed Peak	11.12
Precipitation	38.4 mm	Modeled Peak	28.48

Figure D.19: Panola storm 113.

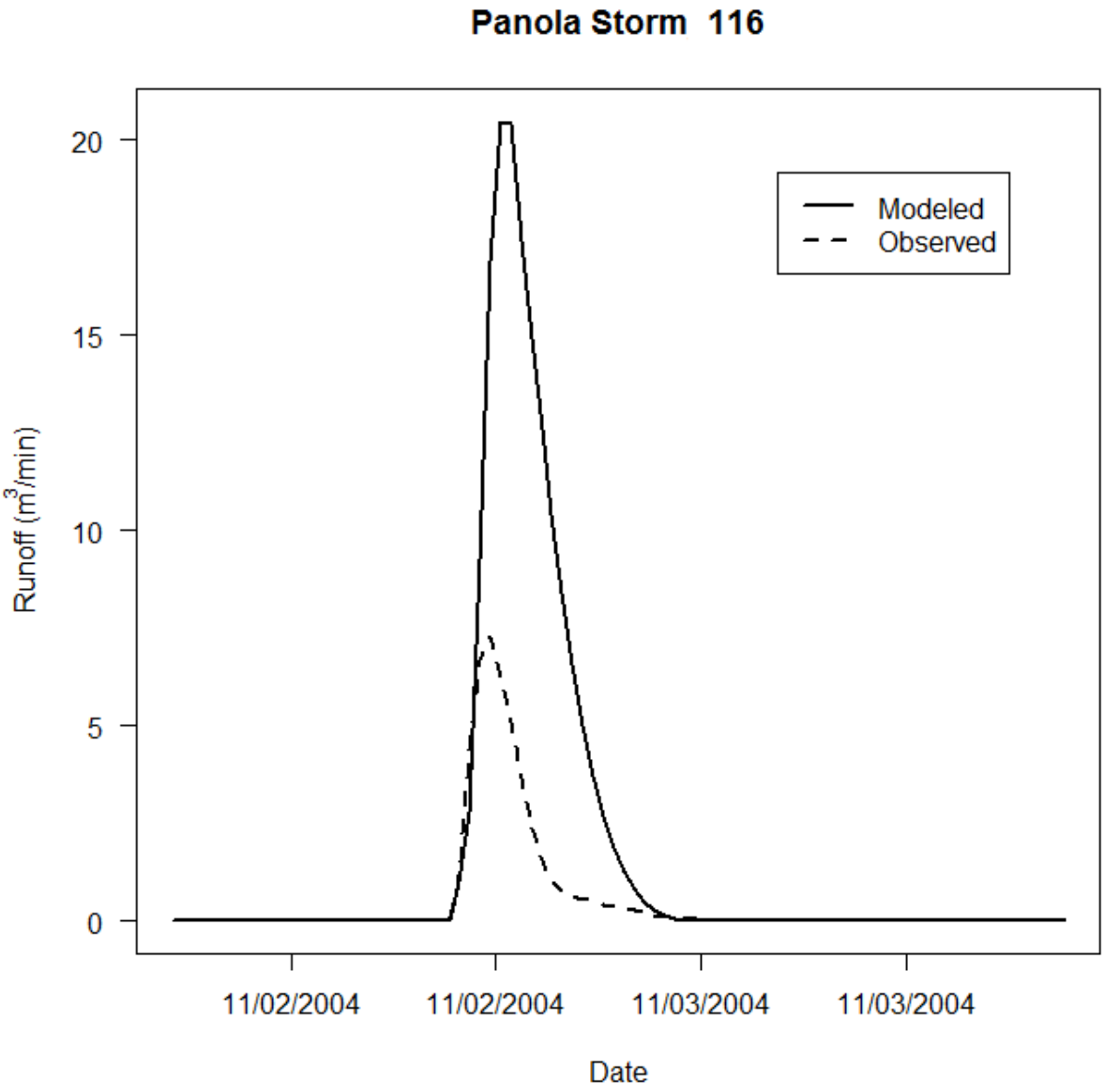

Date	11/02/04	Nash-Sutcliffe	-0.09
Time of Concentration	5 hrs	Modified Nash-Sutcliffe	0.33
Contributing Area	31,584 m^2	Observed Peak	7.29
Precipitation	52.1 mm	Modeled Peak	20.49

Figure D.20: Panola storm 116.

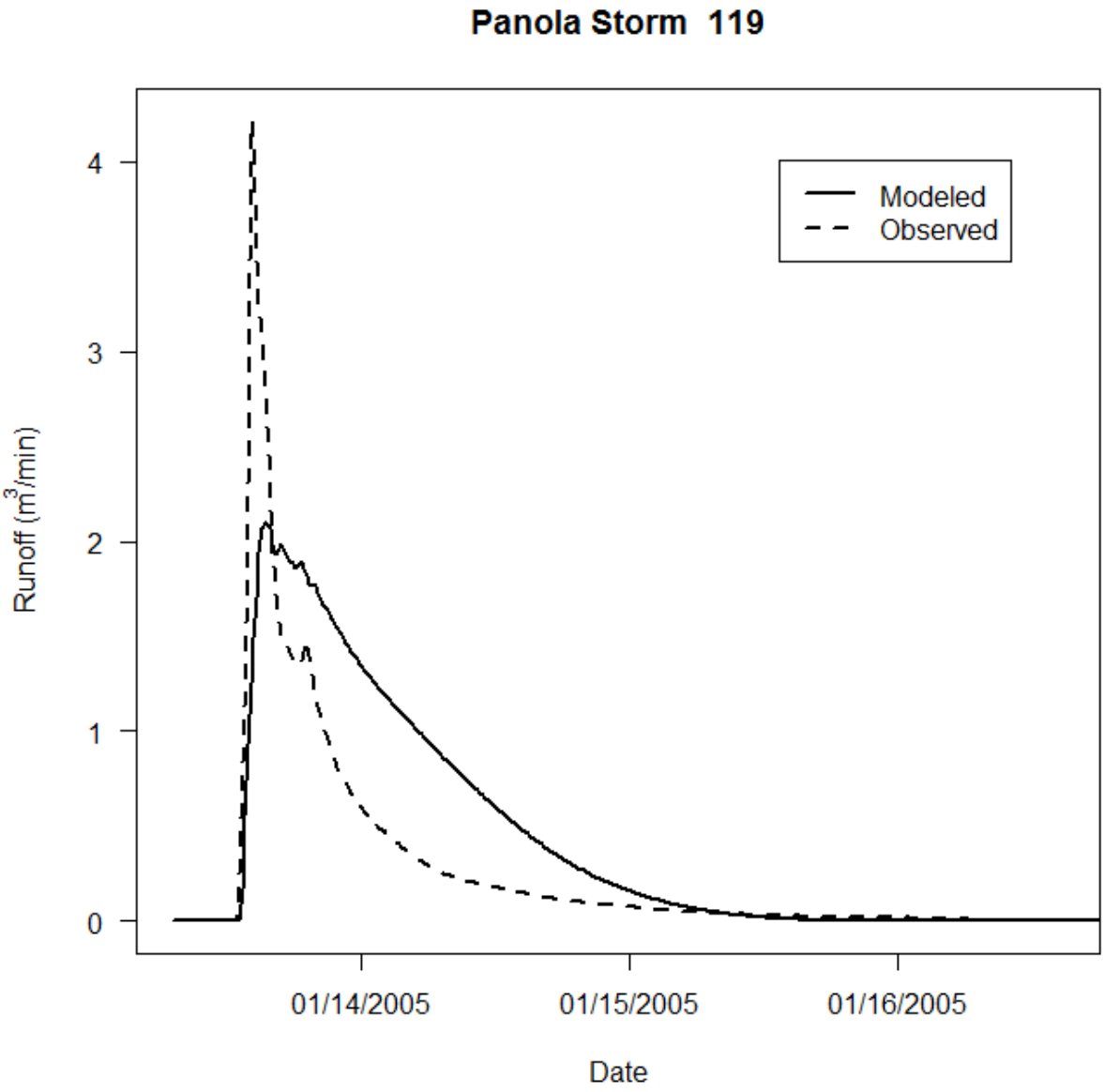

Date	01/13/05	Nash-Sutcliffe	0.63
Time of Concentration	60 hrs	Modified Nash-Sutcliffe	0.50
Contributing Area	19,322 m^2	Observed Peak	4.22
Precipitation	44.7 mm	Modeled Peak	2.09

Figure D.21: Panola storm 119.

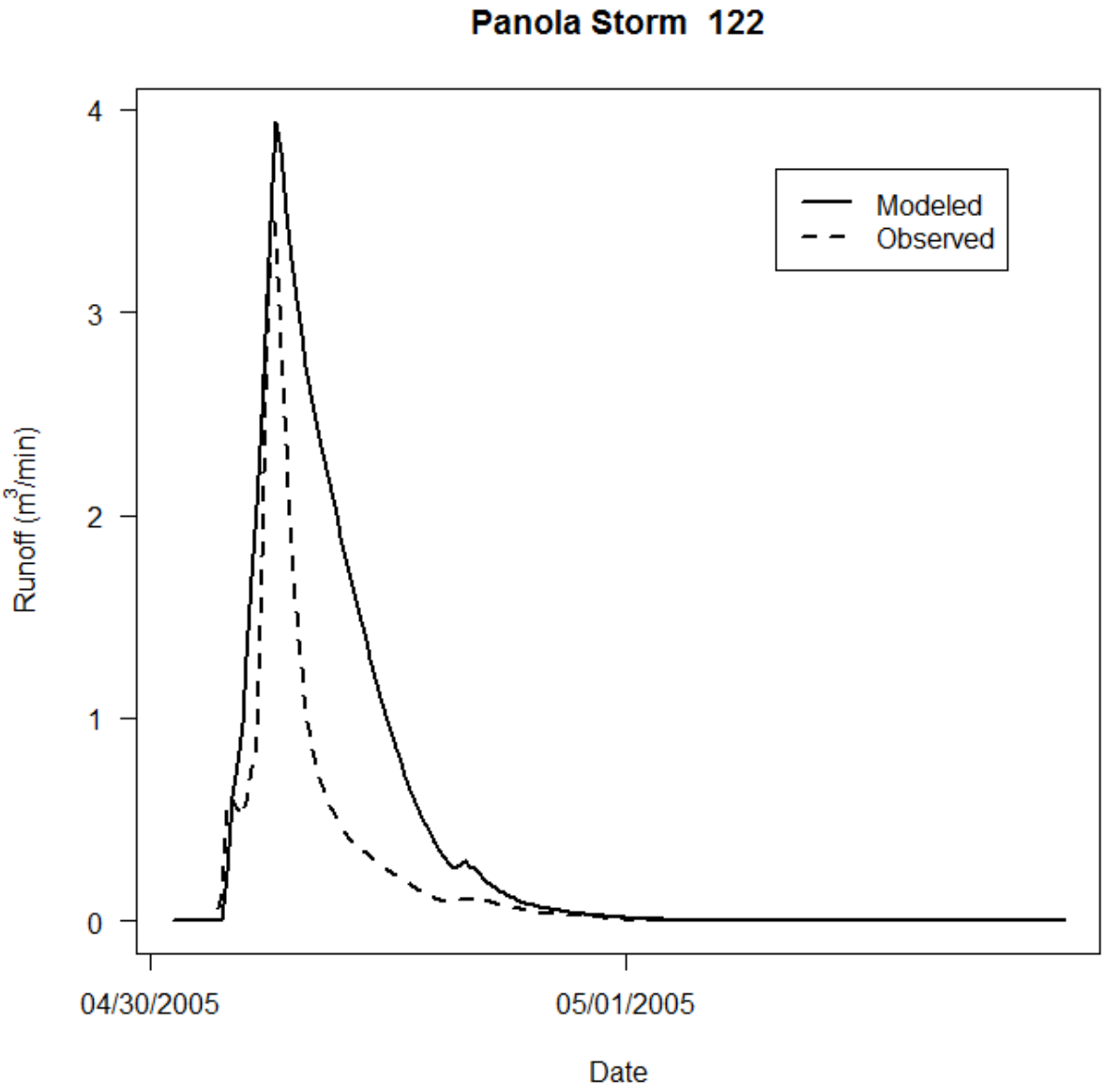

Date	04/30/05	Nash-Sutcliffe	0.36
Time of Concentration	17 hrs	Modified Nash-Sutcliffe	0.38
Contributing Area	16,664 m^2	Observed Peak	3.52
Precipitation	32.3 mm	Modeled Peak	3.94

Figure D.22: Panola storm 122.

Coweeta Modeled Storms

The hydrographs of Coweeta storms presented in this appendix were modeled with D8 networks with an extraction threshold of 155 and using dynamic area estimations. The observed stormflow was separated using the Lynn and Hollick (1979) digital filter.

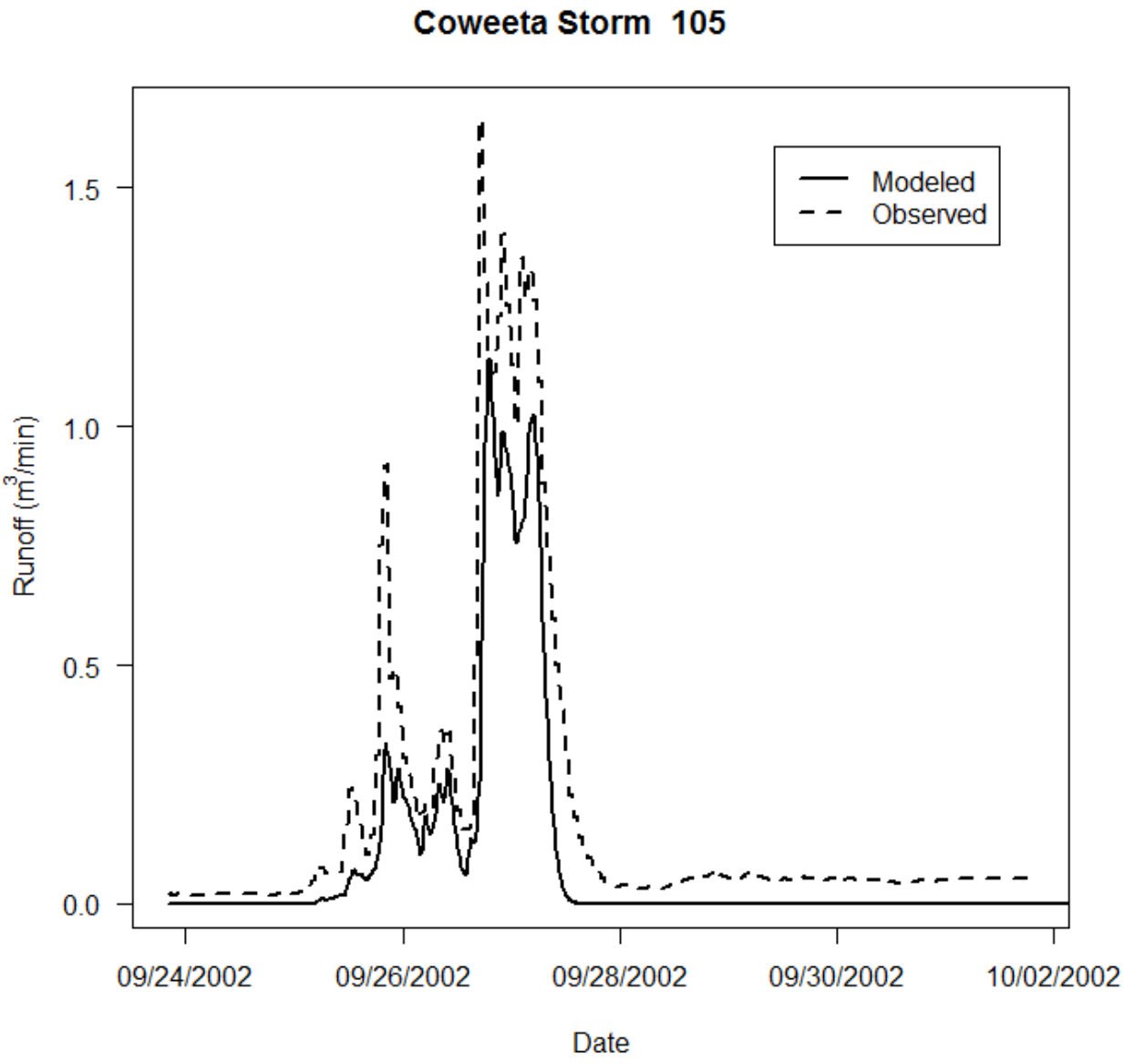

Figure D.23: Coweeta storm 105.

Date: 09/26/02	Nash Sutcliffe	0.77
	Modified Nash Sutcliffe	0.53
Precipitation: 185.4 mm	Observed Peak	1.14
	Modeled Peak	1.30

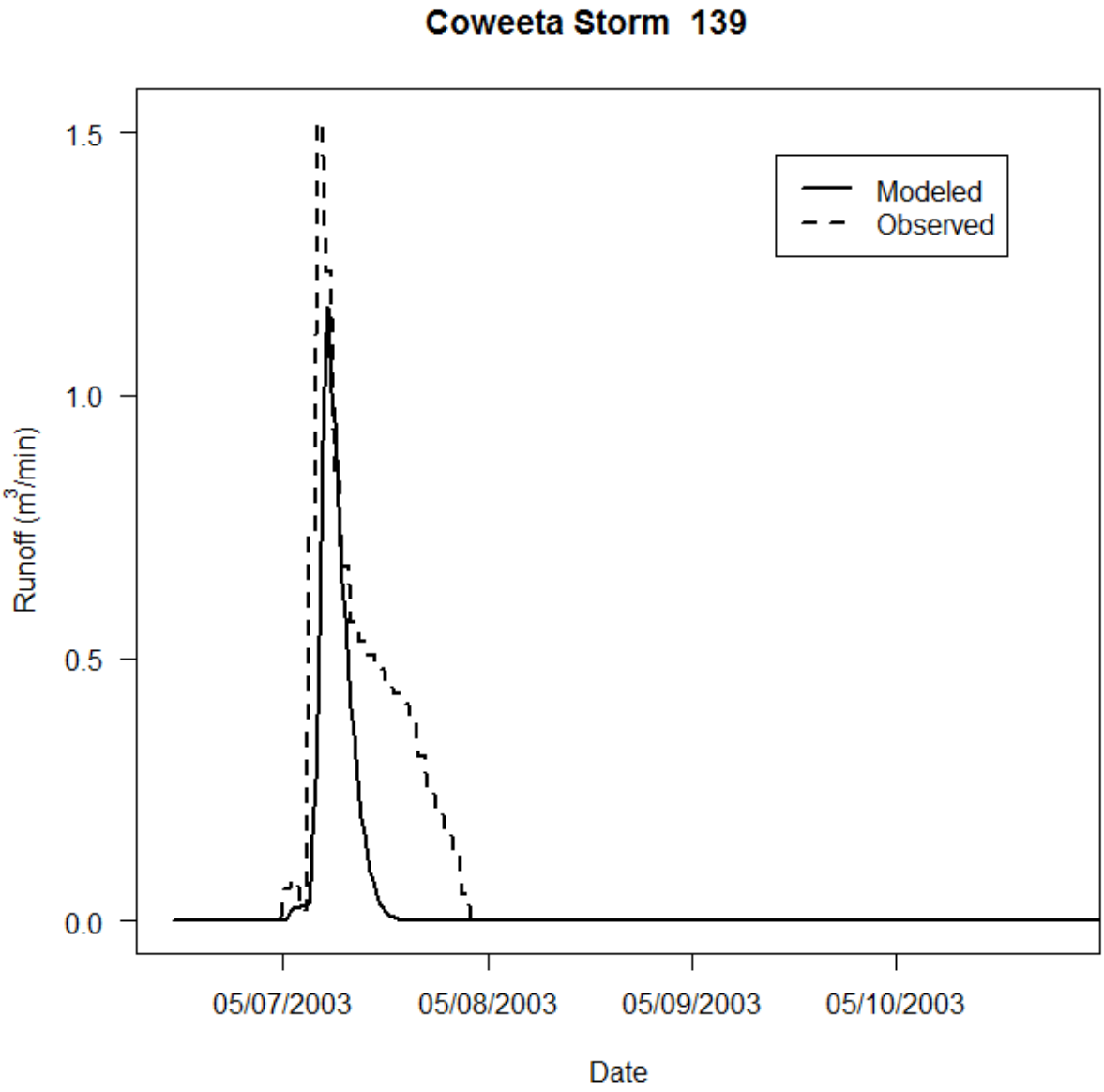

Date: 05/07/03	Nash Sutcliffe	0.58
	Modified Nash Sutcliffe	0.63
Precipitation: 55.9 mm	Observed Peak	1.64
	Modeled Peak	1.14

Figure D.24: Coweeta storm 139.

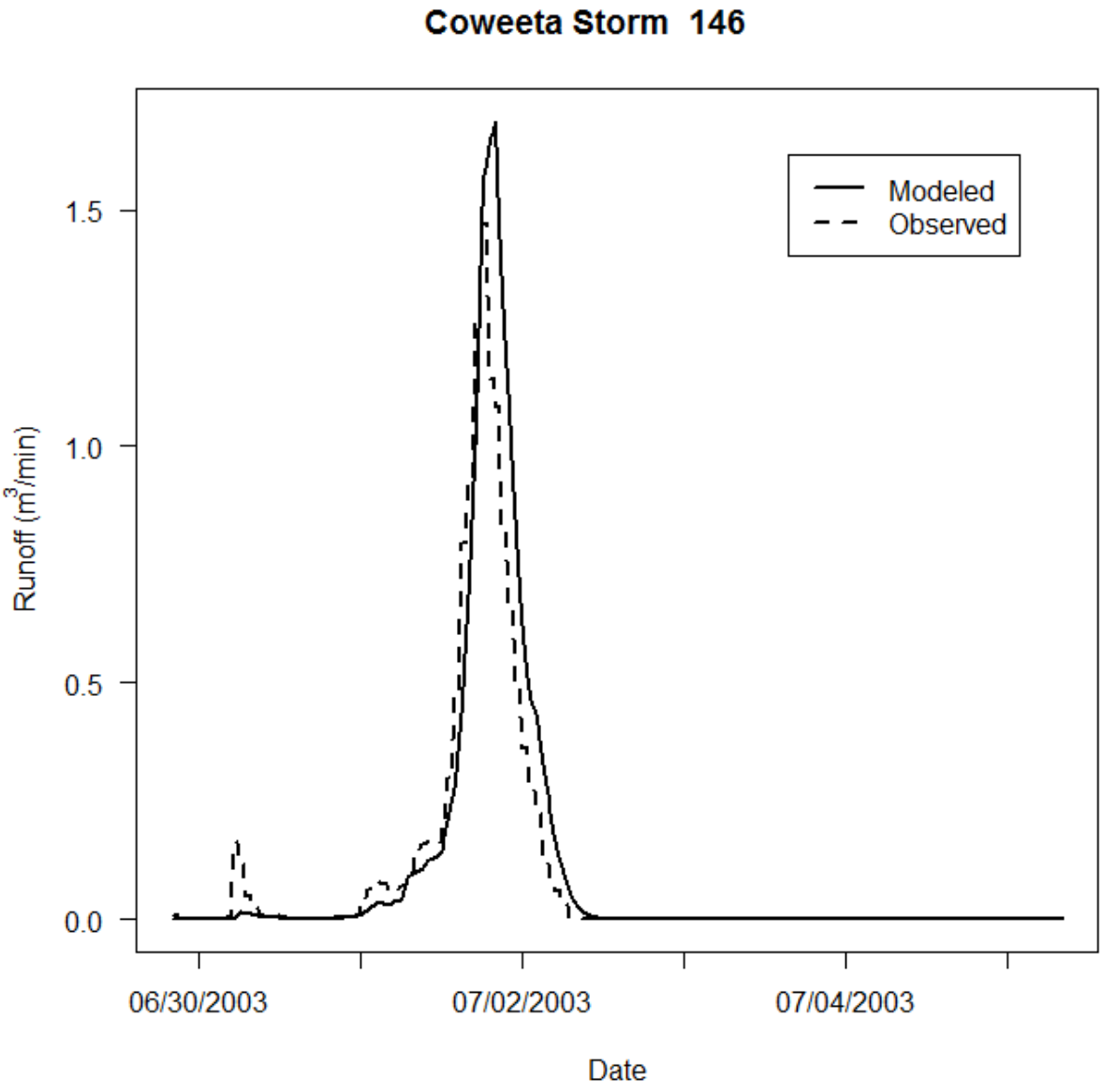

Date: 06/30/03	Nash Sutcliffe	0.90
	Modified Nash Sutcliffe	0.78
Precipitation: 154.9 mm	Observed Peak	1.47
	Modeled Peak	1.69

Figure D.25: Coweeta storm 146.

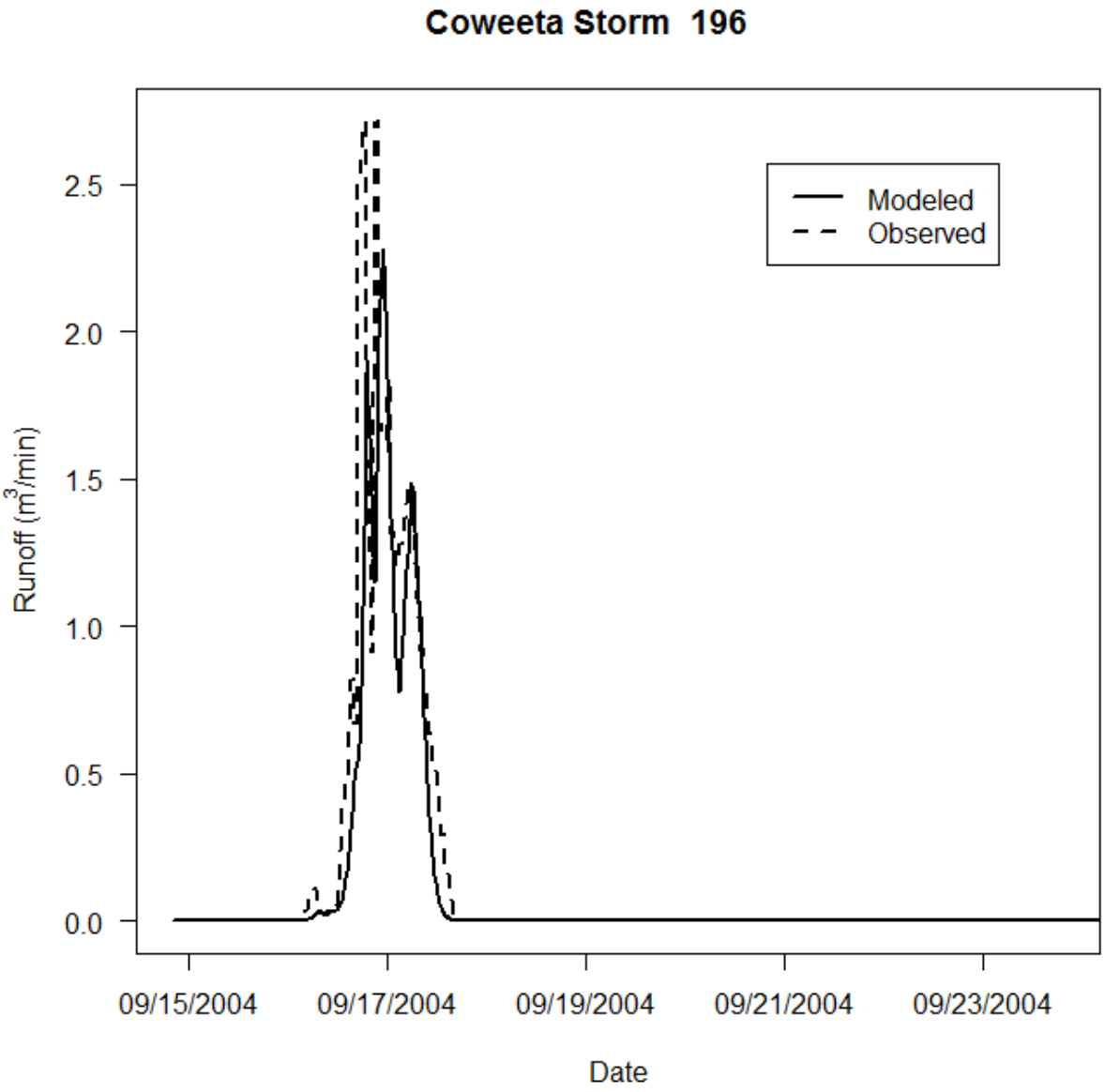

Date: 09/16/04	Nash Sutcliffe	0.88
	Modified Nash Sutcliffe	0.83
Precipitation: 213.4 mm	Observed Peak	2.71
	Modeled Peak	2.28

Figure D.26: Coweeta storm 196.

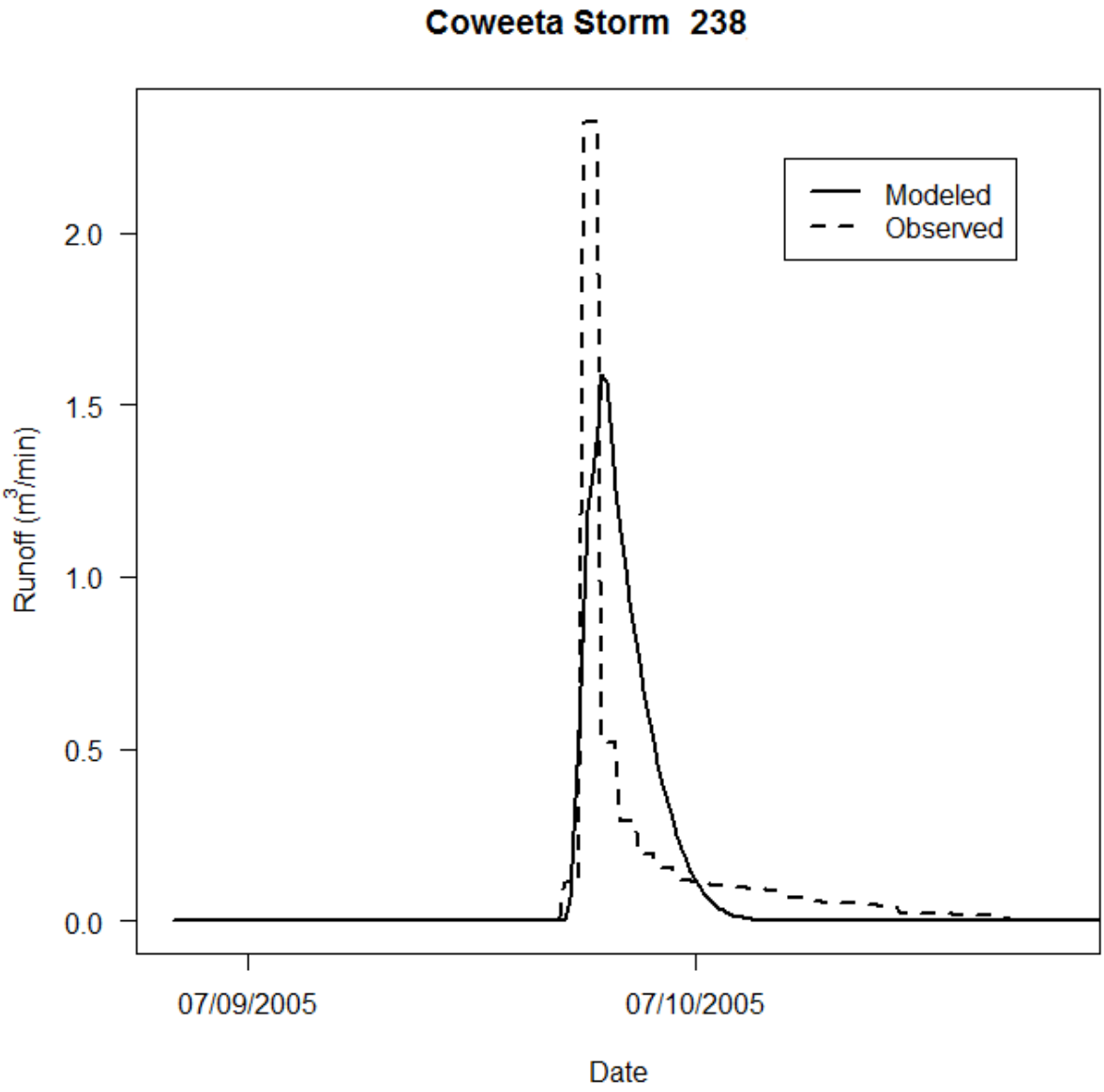

Date: 07/9/05	Nash Sutcliffe	0.51
	Modified Nash Sutcliffe	0.38
Precipitation: 50.8 mm	Observed Peak	2.32
	Modeled Peak	1.59

Figure D.27: Coweeta storm 238.

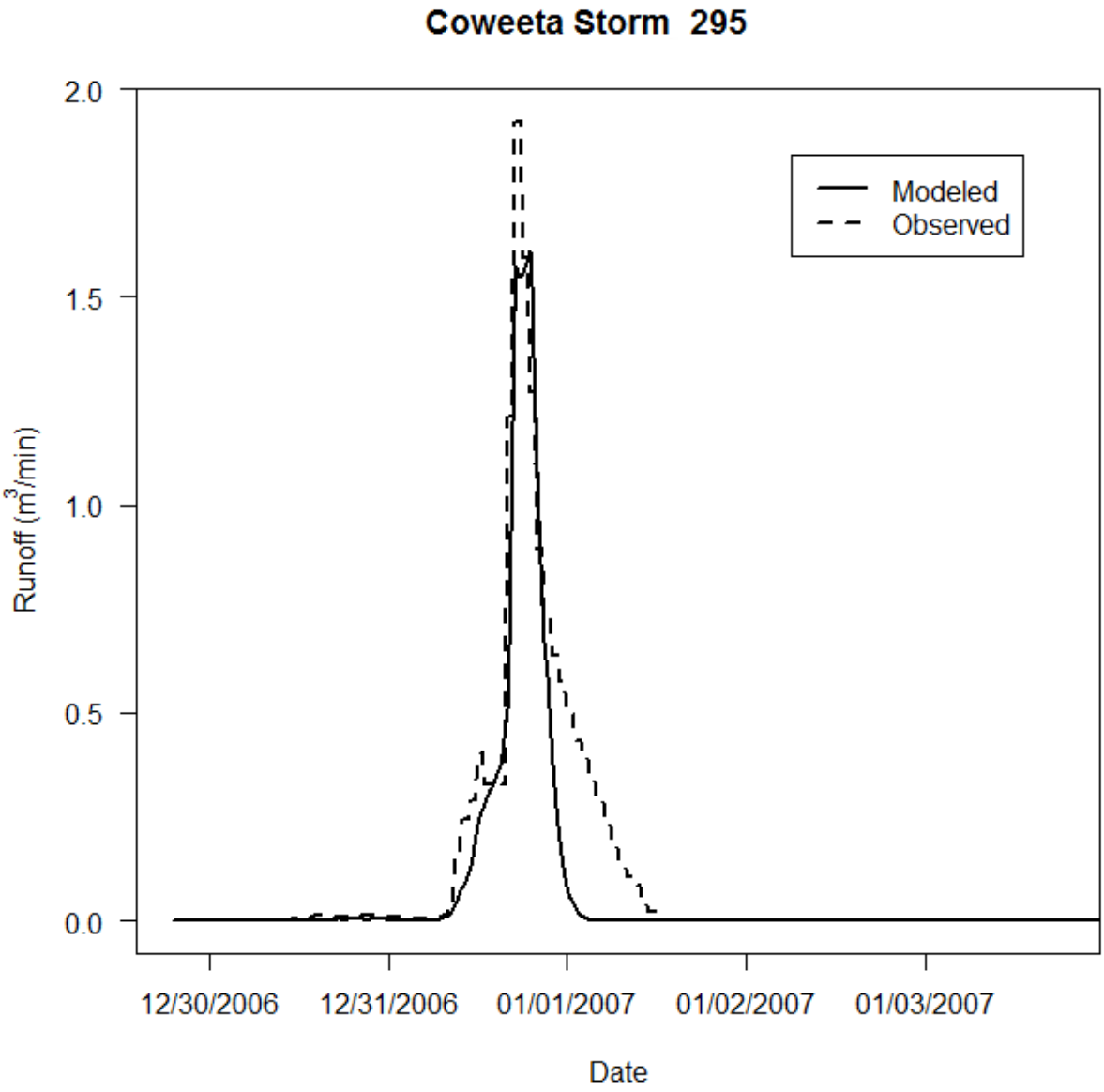

Date: 12/31/06	Nash Sutcliffe	0.81
	Modified Nash Sutcliffe	0.74
Precipitation: 109.2 mm	Observed Peak	1.92
	Modeled Peak	1.61

Figure D.28: Panola storm 295.

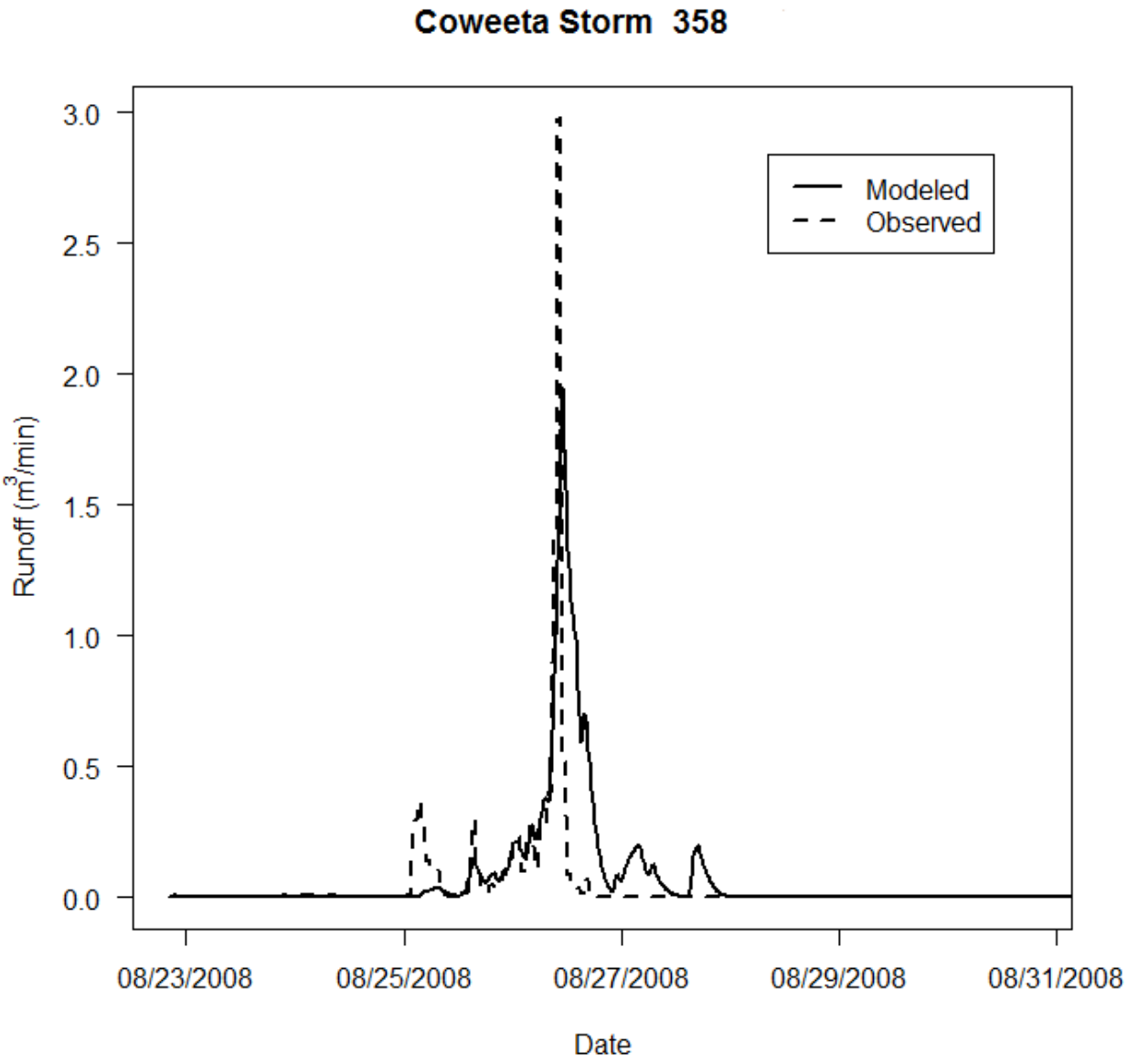

Date: 08/25/08	Nash Sutcliffe	0.09
	Modified Nash Sutcliffe	0.20
Precipitation: 198.1 mm	Observed Peak	2.98
	Modeled Peak	1.95

Figure D.29: Coweeta storm 358.

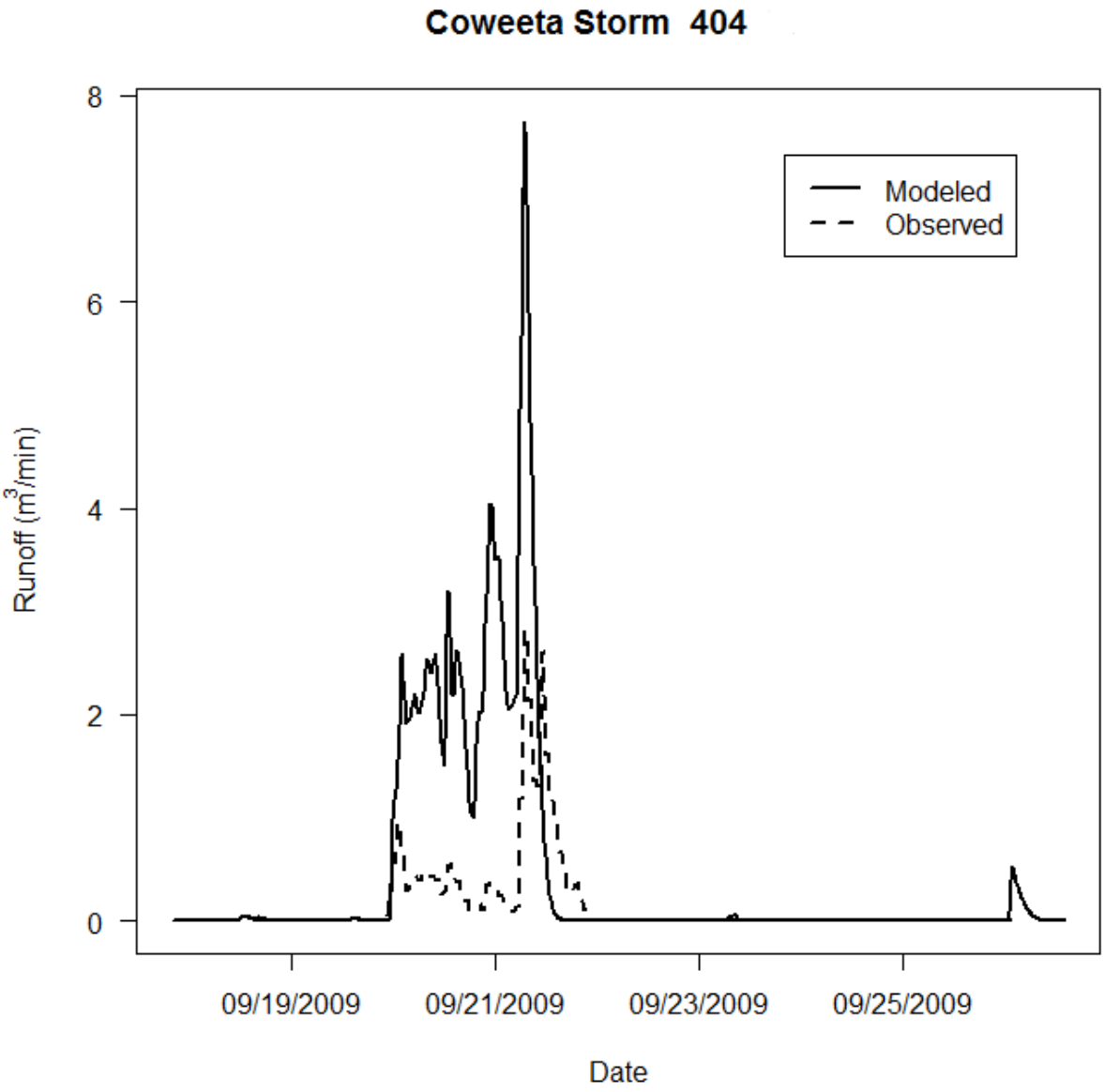

Date: 09/20/09	Nash Sutcliffe	-1.93
	Modified Nash Sutcliffe	-0.22
Precipitation: 251.5 mm	Observed Peak	2.81
	Modeled Peak	7.75

Figure D.30: Coweeta storm 404.

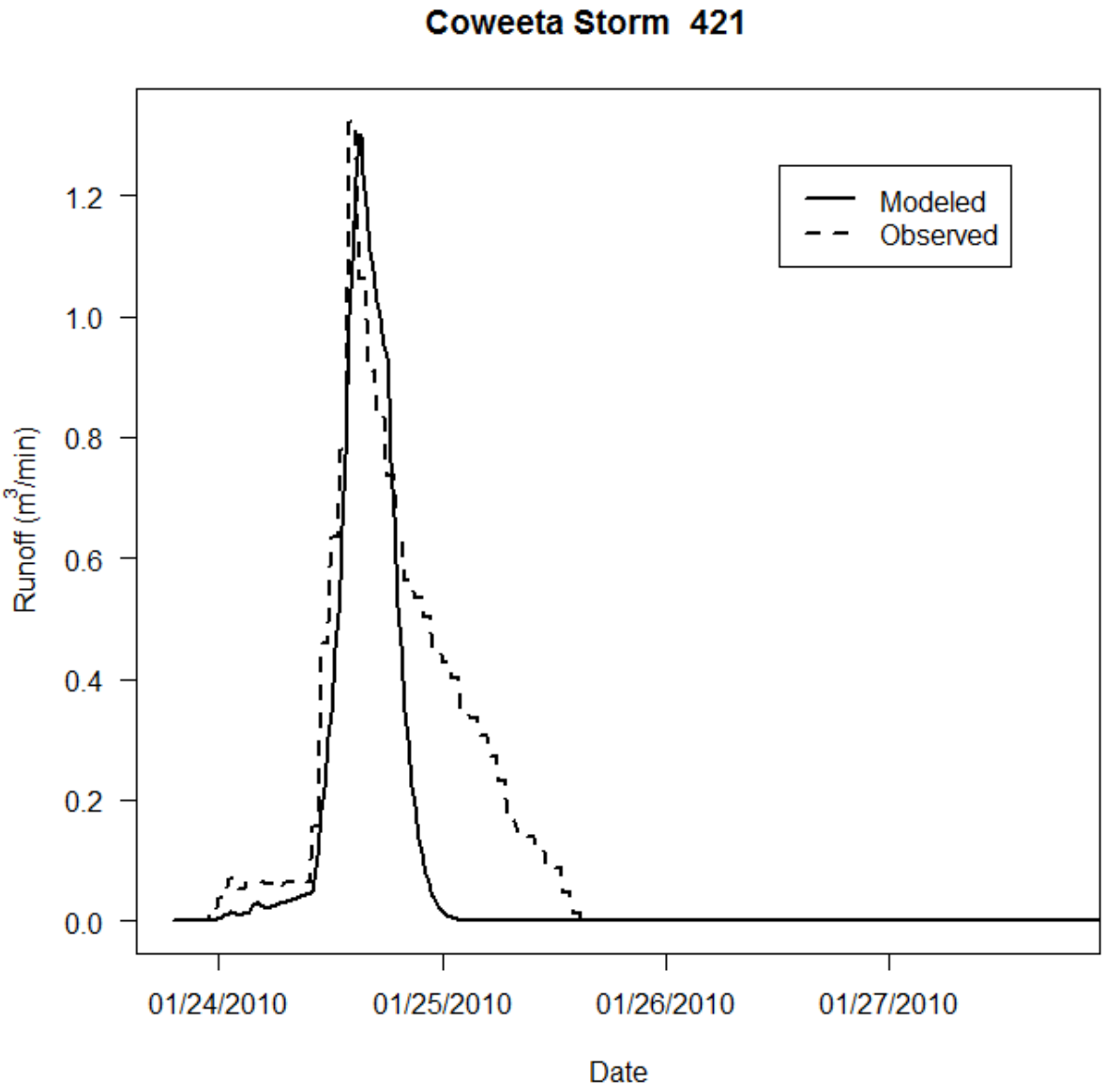

Date: 01/24/10	Nash Sutcliffe	0.69
	Modified Nash Sutcliffe	0.64
Precipitation: 91.4 mm	Observed Peak	1.32
	Modeled Peak	1.30

Figure D.31: Coweeta storm 421.

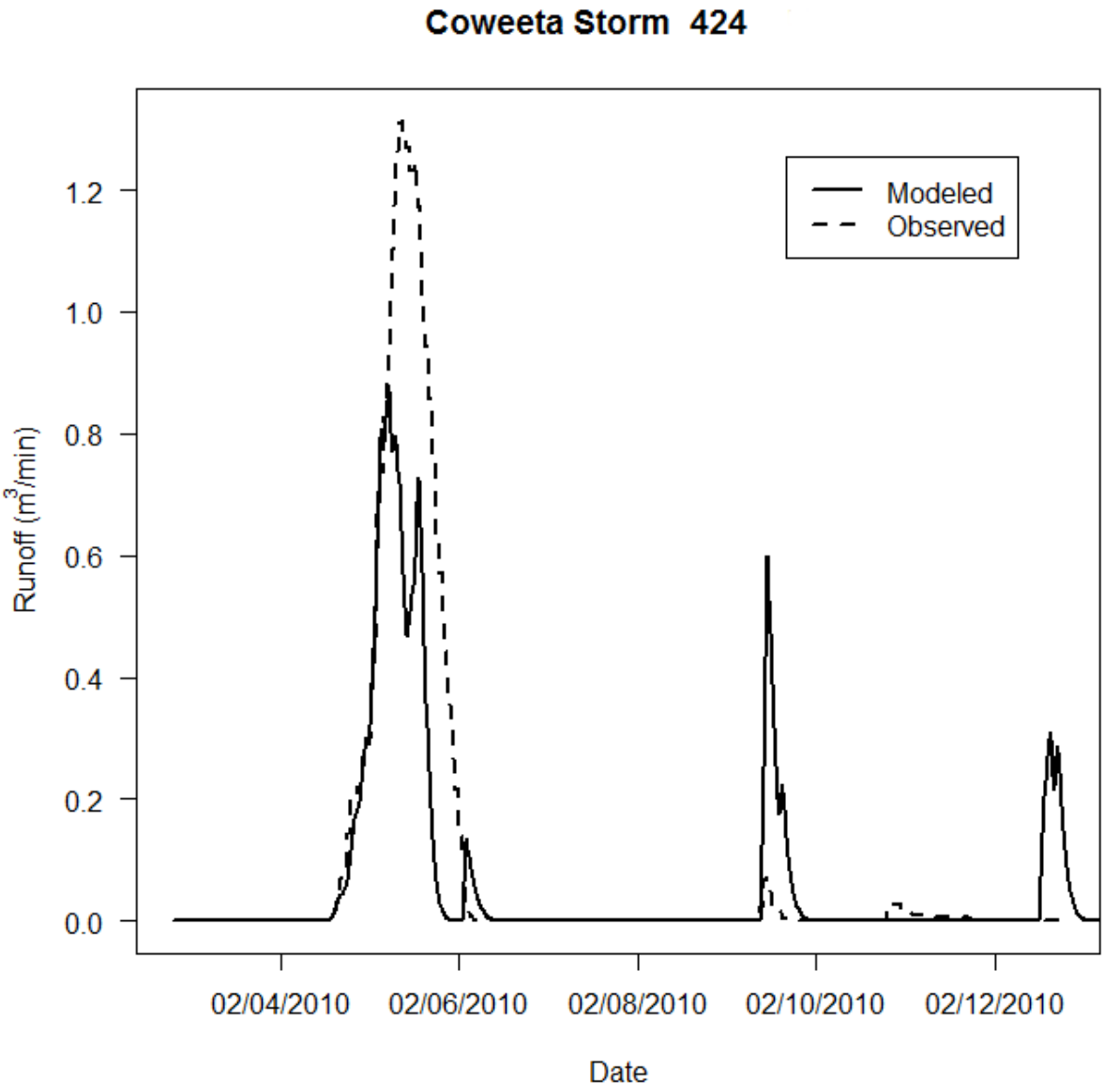

Date: 02/04/10	Nash Sutcliffe	0.65
	Modified Nash Sutcliffe	0.61
Precipitation: 101.6 mm	Observed Peak	1.31
	Modeled Peak	0.88

Figure D.32: Coweeta storm 424.